

**NANOSCALE MODELING OF MATERIALS: POST DEPOSITION
MORPHOLOGICAL EVOLUTION OF FCC METAL SURFACES**

by

ALTAF KARIM

M.Sc., Punjab University, Pakistan, 1995
M.Phil., Quaid-i-Azam University, Pakistan, 1998

AN ABSTRACT OF A DISSERTATION

submitted in partial fulfillment of the
requirements for the degree

DOCTOR OF PHILOSOPHY

Department of Physics
College of Arts and Sciences

KANSAS STATE UNIVERSITY

Manhattan, Kansas

2006

ABSTRACT

This dissertation is an extensive study of several issues related to post deposition morphological evolution of fcc metal surfaces. These studies were carried out by probing the energetics and the dynamics of underlying atomistic mechanisms responsible for surface diffusion. An important aspect is the determination of relative probability of competing atomistic mechanisms and their contribution to controlling shapes and step edge patterns of nano structures on surfaces. In this scenario, the descent of adatoms from Ag islands on Ag(111) surface is examined. It shows an exchange mechanism to dominate over hopping and the process to favor the formation of (100)-microfaceted steps (A-type) over the (111)-microfaceted ones (B-type). Molecular dynamics simulations support these results at low temperature while at high temperature B-type step formation dominates. This change in the trend could happen if these processes leading to the formation of the A and B type steps have different values of their diffusion prefactors. This difference is confirmed on the basis of our calculations of the diffusion coefficients. Further, to understand the macroscopic properties of a system on the basis of its atomic scale information, spatial and temporal fluctuations of step edges on vicinal Cu(1 1 13) and Cu(1 1 19) surfaces is studied using kinetic Monte Carlo (KMC) simulations. These results show excellent agreement with experimental data, highlighting the role of mass transport along step edges, and also showing the validity of tools like KMC which aims at bridging the gap in length and time scales at which a range of

interesting phenomena take place. To facilitate unbiased modeling of material properties, a novel way of performing KMC simulations is presented. In this approach the lists of diffusion processes are automatically collected during the simulation using a saddle-point search method in the potential energy landscape. The speed of the simulations is thus enhanced along with a substantial gain in reliability. Using this method the diffusion and coalescence of two-dimensional Cu and Ag adatom-island on Cu(111) and Ag(111) is studied. Together with input from molecular dynamics simulations, new processes involving the concerted motion of smaller islands are revealed. A significant difference in the scaling of the effective diffusion barriers with island size is observed for the sets of smaller (less than 10 atoms) and larger islands. In particular, the presence of concerted island motion leads to an almost linear increase in the effective diffusion barrier with size, while its absence accounts for strong size-dependent oscillations and anomalous behavior for trimers and heptamers. A crossover from diffusion due to the collective motion of the smaller island to a regime in which the island diffuses through the periphery dominated mass transport (large islands, 19 to 100 atoms) is predicted. For islands containing 19 to 100 atoms the scaling exponent is found to be in good agreement with that found in previous studies.

**NANOSCALE MODELING OF MATERIALS: POST DEPOSITION
MORPHOLOGICAL EVOLUTION OF FCC METAL SURFACES**

by

ALTAF KARIM

M.Sc., Punjab University, Pakistan, 1995
M.Phil., Quaid-i-Azam University, Pakistan, 1998

A DISSERTATION

submitted in partial fulfillment of the

requirements for the degree

DOCTOR OF PHILOSOPHY

Department of Physics
College of Arts and Sciences

KANSAS STATE UNIVERSITY
Manhattan, Kansas

2006

Approved by:

Major Professor
Talat S. Rahman

ABSTRACT

This dissertation is an extensive study of several issues related to post deposition morphological evolution of fcc metal surfaces. These studies were carried out by probing the energetics and the dynamics of underlying atomistic mechanisms responsible for surface diffusion. An important aspect is the determination of relative probability of competing atomistic mechanisms and their contribution to controlling shapes and step edge patterns of nano structures on surfaces. In this scenario, the descent of adatoms from Ag islands on Ag(111) surface is examined. It shows an exchange mechanism to dominate over hopping and the process to favor the formation of (100)-microfaceted steps (A-type) over the (111)-microfaceted ones (B-type). Molecular dynamics simulations support these results at low temperature while at high temperature B-type step formation dominates. This change in the trend could happen if these processes leading to the formation of the A and B type steps have different values of their diffusion prefactors. This difference is confirmed on the basis of our calculations of the diffusion coefficients. Further, to understand the macroscopic properties of a system on the basis of its atomic scale information, spatial and temporal fluctuations of step edges on vicinal Cu(1 1 13) and Cu(1 1 19) surfaces is studied using kinetic Monte Carlo (KMC) simulations. These results show excellent agreement with experimental data, highlighting the role of mass transport along step edges, and also showing the validity of tools like KMC which aims at bridging the gap in length and time scales at which a range of

interesting phenomena take place. To facilitate unbiased modeling of material properties, a novel way of performing KMC simulations is presented. In this approach the lists of diffusion processes are automatically collected during the simulation using a saddle-point search method in the potential energy landscape. The speed of the simulations is thus enhanced along with a substantial gain in reliability. Using this method the diffusion and coalescence of two-dimensional Cu and Ag adatom-island on Cu(111) and Ag(111) is studied. Together with input from molecular dynamics simulations, new processes involving the concerted motion of smaller islands are revealed. A significant difference in the scaling of the effective diffusion barriers with island size is observed for the sets of smaller (less than 10 atoms) and larger islands. In particular, the presence of concerted island motion leads to an almost linear increase in the effective diffusion barrier with size, while its absence accounts for strong size-dependent oscillations and anomalous behavior for trimers and heptamers. A crossover from diffusion due to the collective motion of the smaller island to a regime in which the island diffuses through the periphery dominated mass transport (large islands, 19 to 100 atoms) is predicted. For islands containing 19 to 100 atoms the scaling exponent is found to be in good agreement with that found in previous studies.

TABLE OF CONTENTS

TABLE OF CONTENTS	i
LIST OF FIGURES	v
LIST OF TABLES	xi
ACKNOWLEDGEMENTS	xii
DEDICATION	xiv
I INTRODUCTION	1
II THEORETICAL TECHNIQUES	8
2.1 Methods for Determining the Total Energy	8
2.1.1 The Density Functional Theory Method	8
2.1.2 EAM Interaction Potentials	10
2.2 Methods for Simulating Morphological Evolution of Surfaces	11
2.2.1 Molecular Dynamics Methods	11
2.2.2 The Kinetic Monte Carlo Technique	15
2.3 Determination of Diffusion Prefactors, Paths, and Energy Barriers	20
2.3.1 Diffusion Prefactors	20
2.3.2 Diffusion Paths and Energy Barriers from the Nudged Elastic Band Method	21

2.3.3	Estimation of Final States from the Spherical Repulsion Method	23
2.3.4	Energy Barriers from the Drag Method	23
2.3.5	The Grid Method	26
III	EXPERIMENTAL METHODS	27
3.1	The Scanning Tunneling Microscopy	27
3.2	Field Ion Microscopy	28
3.3	Low Energy Electron Diffraction	29
IV	PATHS, BARRIERS, AND PREFACTORS FOR ADATOM DESCENT FROM AG ISLANDS ON AG (111)	31
4.1	Introduction	31
4.2	Details of the Calculations	33
4.3	Results of Calculations of the Surface Energetics	34
4.4	Results of Molecular Dynamics Simulations	38
4.5	Conclusion	41
V	FLUCTUATIONS OF SURFACE STEPS IN EQUILIBRIUM: A KI- NETIC MONTE CARLO STUDY	42
5.1	Introduction	42
5.2	The Model	43
5.3	Spatial correlations	45
5.4	Temporal correlations	46

5.5	Results	46
5.6	Summary and conclusions	51
VI SELF-LEARNING KINETIC MONTE-CARLO METHOD: APPLICA-		
	TION TO CU(111)	52
6.1	Introduction	52
6.2	Essentials of Self-Learning Kinetic Monte Carlo Method	55
6.2.1	Model System	55
6.2.2	Some Ingredients of Kinetic Monte Carlo	56
6.2.3	Self Learning Kinetic Monte Carlo Method	58
6.3	Application of SLKMC to Morphological Evolution of 2D islands on Cu(111)	62
6.3.1	Model Systems	62
6.3.2	Examination of the collected database	62
6.3.3	Morphological Evolution	66
6.4	Conclusion	71
VII DIFFUSION OF SMALL TWO-DIMENSIONAL CU ISLANDS ON CU		
	(111)	73
7.1	Introduction	73
7.2	Calculational Details	77
7.3	Results and Discussions	81
7.3.1	Monomer	83

7.3.2	Dimer	85
7.3.3	Trimer	88
7.3.4	Tetramer	91
7.3.5	Islands containing 5 to 10 atoms	91
7.3.6	Key mechanisms and their occurrence frequencies	93
7.4	Conclusions	96
VIII THE CROSSOVER FROM COLLECTIVE MOTION TO PERIPHERY		
	DIFFUSION FOR ADATOM-ISLANDS ON CU(111) AND AG(111)	98
8.1	Introduction	98
8.2	Calculational Details	100
8.3	Results and Discussions	100
8.4	Conclusions	104
IX	CONCLUSIONS	112
	Bibliography	116
APPENDIX A	— LIST OF PUBLICATIONS	124

LIST OF FIGURES

1	Island shapes on Pt (111) at different temperatures, a) 200K, b) 400K, c) 455K, d) 640K, e1) 710K, e2) 425K. This Figure is taken from: T. Michely, M. Hohage, M. Bott, and G. Comsa, Phys. Rev. Lett. 70 , 3943 (1993). . .	3
2	Formation of A or B type face via exchange mechanism.	4
3	Some atomic processes involved in epitaxial growth	15
4	Illustration of energy profile with saddle and equilibrium points	17
5	Flowchart of KMC code used for (100) surfaces	18
6	Binary tree structure for selection of transition in the BKL Monte method.	19
7	Linear search method.	19
8	Nudged Elastic Band method, images connected via elastic bands.	22
9	a) A repulsive potential is added in potential to make it biased, b) final shape of total potential. Reference: Oleg Trushin et. al., 2002.	24
10	Illustration of Drag method	25
11	Adatom decent from a small island: a) two possible scenarios; b) their paths and their energies.	26
12	Scanning tunnelling microscope	28
13	Field ion microscope	29
14	Low energy electron diffraction system	30
15	Formation of A or B type face via exchange mechanism.	35

16	The grid	36
17	Diffusion paths and barriers	37
18	Schematics of the barrier energies	38
19	Arrhenius plot of the diffusion coefficient of processes leading to A and B type steps	40
20	fcc (1 1 13) vicinal surface.	44
21	Equilibrium step profiles of the Cu (1,1,13) at (a) $T = 320$ K and (b) $T =$ 370 K.	47
22	Arrhenius plot of the diffusivities for the Cu (1,1,13) and Cu (1,1,19). The inset displays a series of spatial correlation functions $G(y)$ at several temper- atures for Cu (1,1,13).	48
23	Temporal correlation functions $G(t)$ on a log-log scale for Cu(1,1,13). Solid lines are obtained by fitting the simulation data to Eq. 6.5.	50
24	Arrhenius plots of Eq. 6.5 for the Cu(1,1,13) and Cu(1,1,19).	51
25	(a) The three-shell indexing around the central atom labeled 1; (b) signature of a particular 2D cluster configuration in base 2 and base 10	59
26	Sample (a) single-atom and (b) multiple-atom processes involved in the dif- fusion of 2D clusters presented with their specific labels for our database . .	59
27	Flow chart for SLKMC simulation	60
28	Selected single atom processes on the two types of steps A (100 microfaceted) and B (111 microfaceted), on fcc (111) surface. Process 1 is kink-detachment from a step, and 4 is adatom diffusion along step. The labels a and b refer to steps A and B, respectively.	63

29	Distribution (percentage) of activation energies of stored processes in the database during a SLKMC simulation	65
30	Variations in the number of KMC steps per CPU time (i.e., performance) and the buildup of the database as a function of the number of KMC steps (inset)	65
31	Trace of center of mass of 19- and 38-atom Cu clusters on Cu (111) at 300K as obtained from SLKMC simulations (10 million steps)	66
32	Mean square displacement (MSD) for 19- and 38-atom Cu clusters on Cu (111), as function of time at 300 K	67
33	Coalescence of a small Cu cluster (78 atoms) with a larger one (498 atoms) on Cu (111) at 300 K, using the SLKMC simulation (10 million steps).	70
34	Some examples of adatom diffusion and hops on the fcc (111) surface. Dark-colored atoms are active and placed at fcc sites, whereas light-colored atoms serve as the substrate. The lower edge of the layer containing active atoms forms a (111) microfacet, so it is called the B-type step edge while the upper edge of the layer containing active atoms forms a (100) microfacet which is called an A-type step.	82
35	Diffusion coefficients as a function of the island size; (a) KMC results without including concerted motion mechanisms; (b) KMC results after including concerted motion mechanisms obtained from MD simulations.	83
36	Effective diffusion barriers of 1-10 atom islands plotted as a function of island size. The dotted line with squares represents full KMC simulation results including concerted motion, whereas the dotted line with circles shows results of the KMC simulation without including concerted motion mechanisms. The inset shows Arrhenius plots of diffusion coefficients as a function of temperature.	85

37	(a) Illustration of two simple mechanisms for dimer diffusion and their energy barriers, where atoms jump from fcc to fcc sites. (b) 13 mechanisms for dimer diffusion via fcc to hcp sites and their energy barriers. These mechanisms were found from MD simulations.	87
38	(a) Nine mechanisms for trimer diffusion with their corresponding energy barriers, where atoms are allowed to jump from fcc to fcc sites. (b) Trimer diffusion mechanisms observed during MD simulations. These mechanisms are conducted through a collective motion of three atoms by rotation and gliding over the bridge sites from fcc to hcp sites, or vice versa.	89
39	Distribution of normalized frequencies of event occurrences in the case of trimer diffusion. The lines with filled symbols show the distributions of events at different temperatures when only single atom mechanisms were included, and lines with open symbols show the distributions of all events including the collective motion of three atoms by rotation and gliding.	90
40	(a) Illustration of 28 mechanisms and their corresponding energy barriers for tetramer diffusion, where jumps are allowed from fcc to fcc sites only. (b) Tetramer diffusion mechanisms revealed from MD simulations: (1) diagonal glide, (2) vertical glide of 4 atom island over the bridge sites and the corresponding energy barriers, and (3) shearing mechanism.	92
41	A few examples of single and multiple atom mechanisms and their corresponding energy barriers used in our KMC simulations for island larger than 4 atoms. Jumps are allowed from fcc to fcc sites only.	94
42	Diffusion mechanisms found by performing MD simulations for the island sizes of 5-10 atoms and their corresponding energy barriers when they glide over the bridge sites exhibiting collective motion of all atoms.	95

43	Distribution of normalized frequencies of concerted motion events as a function of island size.	97
44	Adatom island diffusion coefficient D vs N for $1 \leq N \leq 100$ at $T = 300\text{K}$, 500K , and 700K , a) Cu on Cu(111), b) Ag on Ag(111).	101
45	Effective diffusion barriers as a function of the island size, a) Cu on Cu(111), b) Ag on Ag(111).	102
46	Comparison of effective and collective diffusion barriers as function of the island size, a) Cu on Cu(111), b) Ag on Ag(111).	103
47	Fit of the proposed theoretical model on simulation data of D , a) Cu on Cu(111), b) Ag on Ag(111).	103
48	Frequencies of different processes as function of the island size, a) Cu on Cu(111), b) Ag on Ag(111).	105
49	Some important multiple atom mechanisms for island diffusion, a) Cu on Cu(111), b) Ag on Ag(111).	105
50	Comparison of Cu and Ag trimer energetics, light colored labels represent energetics of Cu, whereas dark colored labels represent energetics of Ag. (a) Nine mechanisms for trimer diffusion with their corresponding energy barriers, where atoms are allowed to jump from fcc to fcc sites. (b) Trimer diffusion mechanisms observed during MD simulations. These mechanisms are conducted through a collective motion of three atoms by rotation and gliding over the bridge sites from fcc to hcp sites, or vice versa.	107

51	Comparison of Cu and Ag tetramer energetics, light colored labels represent energetics of Cu, whereas dark colored labels represent energetics of Ag. (a) Illustration of 28 mechanisms and their corresponding energy barriers for tetramer diffusion, where jumps are allowed from fcc to fcc sites only. (b) Tetramer diffusion mechanisms revealed from MD simulations: (1) diagonal glide, (2) vertical glide of 4 atom island over the bridge sites and the corresponding energy barriers, and (3) shearing mechanism.	108
52	Comparison of Cu and Ag single atom energetics, light colored labels represent energetics of Cu, whereas dark colored labels represent energetics of Ag. A few examples of single and multiple atom mechanisms and their corresponding energy barriers used in our KMC simulations for island larger than 4 atoms. Jumps are allowed from fcc to fcc sites only.	109
53	Comparison of Cu and Ag concerted motion energetics, light colored labels represent energetics of Cu, whereas dark colored labels represent energetics of Ag. Diffusion mechanisms found by performing MD simulations for the island sizes of 5-10 atoms and their corresponding energy barriers when they glide over the bridge sites exhibiting collective motion of all atoms.	110

LIST OF TABLES

1	M.D. statistics for 4+1 island	40
2	Descending times (DT) and formation probabilities (FP) for A and B types	41
3	Diffusion coefficients (D) for A and B types	41
4	Summary of step parameters for the Cu (100) vicinals	49
5	Diffusion energy barriers for selected mechanisms as shown in Fig. 6.4 . . .	63
6	Diffusion coefficient for 2D Cu islands on Cu(111) (Å ² /sec)	66
7	Frequencies of diffusion processes for the 19 atom cluster at two temperatures	68
8	Frequency of selected processes during the coalescence of 2 islands	68
9	Diffusion coefficients of a trimer and a tetramer at different temperatures. .	83
10	Diffusion coefficients of 1 to 10 atom islands at different temperatures and their effective diffusion barriers with diffusion prefactors.	84
11	Diffusion coefficients of 1 to 10 atom islands at different temperatures and their effective diffusion barriers.	106

ACKNOWLEDGEMENTS

I would like to take a moment to acknowledge those who have been a part of my education, as teachers, friends, and family.

First, I gratefully appreciate the priceless guidance and supervision of my advisor Professor Talat S. Rahman during this work. I thank Dr. Abdelkader Kara for numerous stimulating discussions, ideas, and invaluable help throughout my research work at K-State. I also gratefully acknowledge the help and contributions of all my group members, especially Dr. Ahlam Al-Rawi, Dr. Chandana Ghosh, Dr. Sampyo Hong, Dr. John Spangler, and Dr. Sergey Stolbov. Charlie Thornton and Dr. Al-Rawi's son Ali Mohammad are thanked for their assistance with some visualization tools and problems. I also thank Sophie Exdell for her assistance in proofreading my script.

Secondly, I am grateful to my fellows at Helsinki University of Technology, Finland, and Fritz-Haber-Institut der Max-Planck-Gesellschaft, Germany. These institutions showed me great hospitality during my stay in Finland and Germany in 2001-2003. In this regard, special thanks go to Professor Tapio Ala-Nissila and Dr. Marko Rusanen; with their help and collaborative efforts I learnt the basic principles of KMC techniques and accomplished the major part of my work. I am also greatly thankful to Dr. Oleg Trushin, Institute of Microelectronics and Informatics of Russian Academy of Sciences. His unforgettable cooperation and role in developing SLKMC techniques and various other computational methods for determining energy barriers led us to the frontiers of ongoing research in the field. This collaborative work made the major contributions to Chapter 6 of this dissertation.

I can't finish this acknowledgment without remembering my old teachers in Pakistan, especially Ustad Ibadat Ali, Government Islamia Primary School Kamalia, and Professor Moulvi Bashir, Government College Faisalabad. I can never forget the charisma and power of their teaching style and unshakable moral character. I perceive their magical contribution to my personal development and education as a special gift from God. Without having been

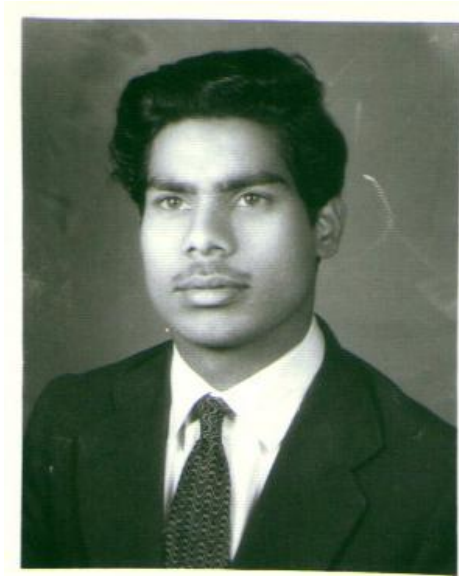
inspired and motivated by them, I would not have been able to pursue the best possible education with profound devotion.

I also proudly express my admiration and gratitude to all my lovely and wonderful friends, bhabies, aunties, uncles, and their kids in Kansas. They have always been my surrogate family through thick and thin.

Finally, I remember the passionate encouragement and contributions of my parents, brother, and sister throughout my life. And with much fondness, I recall my childhood and early youth illuminated by my grandmother's smiles and her unfailing prayers. No word can describe my family's unconditional love filled with sacrifices.

*To my father,
Nazir Ahmad,*

who bought me a set of scientific instruments to entertain my very first interest in science and helped me with setting up a lab in our home when I was a little kid.



CHAPTER I

INTRODUCTION

In the field of surface science, modern microscopic techniques used for probing solid surfaces, such as scanning tunneling microscopy (STM) [1, 2] have produced a paradigm shift in the study of surface systems on the atomic scale. Their potential applications motivated studies of nanostructures on surfaces. These studies provide intriguing examples of both equilibrium and nonequilibrium physics. In this regard, novel experiments were performed which led to the discovery of entirely new phenomena and features. Evolution of surface morphology based on pattern formation, their self-assembly, adatom/vacancy island diffusion, and step edge fluctuations provide us good examples of these challenging topics in surface science. Research in these topics certainly needs a strong communication between experiments and theoretical models.

In terms of theoretical or computational studies, one of the challenges in recent research of nanostructures and pattern formations on surfaces is the development of an understanding of microscopic processes that control the evolution of surface morphology. Also, thermodynamic principles governing these microscopic processes need to be understood in terms of underlying atomic structures and their energetics. In this regard we are fortunate to have methods like *ab-initio* electronic structure calculations [3] for the extraction of relevant energetics and dynamics of selected systems of interest. Such calculations are becoming feasible for complex systems, even though they remain computationally intensive. A reasonable alternative has been provided by several genres of many body interatomic potentials [4]. These potentials have already provided a wealth of information on the microscopic properties of a selected group of metal surfaces that have been tested by comparison with experimental data. With these interatomic potentials it has been possible to carry out computational and theoretical studies of a range of surface phenomena using techniques

like molecular dynamics (MD) and kinetic Monte-Carlo (KMC) simulations. While molecular dynamics simulations carried out with reliable interatomic potentials are capable of revealing the essential details of microscopic phenomena as they unfold as a function of temperature, pressure, and other global variables, they are limited to time scales (microseconds) which are many orders of magnitude smaller than those for events in laboratory take place on all time scales. For examples, surface morphological changes take place in minutes and hours. Furthermore, key atomistic processes that may eventually control the formation of different patterns and ensuing characteristics of systems are “infrequent” events on the time scales so far accessible to standard molecular dynamics techniques. Recently several attempts [5] have thus been made to overcome this huge difference in time scales by finding ways in which rare events are forced to appear more frequently.

The basic ingredients in atomistic modeling of surface morphological evolution are thus linked with those responsible for the characterization of the diffusion of adatoms, vacancies, and their islands on surfaces with specific crystallographic orientations and marked with defects and other local environments. When diffusion is driven by thermally activated processes, entities move on a temperature dependent dynamical surface provided by the substrate. The diffusing entities vibrate about their equilibrium positions and occasionally overcome the energy barrier to move to another site of low occupation energy. To simulate the evolution of surface morphology, first we need a tabulation of all possible diffusion pathways, and the probability (or rate) with which a particular path (or process) might be undertaken. One way to obtain such information is through molecular dynamics (MD) simulations. But, as straight forward as the method is, it has drastic limitations which leave it uncompetitive for such studies.

An alternative to MD simulations is offered by the kinetic Monte-Carlo (KMC) technique. Kinetic Monte Carlo (KMC) is an extremely efficient method which may be used to carry out dynamical simulations of stochastic and/or thermally activated processes when the relevant activated atomic-scale processes are known [6, 7, 8]. KMC simulations have been successfully used to model a wide variety of dynamical processes ranging from catalysis to growth [9, 10]. In particular, for problems such as evolution of surface morphology

in which the possible rates or probabilities for events can vary by several orders of magnitude, the kinetic Monte Carlo algorithm can be orders of magnitude more efficient than Metropolis Monte Carlo algorithm [11].

This dissertation aims to develop a theoretical framework based on the understanding of processes that control surface morphology through pattern formation, step edges fluctuations, and adatom island diffusion by applying the above mentioned classical molecular dynamics and kinetic Monte Carlo techniques. This framework is thus extended to the study of systems of realistic dimensions of length and time scales. By virtue of these developments, our work nicely complement and supplement experimental observations in the area.

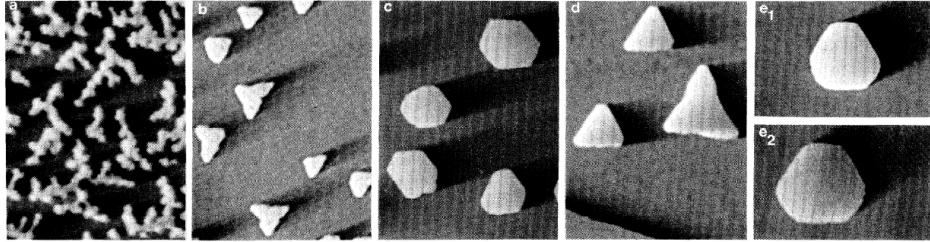


Figure 1: Island shapes on Pt (111) at different temperatures, a) 200K, b) 400K, c) 455K, d) 640K, e1) 710K, e2) 425K. This Figure is taken from: T. Michely, M. Hohage, M. Bott, and G. Comsa, Phys. Rev. Lett. **70**, 3943 (1993).

One of the important aspects of this work is to determine the equilibrium shapes of islands by studying emerging patterns on surfaces [12], as shown in Fig. 1. A variety of experimental studies of homo- and heteroepitaxy on the (100), (110) and (111) surfaces of several transition metals has led to interesting observations. Among these, the case of homoepitaxial growth on fcc (111) surfaces has been particularly intriguing, since the innate geometry of the surface forces the steps formed by nucleating two-dimensional island to take two types of configurations. Monoatomic closed-packed steps formed on this surface may have either a (100)-microfacet (A-type) or a (111)-microfacet (B-type) (see Fig. 2). The relative abundance of one type of step over the other may thus lead to very distinct features in the growth patterns. Since the local structural, dynamical and electronic properties of these steps may be different from each other, it is not surprising that experimental

observations of homoepitaxial growth on several fcc (111) surfaces display very distinct characteristics. In the case of Pt(111), for example, the relative abundances of the A-type or the B-type steps depends on the surface temperature [12].

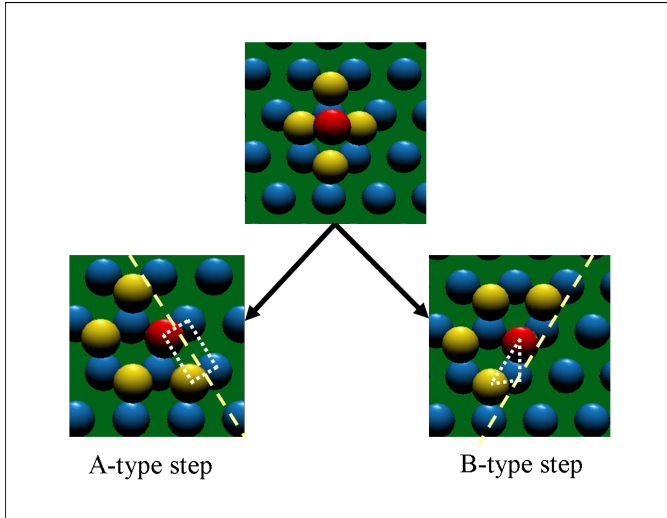


Figure 2: Formation of A or B type face via exchange mechanism.

In this scenario, the descent of adatoms from Ag islands on Ag(111) surface is examined, as shown in Fig. 2. An extensive study of the energetics of an initial stage of formation of steps on the Ag (111) surface is carried out by examining the potential energy surface. It shows the exchange mechanism to dominate over hopping and the process to favor the formation of the 100-microfaceted steps (A-type) over the 111-microfaceted ones (B-type). Our molecular dynamics simulations support these results at low temperature. However, a flip in the trend favors the B-type step formation at high temperatures. This temperature dependent change in the trend of A-type and B-type step formation can be understood if we expect the potential energy surface to undergo modulations with temperature and the characteristics of surface vibrations to play a role in the diffusion process. We have thus carried out molecular dynamics (MD) simulations of the system of interest here for the temperature range 300K to 700K. Interestingly, our results show that predictions of diffusion coefficients made from considerations of surface energetics alone are not enough to give us reliable results at finite temperatures. In particular, we show that the diffusion

pre-exponential factors for the formation of A and B type steps may differ significantly from each other.

As we mentioned above, molecular dynamics simulations can only be carried out adequately at small length and time scales. Further implementations of MD is certainly not a practical idea if we study phenomena taking place at large length and time scales. So we have to use other tools like KMC that aims at bridging the gap in length and time scales at which a range of interesting phenomena take place. Post deposition morphological evolution, epitaxial growth, and step edge fluctuations are good examples of such phenomena.

For nanostructuring of materials and controlling epitaxial growth of thin films on substrates, a knowledge of the stability and atomistic quality of the surface is essential. This is particularly important for the case of vicinal surfaces with regular arrays of steps, which can be used, for example, for stabilizing layer-by-layer Molecular Beam Epitaxy (MBE) growth mode, or for forming quasi-1D nanostructures, by decoration techniques [13]. Because of the availability of specific experimental data [14, 15], we concentrate here on the Cu(1 1 13) and Cu(1 1 19) surfaces, both of which have well separated steps and to a first approximation step-step interaction may be ignored. In this regard, to understand the macroscopic properties on the bases of atomic scale information, spatial and temporal fluctuations of step edges on these vicinal surfaces are studied using kinetic Monte Carlo (KMC) simulations. Analysis of the STM data for these cases has already led to predictions about the microscopic mechanisms of surface mass transport and to quantitative determination of the kink formation energy. From the observed evolution of the step profiles, values of key macroscopic parameters such as diffusivity and step stiffness have also been obtained. We find that our atomistic calculations provide results in excellent agreement with experiments. However, there are some limitations of this type of KMC models using limited information of atomistic processes based on a set of bond counting rules.

To facilitate unbiased modeling of material properties, a novel way of performing KMC simulations is presented. In this approach the lists of diffusion processes are automatically collected during the simulation using a saddle-point search method in the potential energy

landscape. Here we employ a pattern recognition scheme that allows efficient storage and subsequent retrieval of information from a database of diffusion processes, their paths and their activation energy barriers. This technique is thus efficient and reliable. The removal of redundancies and repetitions in the calculations of energetics of system dynamics speeds up the simulations by several orders of magnitude making it feasible for a range of applications. Since the generation of the database and its future usage through recognition patterns is akin to the simulation procedure learning from itself, we call this method self learning KMC (SLKMC). Using this method the diffusion and coalescence of two-dimensional Cu and Ag adatom islands on Cu(111) and Ag(111) are studied.

Further, to determine the microscopic factors that control the diffusion of small Cu islands on Cu(111) in an unbiased manner, SLKMC simulations of diffusion of small islands (up to 10 atoms) are carried out. Results obtained from these simulations in which atoms hop from one fcc hollow site to another are compared with those obtained from a parallel set of simulations in which the database is supplemented by processes revealed in complementary molecular dynamics simulations at 500 K. They include processes involving the hcp stacking-fault sites, which facilitate concerted motion of the islands involving simultaneous motion of all atoms in the island. A significant difference in the scaling of the effective diffusion barriers with island size is observed in the two cases. In particular, the presence of concerted island motion leads to an almost linear increase in the effective diffusion barrier with size, while its absence accounts for strong size-dependent oscillations and anomalous behavior for trimers and heptamers. We also identify and discuss in detail the key microscopic processes responsible for the diffusion and examine the frequencies of their occurrence, as a function of island size and substrate temperature.

These studies are also extended to the case of Ag island (up to 100 atoms) diffusion on Ag(111) surfaces in comparison with Cu island diffusion. Because of the inherent differences in the microscopic processes responsible for the diffusion and its scaling behavior with size, the discussion is naturally bifurcated into those for the larger islands, usually containing more than 10 atoms, and the smaller ones ($N < 10$). For the larger islands, a very important study of diffusion on metal surfaces was done by Voter [7]. He showed that the diffusion

coefficients obeys a scaling law [7] $D \propto \exp(-E_{eff}/k_B T) N^{-\alpha}$. The diffusion coefficients of large islands appear to scale as a function of the size and the scaling exponent is expected to reflect the intervening atomistic processes responsible for the diffusion [16, 17]. For larger islands short-range diffusion of the atoms around the periphery, followed by adjustment of island shape, has been proposed to be the dominant mechanism for the diffusion [18, 19]. In such cases, elastic continuum modeling methods lead to a scaling exponent $\alpha = 3/2$ [7]. However, this scaling law may not be valid for small island diffusion for which collective motion may overwhelm periphery diffusion. Our KMC studies complement the validity of the scaling law only in the case of the larger (> 13 atoms) Cu and Ag island diffusion. During the simulations, a variety of multiple and single atom processes are revealed. The size dependence of the diffusion coefficients and effective diffusion barriers are calculated. From the tabulated frequencies of events found in the simulation, we show a crossover from diffusion due to the collective motion of the island to a regime in which the island diffuses through the periphery dominated mass transport. This crossover occurs for island sizes of 8 to 11 atoms. For islands containing 19 to 100 atoms the scaling exponent is to be approximately 3/2, which is in good agreement with previous work. The diffusion of islands containing 2 to 10 atoms can be explained primarily on the basis of a linear increase of the barrier for the collective motion with the size of the island.

This dissertation is organized as follows. Chapter 2 contains a few details of theoretical techniques employed for the atomistic studies of surfaces. Some of the experimental techniques used for detecting and characterizing surface diffusion are summarized in Chapter 3. The focus in Chapter 4 is on the processes and energetics for adatom descent from Ag islands on Ag (111) and on their respective diffusion prefactors. Details of spatial and temporal step edge fluctuations on Cu vicinal surfaces using KMC method are given in Chapter 5, whereas Chapter 6 is devoted for the description of self learning kinetic Monte Carlo methods. Chapter 7 and 8 provide a detailed study of small and large island diffusion based on all possible atomistic jump processes (*i.e.*, single atom jump, multiple atom jump, and collective island motion). Finally, the conclusion of the whole dissertation is presented in Chapter 9.

CHAPTER II

THEORETICAL TECHNIQUES

In this chapter we present some details of theoretical techniques used for atomistics studies of post deposition morphological evolution of metal surfaces. The first step towards any atomistics modeling is based on a reliable procedure that can determine the total energy of the system using robust forms of interatomic potentials. The dynamical and spatial evolution of the system at different length and time scales can next be studied by employing techniques like Molecular Dynamics (MD) and kinetic Monte Carlo (KMC). Phenomenon occurring at long time (seconds/minutes) and length (nanometer) scales can adequately be simulated using kinetic Monte Carlo methods. To perform such simulations, a detailed information of the system energetics including activation energy barriers, diffusion paths, and the potential energy surface is needed, which can then be mapped out using standard techniques such as the Nudged Elastic Band (NEB) method [27], the Drag/Grid method, etc. These methods are presented in the following sections.

2.1 Methods for Determining the Total Energy

Theoretical methods for the calculation of total energy of any atomic system are available in a large variety. Their spectrum varies from first principle electronic structure calculations to methods based on empirical or semi-empirical model potentials. Although there are lots of methods available for the first principles or *ab initio* calculations already known to physicists and chemists, for structural and dynamical studies of metal surfaces the density functional theory (DFT) [20] method is being used by our group.

2.1.1 The Density Functional Theory Method

In Density Functional Theory (DFT) method, quantum mechanical equations are solved for the system electrons in the presence of ion cores. The ion cores are allowed to relax to their minimum of energy position, corresponding to 0 K, through calculations of the

forces that act on them. Calculations of quantities like the total potential energy of the structure, equilibrium configurations of surface atoms (which are generally different from the bulk terminated ones), surface stress and surface energy are then performed with the ion cores at the minimum energy configuration corresponding to 0 K. These calculations are accurate and provide good insight into the electronic structural changes at surfaces that manifest themselves in a variety of forms. First principles electronic structure calculations have received further boost in the recent past [3] with the introduction of new schemes [21] for obtaining solutions to the following Kohn-Sham equations for the total energy of the system.

$$\left(-\frac{\hbar^2}{2m}\nabla^2 + V_H(r) + V_{xc}(r) + V_{ext}(r)\right)\psi_i = \varepsilon_i\psi_i \quad (1)$$

where V_H is the Hartree potential, V_{xc} is the exchange-correlation potential, and V_{ext} is the external potential containing the effect of the nuclei on the electron of the system. And $n(r)$, the ground-state electron density is defined as:

$$n(r) = \sum_{i=1}^N \theta(\mu - \varepsilon_i) |\psi_i|^2 \quad (2)$$

where μ is the chemical potential, and $\theta(\mu - \varepsilon_i)$ is the step function ensuring that all ψ_i with $\mu > \varepsilon_i$ are occupied and those with $\mu < \varepsilon_i$ are empty.

$$E = \sum_{i=1}^N \varepsilon_i + E_{XC}[n(r)] - \int V_{XC}(r)n(r)d^3r - \frac{1}{2} \int \frac{n(r)n(r')}{|r-r'|}d^3rd^3r' \quad (3)$$

The set of Kohn-Sham equations is solved self-consistently following a standard procedure in which an initial educated guess of the density $n(r)$ is made. Then $n(r)$ is used to build the potential, $V_{eff}(r) = V_H(r) + V_{xc}(r) + V_{ext}(r)$. This effective potential is used to solve Eq. 1 for ψ_i and ε_i . The new density $n(r)$ is then constructed from Eq. 2. Using this new density, a new effective potential is developed to solve Eq. 1. This process is repeated until $n(r)$ becomes almost constant. Finally, Eq. 3 is used to calculate the total energy for the ground state charge density.

This theoretical model has a predictive power because it does not require any fitting

parameters. This virtue makes it desirable for exploring the structure and the dynamics at any solid surface. Presently, in this method there are few problems of technical and conceptual nature. These issues keep this method away from its broad applicability. So different techniques for the simulation of surface diffusion processes will have to rely on model interaction potentials until such *ab initio* methods become more feasible for realistic length and time scales.

Because of these genuine reasons, a class of many body interatomic potentials is being used to solve a variety of problems during the past few decades. These potentials have already provided a good deal of information on the microscopic properties of fcc metals and their surfaces. They have also been tested successfully by comparison with experimental data. In our work we used the same kind of potentials based on the embedded atom method (EAM) [4], developed by Foiles, Baskes, and Daw.

2.1.2 EAM Interaction Potentials

The Embedded Atom Method (EAM) is based on a formulation that provides us many-body semi-empirical potentials. These potentials have been quite successful for describing the energetics of diffusion processes of Cu and Ag on surfaces [22, 23]. According to this method the ground state of an interacting electron gas can be defined as a functional of the total electron charge density [20]. Hence the energy E of an impurity in a host can be represented as a functional $F_{z,R}(\rho_h)$ of the unperturbed host electron density $\rho_h(R)$. In the functional $F_{z,R}(\rho_h)$, R is the position of the impurity in the host and Z is the type of the impurity. In this method each atom of the system is considered as an impurity atom embedded in the host. So the energy of an atom can be represented as follows:

$$E_i = F_i(\rho_i(R_i)) + \frac{1}{2} \sum_j \varphi(R_{ij}) \quad (4)$$

where φ is a short range electrostatic pair potential between atom i and j , which is a function of R_{ij} (the distance between atoms i and j). The electron density of the host ρ_i can be represented as a superposition of functions f_j representing the electron density of

any atom j as a function of R_{ij} .

$$\rho_i = \sum_{j \neq i} f_j(R_{ij}), \quad (5)$$

Therefore, the total energy of the system can be calculated by taking a sum over all atoms, which is given by

$$E_{tot} = \sum_i F_i(\rho_i(R_i)) + \frac{1}{2} \sum_{i,j} \varphi(R_{ij}). \quad (6)$$

For the six fcc metals Ni, Pd, Pt, Cu, Ag and Au, and their alloys, these potentials have done an excellent job of reproducing many of the observed properties of the bulk and surface systems. There are also several other realistic many-body potentials available [24]. Our choice of EAM is based mostly on familiarity and easy access rather than a technical or philosophical difference with the others.

Using these potentials for a model system representing surface or bulk, the steepest descent or conjugate gradient methods [25] are used for energy minimization in order to relax the system to the 0 K equilibrium configuration.

2.2 Methods for Simulating Morphological Evolution of Surfaces

The hierarchy of models for simulating spatial and temporal morphological evolution of surfaces ranges from atomic to macroscopic scales. To deal with a system having only a few thousand atoms, molecular dynamics or molecular static methods are applied with potentials based on *ab-initio* or EAM. On the other hand, Kinetic Monte-Carlo simulations are applied to study the systems evolving at large time/length scales or macroscopic level. The information obtained at the atomic level (energy barriers, and pre-factors) is used in Kinetic Monte-Carlo simulations. We present below some details of these methods.

2.2.1 Molecular Dynamics Methods

In the molecular dynamics (MD) technique classical equations of motion, for atoms interacting with a known interatomic potential, are solved numerically using a suitable algorithm. The basic form of these classical equations are given below:

$$\begin{aligned}
m_i \ddot{\mathbf{r}}_i &= \mathbf{f}_i = -\nabla_{\mathbf{r}_i} V \\
\dot{\mathbf{p}}_i &= \mathbf{f}_i = -\nabla_{\mathbf{r}_i} V \\
\dot{\mathbf{r}}_i &= \frac{\mathbf{p}_i}{m_i}
\end{aligned}
\tag{7}$$

The MD cell generally consists of a few thousand atoms arranged in ten to twenty layers. The minimum size of the cell depends on the nature of the dynamical property that one is interested in investigating. For atomistic simulations of surfaces, periodic boundary conditions are applied in the two directions parallel to the surface while no such constraint is imposed in the direction normal to the surface. It is essential to assign initial velocities to the atoms. This can be done by randomly selecting velocities from a Maxwell-Boltzmann distribution at the temperature of interest:

$$p(v_{ix}) = \left(\frac{m_i}{2\pi k_B T} \right)^{\frac{1}{2}} \exp \left[-\frac{1}{2} \frac{m_i v_{ix}^2}{k_B T} \right]
\tag{8}$$

This equation provides the probability that an atom i of mass m_i has a velocity component v_{ix} in the x direction at a temperature T . A Maxwell Boltzmann distribution is a Gaussian distribution, which can be generated using a random number generator. The initial velocities are always adjusted in such a way that the total momentum of the system is zero.

An algorithm like a Predictor-Corrector method [29] with a time-step of 10^{-15} s is then used to solve Newton's equations for all the atoms in the MD cell. Its general idea is as follows: given the atomic positions, velocities, and other dynamics information at time t , we try to obtain the positions, velocities, etc. at a later time $t + \delta t$, to a required degree of accuracy. The equations are solved on a step-by-step basis; the choice of the time interval δt will depend somewhat on the method of solution, but δt will be significantly smaller than the typical time taken for an atom to travel its own length.

For the continuous classical trajectory, an estimate of the positions, velocities, and accelerations at time $t + \delta t$ can be obtained by using Taylor expansion about time t ;

$$\begin{aligned}
\mathbf{r}^p(t + \delta t) &= \mathbf{r}(t) + \delta t \mathbf{v}(t) + \frac{1}{2} \delta t^2 \mathbf{a}(t) + \dots & (9) \\
\mathbf{v}^p(t + \delta t) &= \mathbf{v}(t) + \delta t \mathbf{a}(t) + \dots \\
\mathbf{a}^p(t + \delta t) &= \mathbf{a}(t) + \dots
\end{aligned}$$

Left hand sides of the above set of equations represent “predicted” values. These values need to be “corrected” afterwards. In these equations, \mathbf{r} and \mathbf{v} represent positions and velocities, whereas acceleration is denoted by \mathbf{a} . These equations may not generate correct trajectories as time advances if we do not introduce the equations of motion. Therefore, it is necessary to use equations of motion to remove any possible error in calculated quantities at $t + \delta t$. We can calculate the forces at time $t + \delta t$ using new positions \mathbf{r}^p , and from these forces the “correct” accelerations $\mathbf{a}^c(t + \delta t)$ can be easily found. By comparing the corrected values of accelerations with the predicted ones, we can estimate the size of the error:

$$\Delta \mathbf{a}(t + \delta t) = \mathbf{a}^c(t + \delta t) - \mathbf{a}^p(t + \delta t) \quad (10)$$

This error is then substituted into the corrector step,

$$\begin{aligned}
\mathbf{r}^c(t + \delta t) &= \mathbf{r}^p(t + \delta t) + c_0 \Delta \mathbf{a}(t + \delta t) & (11) \\
\mathbf{v}^c(t + \delta t) &= \mathbf{v}^p(t + \delta t) + c_1 \Delta \mathbf{a}(t + \delta t) \\
\mathbf{a}^c(t + \delta t) &= \mathbf{a}^p(t + \delta t) + c_2 \Delta \mathbf{a}(t + \delta t)
\end{aligned}$$

where the $\mathbf{r}^c(t + \delta t)$ and $\mathbf{v}^c(t + \delta t)$ are better approximations to the true positions and velocities. The best choice for the coefficients c_0, c_1, c_2, \dots is discussed in detail in Gear’s work [30]. This choice is related to issues like optimum stability and accuracy of the trajectories. The predictor step provides an initial guess, which in principle does not have to be a very good one since the successive corrector iterations should then converge rapidly onto the correct answer. The general scheme of MD simulation can be summarized as follows:

1. Using current values of the positions, velocities, and accelerations, predict their values at later time $t + \delta t$;
2. From the new positions, evaluate the forces, and hence acceleration $a_i = f_i/m_i$;
3. Using new accelerations, correct the predicted positions, velocities, and accelerations;
4. Check if the system is ready for the accumulation of time averages, if not then return to step 1, if yes then move to the next step;
5. Calculate variables of interest, such as total energy, lattice constants, and any order parameters;

These MD simulations can also be performed under conditions of constant temperature and constant pressure (NVT). A simple way to control the temperature is to multiply the velocities at each time step by a factor $\lambda = \sqrt{T_{des}/T_{act}}$ where T_{des} is the desired temperature and T_{act} is the actual temperature. For NVT simulations, the system of interest is first equilibrated under conditions of constant volume and constant temperature. In the next step, the system is allowed to evolve in a much longer run of a few nano seconds, with its energy maintained as constant (microcanonical ensemble). Similarly, a simulation for constant pressure canonical ensemble NPT can also be performed. The pressure can be maintained at a constant value by scaling the volume [29]. The rate of change of pressure can be described as:

$$\frac{dP(t)}{dt} = \frac{1}{\tau} (P_{bath} - P(t)) \quad (12)$$

where τ is the coupling constant, P_{bath} is the pressure of the "bath," and $P(t)$ is the actual pressure at time t . The volume of the simulation box is scaled by a factor λ , which is equivalent to scaling the atomic coordinates by a factor $\lambda^{1/3}$. We have $\lambda = 1 - \kappa \frac{\delta t}{\tau} (P - P_{bath})$, where κ is the isothermal compressibility.

Statistics on the positions and velocities of the atoms are recorded. Structural and dynamical properties of the system can now be obtained from appropriate correlation functions involving atomic positions and velocities. If forces are calculated from *ab initio* methods, MD simulations are capable of providing details of all atomistic processes on surfaces. However, as we have already noted, it would take a lot of computer time to span length scales

from 10^{-15} s to 10^{-3} s or more. It will also generate more data than one can absorb and unless creative methods are developed for extracting important information from the pile, it is not clear how viable this technique will be for developing an understanding of material properties from microscopic considerations.

2.2.2 The Kinetic Monte Carlo Technique

The main ingredient of any KMC technique comes from the rates of various possible processes. These rates are provided to KMC codes as an input. If this input of processes and their associated energetics is complete and reasonable then KMC simulations can be performed for the time scales as in real experiments. Few examples of such atomistic processes leading the system to surface diffusion, evolution, and growth are shown in Fig. 3. These include adsorption (a), followed by the diffusion of the atom (called adatom) on the terrace (b), or its nucleation (c), or the attachment of an adatom to an existing island (d), or the reverse process of an adatom detachment from an existing island (e). In the same way we have few more processes such as the adatom diffuses along a step edge (f), or down the step (g), or nucleates on top of an island (h) [31]. The diffusion of the dimer (i), as well as, that of clusters with larger number of atoms, may proceed with significant rates as compared to other single processes [32].

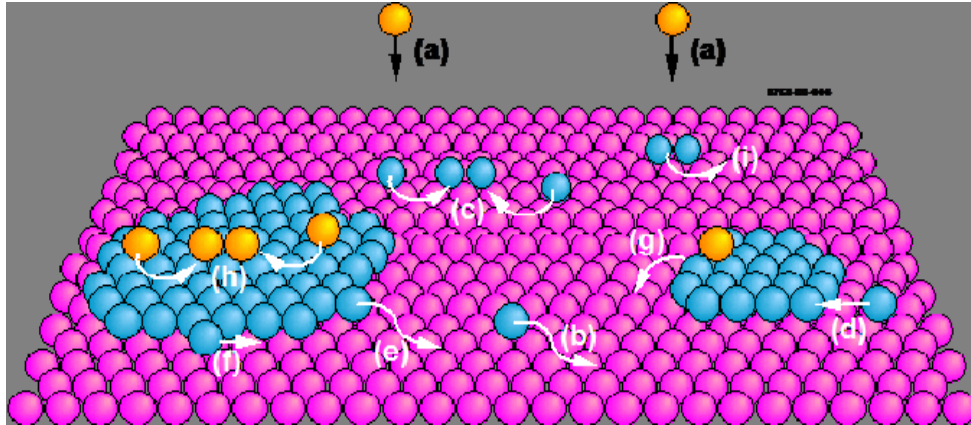


Figure 3: Some atomic processes involved in epitaxial growth

Since the methods of producing a complete set of all possible processes are very complex, standard KMC simulations are generally based on a list of only a few processes. However, in

these simple KMC simulations a large number of processes are ignored. In some cases, such processes and their energetics are included using some approximations or so called bond counting formulas. In this regard, several efforts have recently been made to overcome this problem, in particular in the work of Henkelman and Jonsson [33]. For this purpose, we also developed our own self-learning KMC technique and code. Details of the self-learning method are discussed in another chapter. Here we discuss only about the general scheme of KMC.

As we mentioned above, the first step is a tabulation of all possible diffusion pathways, and the probabilities (or rates). For a given mechanism the diffusion rate is invariably obtained by making use of transition state theory. This theory is based on an assumption that a process happens following the minimum energy path in the potential energy surface through a well defined saddle point. Therefore, the diffusion rate for process ‘ i ’ is then defined by using a Boltzmann factor as given in the following expression:

$$D_i = D_{0i} \exp(-\Delta E_i/k_B T) \quad (13)$$

where ΔE_i is the activation energy for the process, k_B is the Boltzmann constant, T is temperature, and D_{0i} is the so-called pre-exponential or prefactor for the particular process. The above equation leads to the well known Arrhenius behavior. Hence, the modeling of surface morphology using KMC is based on the knowledge of processes/mechanisms by which surfaces undergo spatial and temporal changes. The hopping of an adatom from one site to the next is an example of such mechanism. These processes may be more complex. For example motion of the whole island through hopping of multiple atoms or diffusion of entities via exchange of atoms between layers. Once diffusion mechanism and its path are known, the activation energy barrier can easily be obtained. The activation barrier can be defined as the difference of the total energy of the system at the saddle and basin points along the path, as shown in Fig. 4.

To calculate the probability of any possible event, the numerical values of the total rate and the macroscopic rates are required. Say, for the process i , there are n_i adatoms entities capable of performing the same process in the whole system. The macroscopic rate of such

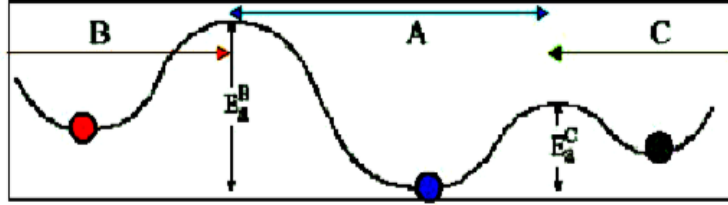


Figure 4: Illustration of energy profile with saddle and equilibrium points

a process can simply be written as $R_i = n_i D_i$, where D_i is the diffusion rate from Eq. 13. The total rate R of the system is then a sum over all possible events:

$$R = \sum_i R_i \quad (14)$$

In these simulations, the time forwards according to the rates of events occurring at each KMC step. The time step is generally considered as the reciprocal of the total rate. At each step in KMC simulations, the acceptance of the chosen event is always set to one. The probability of the event is then calculated by its relative rate $P_i = R_i/R$. Further in KMC simulations, a probability distribution is constructed. Finally, the Bortz-Kalos-Lebowitz (BKL) algorithm [6] is used for the random selection of events. A typical flowchart of a KMC simulation applied to fcc(100) is shown in Fig. 5, whereas the flowchart for fcc(111) will be described later under another chapter.

2.2.2.1 The Bortz-Kalos-Lebowitz (BKL) Algorithm

Binary Tree Search A binary search tree is shown in Fig. 6. The transition rates associated with each site in the lattice fill the lowest level nodes of the binary tree. In other words, each node of the tree in the lowest level contains a numerical value representing the rate P_i associated with a particular site in the lattice. Every parent node in the tree has two children. Each parent node is assigned by a numerical value which is the sum of their two children nodes. The node on the top of the tree is called the parent of the whole tree, which contains the total rate of the system. The binary search method needs only one random number from $\xi[0, 1[$. In the first step, the random number is multiplied by the total rate

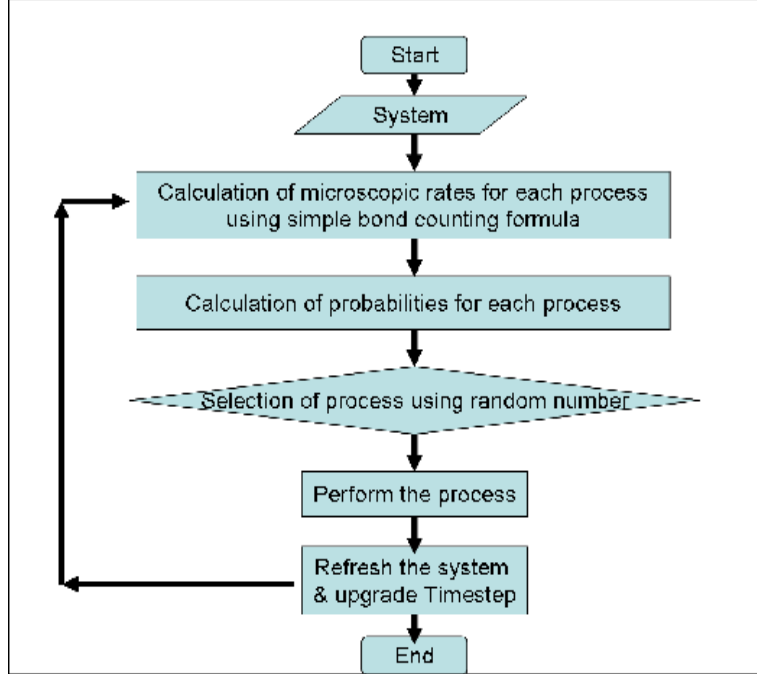


Figure 5: Flowchart of KMC code used for (100) surfaces

R_{tot} . Next, this new value of the total rate is compared to one of the children nodes. If this number turns out to be smaller than the child node (under examination) then that child node is selected. Otherwise, the other child node is selected. To get the new numerical value of the total rate, the rate of the unselected child is subtracted from the old value of the total rate. This process goes on until it gets to the child in the lowest level of the tree. Since each child in the lowest level of the tree defines a particular atomistic process in the lattice, that particular processes is performed according to the rate of the selected child in the lowest level of the tree.

Linear Search This search method is based on a conditional and cumulative probability operation. First, the normalized probabilities of all processes, occurring during the simulation, are calculated. In the next step, the interval (0 to 1) is divided into slices in such a way that the width of each slice corresponds to the numerical value of the normalized probability of each process. Finally, a random number is selected from $\xi[0, 1[$. The process P_n is picked up if the numerical value of the random number falls between P_n and P_{n-1} .

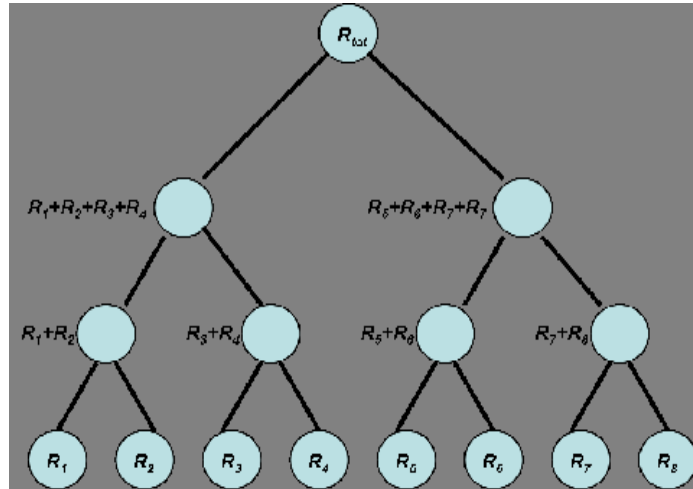


Figure 6: Binary tree structure for selection of transition in the BKL Monte method.

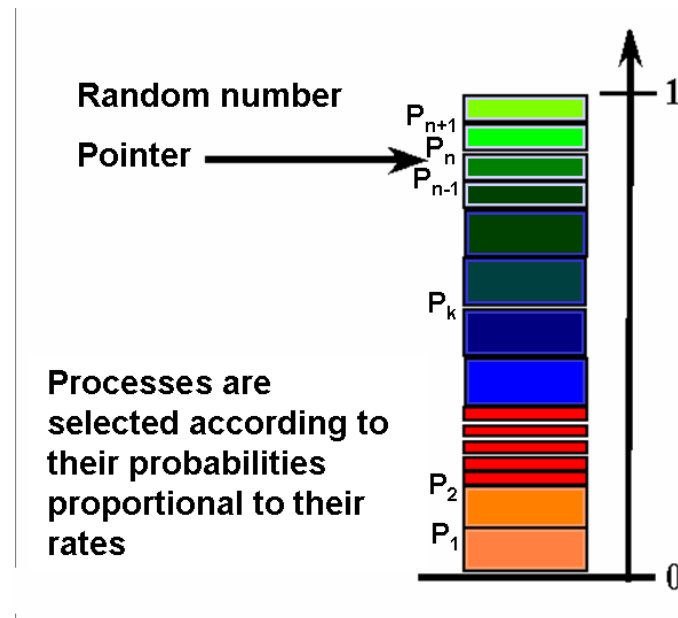


Figure 7: Linear search method.

2.3 Determination of Diffusion Prefactors, Paths, and Energy Barriers

2.3.1 Diffusion Prefactors

The task for determining the diffusion prefactors is not so simple and trivial. One way of defining the prefactors are taking the ratio of the products of system's normal mode frequencies when system entities are at basin (minimum energy point) and saddle point [34]. According to Vineyard *et. al.*, it can be written as:

$$D_{oi} = \frac{\prod_{n=1,N} \nu_n^{b_a \sin}}{\prod_{n=1,N-1} \nu_n^{saddle}} \quad (15)$$

Since the denominator of the above equation has one less vibrational mode as compared to the numerator, D_{oi} can be expressed in units of frequency. It is often approximated by a value equivalent to that of a normal mode that is about 10^{12} or 10^{13} s⁻¹. Alternatively, the prefactor can also be derived from the vibrational partition function. In this case, the diffusion prefactor can be shown by using the following expression:

$$D_{oi} = (k_B T/h)(nl^2/2\alpha) \exp(\Delta S_{vib}/k_B) \exp(-\Delta U_{vib}/k_B T) \quad (16)$$

In this equation, ΔS_{vib} is the change in the vibrational entropy of the system when its diffusing entities are at saddle point, whereas ΔU_{vib} is the change in the vibrational internal energy of the system when its diffusing entities are at the minimum energy points. Also, h is the Planck's constant, l is the length of the jump, n the number of sites available for the jump, and α is the dimensionality of the system. According to Kurpick *et al.* [35, 36], the diffusion prefactors can easily be calculated in case of single crystal surface. The thermodynamical quantities, S_{vib} and U_{vib} , used in the above equation can be obtained by calculating vibrational density of states using standard lattice dynamical methods or MD simulations.

$$\begin{aligned}
U_{vib} &= k_B T \int_0^\infty N(\nu) \left(\frac{1}{2}x + \frac{x}{e^x - 1} \right) d\nu, \\
S_{vib} &= k_B T \int_0^\infty N(\nu) \left(-\ln(1 - e^{-x}) + \frac{x}{e^x - 1} \right) d\nu,
\end{aligned}
\tag{17}$$

In this set of equations, $x = h\nu/k_B T$, whereas $N(\nu)$ is the vibrational density of states that may be expanded as $N(\nu) = \sum_l n_l(\nu)$, where $n_l(\nu)$ is the local density of states (LDOS) of atoms in layer l . Sometimes we get strange numerical values for diffusion prefactors. It is mainly because of the abnormal behavior of the vibrational density of states. Fixing this problem is very tricky and tedious. Therefore, we generally take some constant numerical value representing the prefactor in our simulation. However, considering the same prefactor for all processes is obviously a questionable assumption.

2.3.2 Diffusion Paths and Energy Barriers from the Nudged Elastic Band Method

The Nudge Elastic Band (NEB) method [27] is one of the most reliable, efficient and well tested methods for saddle point search along the diffusion path. To initiate the saddle point search using NEB, initial and final configurations of the system should be known and well defined. Therefore, a method or automatic computational technique is highly desirable, in conjunction with NEB, to determine the final state of the system. In this regard, we have combined the NEB method with a simple technique called Spherical Repulsion [26]. So this whole procedure of locating the saddle point and calculating the energy barrier takes place in two stages. First, a repulsive potential is used in such a way that the diffusing entity can escape from a particular minimum energy state and go to next neighboring minimum energy state. This helps in determining the final states of the systems. Second, the general NEB scheme is used to determine diffusion path between initial and final states. In this section, our main focus is on the NEB method, whereas some details of the spherical repulsion method are given in the next sub-section.

In NEB, the minimum energy path (MEP) is mapped out by constructing an arbitrary set of images between the initial and final states. A simple spring interaction potential is introduced to connect all adjacent stages or images with each other, see Fig. 8. This

connection between images represents an elastic band. Thus, the total force acting on an image can be defined as the sum of the spring force along the local tangent and the true force perpendicular to the local tangent [27]:

$$\mathbf{F}(i) = \mathbf{F}_i^s + \nabla V(\mathbf{R}_i) \quad (18)$$

where V is the potential energy of the system as a function of \mathbf{R}_i (the set of atomic coordinates). The spring force \mathbf{F}_i^s can be defined as:

$$\mathbf{F}_i^s = k_{i+1}(\mathbf{R}_{i+1} - \mathbf{R}_i) - k_i(\mathbf{R}_i - \mathbf{R}_{i-1}) \quad (19)$$

where k is the spring constant. Finally, the images are brought to the MEP by simply using a standard minimization procedure for the force acting on these images. To obtain the set of initial images in NEB, a standard interpolating procedure can be used between initial and final states. However, this may lead to some instability. This problem can easily be resolved by moving to the final state in the presence of a repulsive potential[31].

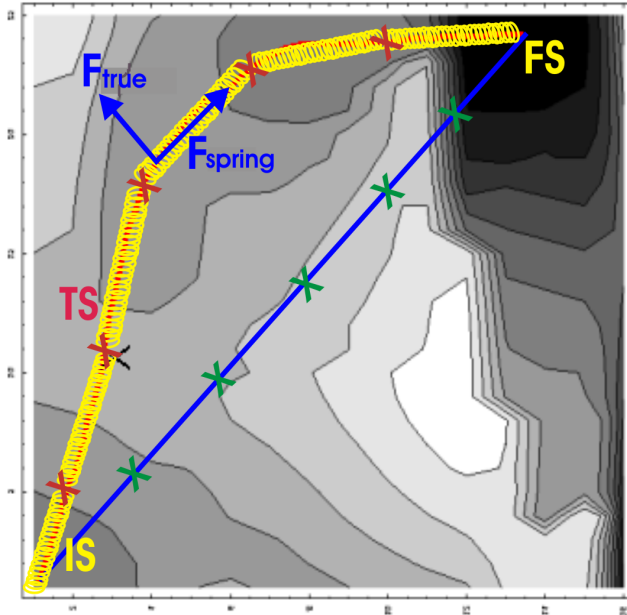


Figure 8: Nudged Elastic Band method, images connected via elastic bands.

2.3.3 Estimation of Final States from the Spherical Repulsion Method

This method is based on modifying locally the potential energy surface by using a spherical repulsive potential in such a way that it makes the specific minimum energy state unstable and leaves the neighboring energy minima unchanged. Further procedure of total energy minimization automatically causes the system to undergo the possible transition. This whole Procedure can be divided into the following steps:

- 1) The initial configuration of the system is prepared and then its total energy is minimized using any standard energy minimization technique.
- 2) Diffusing entity is then slightly displaced in the direction of the nearest available minimum energy state.
- 3) A localized repulsive potential is added to the Hamiltonian of the system as shown in Fig. 9. This may be represented by following expression:

$$U_{tot}(x) = U(x) + U_{rep}(x) \tag{20}$$

where

$$U_{rep}(x) = Ae^{-\alpha(x-x_0)^2}$$

where x_0 represents the coordinates of the initial state [26].

- 4) Further minimization of the total energy lets the diffusing entity fall into a next neighboring state (final).

Different forms of the repulsive potentials and different variations in the initial displacements help to explore a range of final states. To keep the final state unperturbed and maintain the accuracy, the repulsive potential should be sufficiently localized around the initial state.

2.3.4 Energy Barriers from the Drag Method

The NEB method is computationally expensive, but reliable and accurate in terms of calculating diffusion barriers. To make the process fast for calculating energy barrier, we

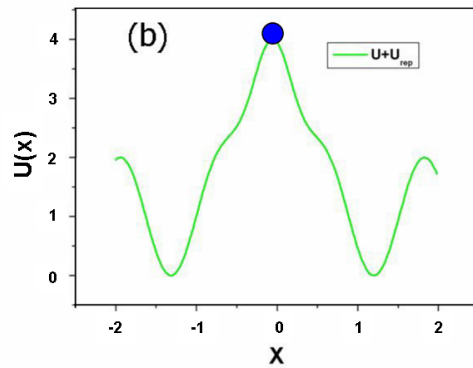
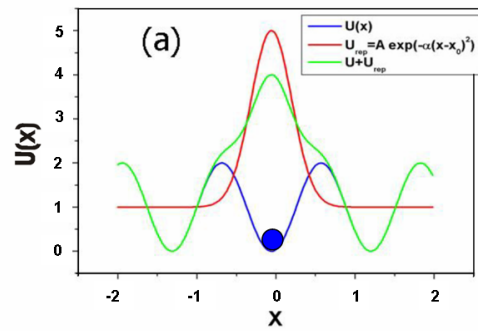


Figure 9: a) A repulsive potential is added in potential to make it biased, b) final shape of total potential. Reference: Oleg Trushin et. al., 2002.

recently developed the drag method, which is implemented in our newly developed “self-learning KMC” code [32]. Generally, in the drag method, the diffusing atom is forced to move to its adjacent vacant site in small steps. At each step the diffusing atom is allowed to relax in the plane perpendicular to the direction of motion, while all other atoms are free to move in any direction. Since the neighboring adatoms are free to follow the diffusing atom, this simple procedure is capable of discovering multiple atom motion mechanisms.

A good guess of the reaction coordinates is highly desirable in order to make this method perform correctly. Thus, it may yield to an unphysical reaction path if the true reaction coordinates lie sizably away from the guess.

In our studies of island diffusion, which we will discuss later in another chapter, the drag method was found to be good enough in order to reproduce the activation energy barriers that were obtained from the more sophisticated methods like NEB. The drag method can be improved by the introduction of a high resolution grid over which the calculations of the energy barriers are done. Such high resolution grid may be able to discover diffusion paths that are inaccessible in a simple drag method. Few details of the grid method are discussed in the next section.

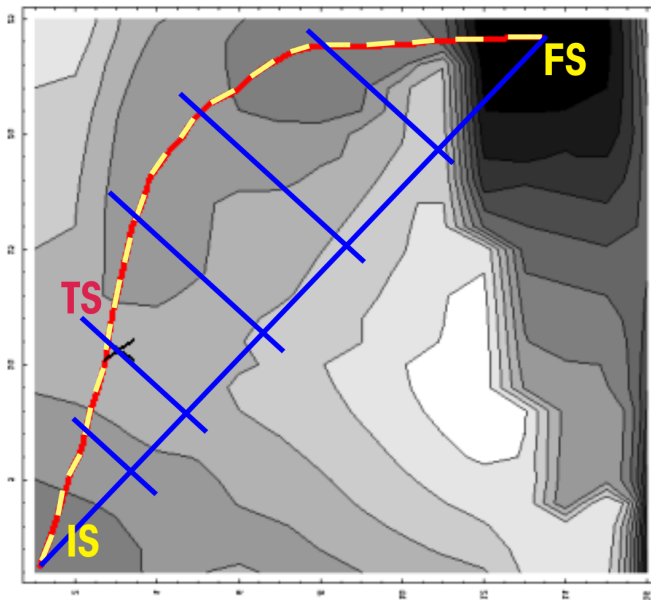


Figure 10: Illustration of Drag method

2.3.5 The Grid Method

To discover complex multi-atom processes and their energetics, a combination of a fine grid and traditional drag method may serve as another powerful tool. To explain this method, we consider the case of a descending adatom from a four-atom island on a fcc(111) surface [28]. This system of Ag atoms is described by EAM potentials in our work. In this particular scenario the Ag adatom prefers to diffuse by exchanging its position with a neighboring Ag atom, rather than by hopping to another site [28]. The adatom ends up forming a step with either a (100) or a (111)-microfacet (Fig.11a) through exchange with one of the four atoms of the island. To determine the diffusion path and energy barrier, the total energy of the constrained system is calculated by placing the exchanged atom at all points on the grid and allowing the other atoms to relax. The exchanged atom is only allowed to relax in perpendicular direction to the surface. The data of the total energy of the system calculated at all grid points is then used to create a contour plot showing the minimum energy path with saddle point and basin. The grid and minimum energy paths with their corresponding energy barriers are shown in Fig. 11b. The presence of a metastable state is noticeable in the lower part of the grid. In this case, the exchange process occurs through the hcp metastable site. This metastable site can not be detected by using simple drag method.

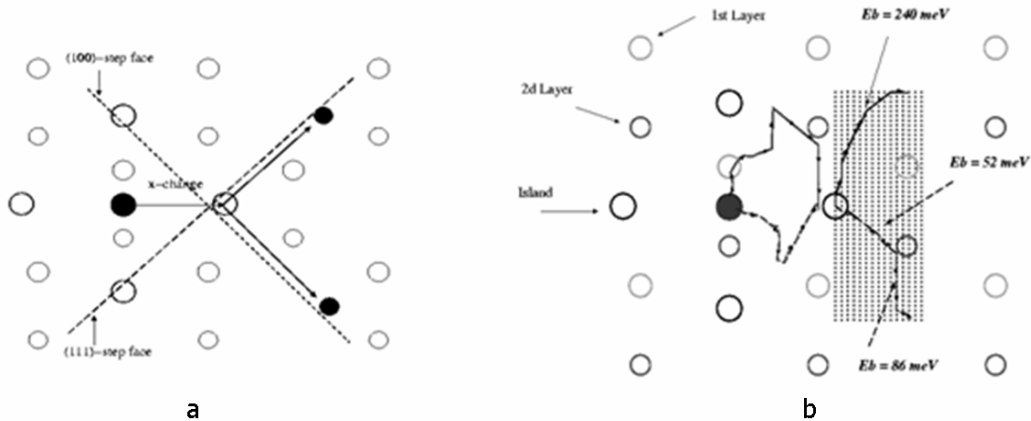


Figure 11: Adatom decent from a small island: a) two possible scenarios; b) their paths and their energies.

CHAPTER III

EXPERIMENTAL METHODS

In this chapter, some experimental techniques for examining surface diffusion are summarized.

3.1 The Scanning Tunneling Microscopy

Scanning tunneling microscopy is a technique developed by Gerd Binnig and Heinrich Rohrer at IBM in 1981[1, 2]. It allows imaging solid surfaces with a resolution having no previous example in history. Its operation is based on the so-called tunneling current. When its tip approaches a conducting surface at a distance of approximately one nanometer the tunneling current starts to flow. The tip is controlled by a piezoelectric tube. This tube permits a tiny movement of the tip by applying a voltage at its electrodes. The electronic feedback system of the STM controls the tip position in such a way that the tunneling current and the tip-surface distance can be kept constant. At the same time it scans a small area of the sample surface. Therefore, the surface topographical image of the sample is recorded and displayed.[37].

STM images also depend on the electronic density of states of the sample. Another factor of tip and sample interaction is also involved in the scanning process. These interactions are not still understood. Metal surfaces look very flat to an STM, which can cause a problem during the process of scanning such surfaces. This is because of the apparent height of individual atoms (corrugation). This height is approximately 1/100 to 1/10 of an atomic diameter. To handle this problem, the distance between the tip and the sample must be kept constant within 1/100 of an atomic diameter in order to resolve individual atoms. This means that the STM should itself be very rigid and it should be kept in isolation, away from environmental vibrations.

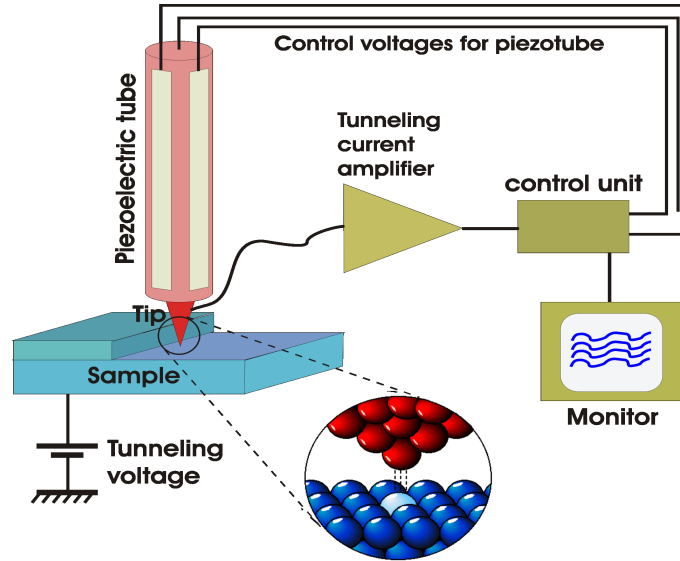


Figure 12: Scanning tunnelling microscope

3.2 *Field Ion Microscopy*

A field ion microscope uses a high electric field to form gas ions. This electric field is applied to the fine needle shaped specimen tip [37]. A strong inhomogeneous field accelerates ions. These accelerated ions form an enlarged direct projection of the surface on the screen. The gas ions can be kept on the field trajectories by keeping the specimen tip at a very low temperature. Using this technique, the atomic resolution can be obtained. Surface atoms can be ionized and desorbed as positive ions by increasing the electric field further above a critical value. This process of field desorption can be used for the following purposes: 1) cleaning the surface, 2) layer by layer removal of surface atoms for studying the sample into depth, 3) analytical study of layer by layer mass spectrometry of atoms.

The combination of the FIM with a time-of-flight mass spectrometer is called atom probe (AP). The chemical nature of the species can be mapped out in two and three dimensions using AP. The FIM also allows the investigation of lattice defects in pure metal crystals and alloys with atomic resolution.

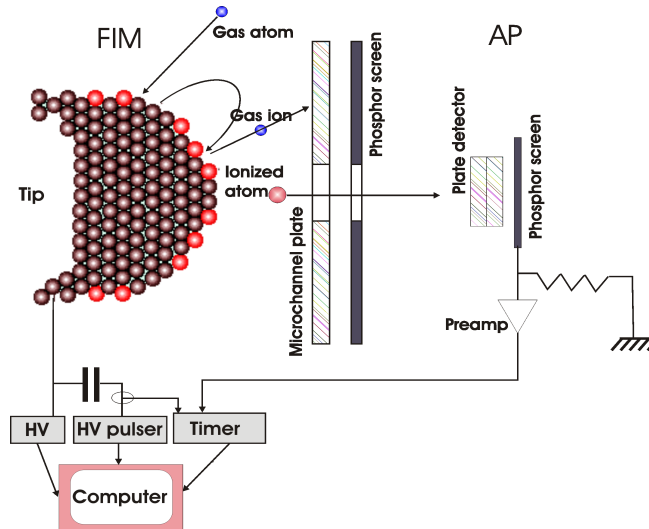


Figure 13: Field ion microscope

3.3 Low Energy Electron Diffraction

Low-energy electrons are used to probe surfaces in a similar way as x-rays are used to probe bulk [38]. This is because of the short mean free path of low energy electrons in surfaces and the electron de Broglie wavelength fits very well with the typical distances in crystals. Therefore we can easily observe diffraction phenomena.

LEED has two major applications. The first application is to study the surface diffraction pattern. In this regard, direct information about surface order and geometry can be obtained easily. The LEED system can also uncover the information of symmetry and periodicity of buried surfaces under adsorbates. Its second application is related to the quantitative structure determination. For the quantitative analysis, the diffraction intensities are measured as a function of the incidence electron energy. This data is then compared to multiple-scattering calculations for a model system. The process of comparison goes on continuously in a loop until a good agreement between calculations and experimental intensities is found. LEED is still known as the most powerful tool for the quantitative surface analysis.

A typical LEED apparatus is shown in Fig. 14. This system is composed of two main parts, 1) an electron gun that produces monochromatic electrons and 2) a detector for

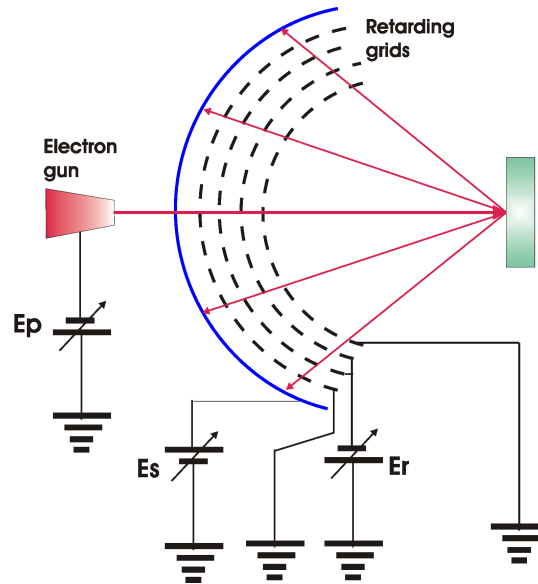


Figure 14: Low energy electron diffraction system

only the elastically scattered electrons. The detector is composed of four metal grids and a fluorescent screen. These grids in the detector are kept at different voltages. In order to provide a field free region around the sample, the closest grid to the sample is kept at ground potential. The next two grids are connected to the retarding voltage. To repel all inelastically scattered electrons, the voltage on the next two grids is kept slightly lower than the kinetic energy of the electrons coming from the gun. The next grid, connected to ground voltage, lets the elastically scattered electrons pass through it. Then these electrons are accelerated towards the fluorescent screen because of its high positive potential. LEED patterns are directly observed through the window behind the screen.

CHAPTER IV

PATHS, BARRIERS, AND PREFACTORS FOR ADATOM DESCENT FROM AG ISLANDS ON AG (111)

We have calculated the energetics and the dynamics for the diffusion of Ag adatoms that land on top of small two-dimensional Ag islands Ag (111), using realistic many-body interaction potentials. Purely energetic considerations of the descent of the adatoms from the island show an exchange mechanism to dominate over hopping and the process to favor the formation of (100)-microfaceted steps (A-type) over the (111)-microfaceted ones (B-type). Accompanying molecular dynamics simulations validate these findings at low temperatures, but show a reversal in the trend above room temperature making the formation of B-type step more probable. Calculations of the diffusion coefficient confirm that the pre-exponential factor for the processes leading to the formation of the A and B type steps are significantly different.

4.1 Introduction

The era of scanning tunneling microscopy (STM) has brought about a tremendous surge in the investigation of growth processes on metal surfaces. A variety of experimental studies of homo- and heteroepitaxy on the (100), (110 and (111) surfaces of several transition metals has led to interesting observations. Among these the case of homoepitaxial growth on fcc (111) surfaces has been particularly intriguing, since the innate geometry of the surface forces the steps formed by nucleating two-dimensional island, to take two types of configurations. Monoatomic closed-packed steps formed on this surface may have either a (100)-microfacet (A-type) or a (111)-microfacet (B-type). The relative abundance of one type of step over the other may thus lead to very distinct features in the growth patterns. Since the local structural, dynamical and electronic properties of these steps may be different from each other, it is not surprising that experimental observations of homoepitaxial growth

on several fcc (111) surfaces display very distinct characteristics. In the case of Pt (111), for example, the relative abundance of the A-type or the B-type steps depend on the surface temperature [12]. The case of Ir (111) is somewhat different and it may be argued that both types of steps are equally probable [39], although the issue is still debatable. Several theoretical papers have also addressed the issue of the relative energetics of the A and B type steps [40]. Theoretical calculations have also examined the energetics of various diffusion processes on fcc (111) surfaces [41],[42],[43]. The intricacies of the processes revealed by these studies have established the need for studying the details of the potential energy surface available to the diffusing atoms as accurately and as extensively as feasible. The object of our work here is to carry out an extensive study of the energetics of an initial stage of formation of steps on Ag (111) surfaces. For this purpose we have carried out an examination of the potential energy surface experienced by an adatom as it attempts to descend from a small two dimensional island of Ag atoms already nucleated on Ag (111). As we shall see, the investigation of the activation energy barriers and diffusion paths for these atoms in low coordinated sites allow us to make some general observations about homoepitaxial growth on fcc (111) surfaces. Since our aim is to predict the minimum energy path for the diffusion of the adatom, we have constructed a very fine grid for the calculation of the total energy of the system. As an *ab initio* calculation of this type would be formidable with the computational resources available to us, we have used reliable manybody interaction potentials from the embedded atom method for the purpose.

Another major undertaken in the present chapter is the examination of the characteristics of diffusion process as a function of the surface temperature. While most theoretical calculations of adatom diffusion focus their attention on the activation energy barriers and assume the diffusion prefactors to be ‘normal’ and the same for all relevant processes, we find no reasons to do so. In fact, we expect the potential energy surface to undergo modulations with temperature and the characteristics of surface vibrations to play a role in the diffusion process. We have thus carried out molecular dynamics (MD) simulations of the system of interest here for the temperature range 300K to 700K. Interestingly, our results show that predictions of diffusion coefficients made from considerations of surface energetics

alone are not enough to give us reliable results at finite temperatures. In particular, we show that diffusion pre-exponential factors for the formation of A and B type steps may differ significantly from each other.

In the next section we provide some details of the theoretical technique that we have used. This is followed by a presentation of the results and their discussion.

4.2 *Details of the Calculations*

For adsorbed two-dimensional islands on metal surfaces, the relaxation patterns near and around the corners may be quite complex [44], as a result of the low local atomic coordination and symmetry as compared to that on flat terraces. These complexities in atomic relaxations can also be expected to affect the potential energy surface in the vicinity of the islands and be reflected in the structural and dynamical phenomena at these sites. Of interest to the work here is the descent of adatoms that land on top of small two-dimensional islands on fcc (111) surface (see Fig. 15). To determine the diffusion path for the adatom accurately, we need to evaluate the potential energy surface near the corners and step edges accurately and reliably. With this in mind we have used a two dimensional drag/grid method for the purpose. According to this method, we minimize the total energy of a N-atom system by allowing $(3N-2)$ degrees of freedom to freely relax while holding 2 degrees of freedom of the atom involved in the diffusion process fixed. In the case studied here, these two degrees of freedom correspond to the x and y components contained in the surface plane. The grid used in these calculations consisting of 100×100 points allows a smooth representation of the full potential energy surface available to the adatom and an *a priori* determination of the diffusion paths. The usage of a sophisticated graphic applications package (XFARBE) further facilitates the extraction of the energy barriers and the minimum energy path for diffusion.

While we expect the calculated energy barriers to give us reliable predictions for the adatom diffusion paths at very low temperatures (at which the assumption of a static lattice is still valid), there is still the question of the relative values of the diffusion pre-exponential for the different competing processes. To check the validity of the method for

determination of diffusion paths at finite temperatures, we supplement the grid calculations with molecular dynamics simulations carried out for the temperature range 300K-700K, for the case of a Ag adatom descending on a small island on Ag (111). These simulations are done in a microcanonical ensemble in which the number of particles, the volume, and the total energy are conserved (NVE). these NVE runs were preceded by simulations in the canonical ensemble for which the number of particles, the volume, and the temperature are kept constant (NVT). This first step is essential to produce a thermalized system at the desired temperature. The molecular dynamics cell consists of 9 layers of fcc (111) with 144 atoms per layer, on top of which we place the 4-atom island and the adatom above it. The two bottom layers of the slab are kept rigid. Using a time step of 1.5 femtosecond, the (NVE) simulations were run until the adatom has diffused down.

To calculate the structure and the dynamics of the systems at hand we use interaction potentials based on the embedded atom method (EAM) [45] which, despite being empirical, have had success in predicting several surface properties of the fcc metals Ag, Cu, and Ni [45]. For example, surface relaxations [46], the dispersion of the surface phonons [47], the vibrational dynamics and thermodynamics of vicinal surfaces [48],[49], and also self diffusion [50] on these transition metal surfaces appear to be in reasonable agreement with experiments where available. We have used here the parameterization by Voter and Chen [51] in which experimental values of the bond length and the binding energy of the diatomic molecule are also included, in addition to several bulk properties, in extracting the interaction potentials. Energy minimization of the system were performed via the conjugated gradient method.

4.3 Results of Calculations of the Surface Energetics

We now turn to the descent of a Ag adatom from a small island on Ag (111). In Fig. 15 we depict the two possible scenarios when an adatom initially deposited on a 4-atom island descends via an exchange process involving one of the island atoms. Depending on which of the two available fcc sites the exchanged island atom will occupy, the long step edge (3 atoms) of the final 5-atoms island will be exhibit a (111) microfacet (B-type) or a (100)

microfacet (A-type), as indicated in the figure.

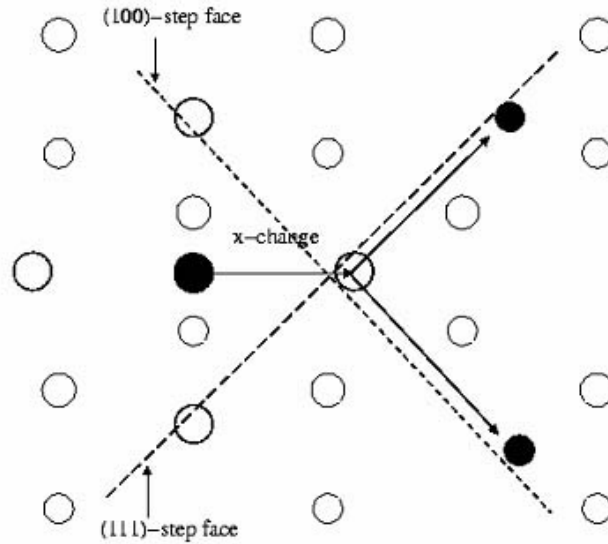


Figure 15: Formation of A or B type face via exchange mechanism.

The determination of the diffusion paths and energy activation barriers was done by calculating the total energy of the constrained system with the exchanged atom placed at all point on the grid and allowing all other atoms to relax, as described above. The grids used in these calculations, for the two scenarios by which the adatom could undergo a simple exchange process with one of the island atoms, are shown in Fig. 16. The collection of the total energy of the system evaluated with the exchanged atom at points of the grid are then used to create a contour plot from which one can extract the minimum energy paths, saddle points and the energy minima.

The relevant information obtained from the contour plots for the two possible exchange events is shown in Fig. 17. The top half of the figure concentrates on the minimum energy paths that would be taken by the adatom and the exchanged atom to eventually lead to the nucleation of a B-type step, while the bottom half illustrates the same for the formation of an A-type step. Quite clearly both sets of paths show concerted motions of the two atoms. Also, the energy at the saddle points (E_b) for the top set of minimum energy paths is higher than that for the bottom ones. This is very interesting because the main difference

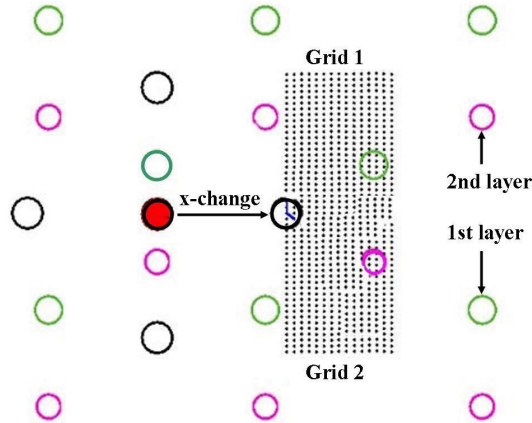


Figure 16: The grid

in the two sets of paths arises from the differences in the local environments because of the locations of atoms in the layer below. In order to land at the fcc site in the top half of the figure, the minimum energy path takes the exchanged atom to the vicinity of the hcp site. This hcp site falls also in the minimum energy path of the adatom itself as it proceeds to descend and exchange with the atom below. It is worth remembering that the potentials used here (EAM) are based on coordination and as a consequence every atom would tend to maximize its coordination at all times. Thus, the exchanged atom, en route to the fcc site, and the adatom both want to go to their final positions via the hcp site. This competition for the hcp site affects the total energy of the system and makes the process energetically unfavorable, as compared to the other possibility.

We turn now to the event in the bottom half of Fig. 17, which would lead to the formation of an A-type step. In this case we see that the exchanged atom, en route to the fcc site, finds an hcp site on the way. Since the adatom is always far away from this hcp site, there is no competition. Here the first saddle point is at an energy of 52meV , beyond which the system actually settles into an equilibrium state that is about 40meV lower than the initial one. Eventually, the exchanged atoms sees a second barrier of about

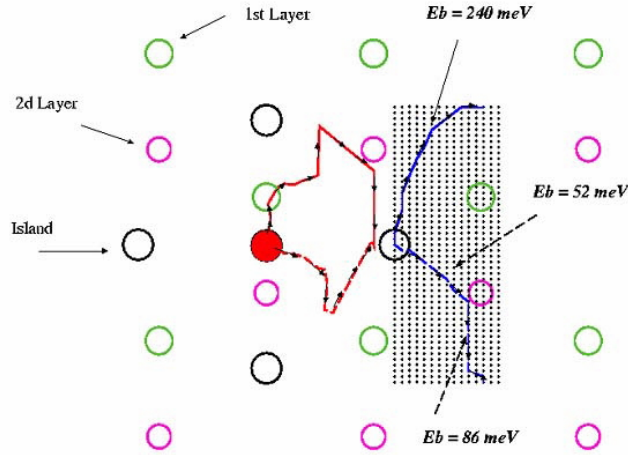


Figure 17: Diffusion paths and barriers

86meV which it has to overcome to make the A-step for this 5-atom flat island. Fig. 18 is a schematic representation of the energy levels for the two events, taking the total energy of the system to be zero when the adatom is on top of the 4-atom island (start 4+1). To follow the path to form a B-step, we encounter a saddle point with an energy of 240meV above the zero, while to form the A-step, one encounters first a saddle point of energy 52meV , then a minimum energy level that is lower than the starting one, and finally a saddle point 86meV above this minimum.

In summary, we have shown above that when an adatom descends from a small island via an exchange process on Ag(111), the atoms involved prefer to arrive at a final fcc site via an hcp site. If the two atoms compete for the same hcp site, the barrier to diffusion is higher than if there is no such competition. This argument is quite general and should be applicable to other fcc (111) surfaces for which local coordination dictates the local structure and dynamics. If it is further assumed that pre-exponential factors are irrelevant, and that activation barriers calculated for a static lattice control the diffusion process, the above arguments would predict the formation of an A-type step in this adatom descent. Further, from the simple calculation presented below, relative rates of formation of the A and B type steps, as a function of the surface temperature, could also be deciphered.

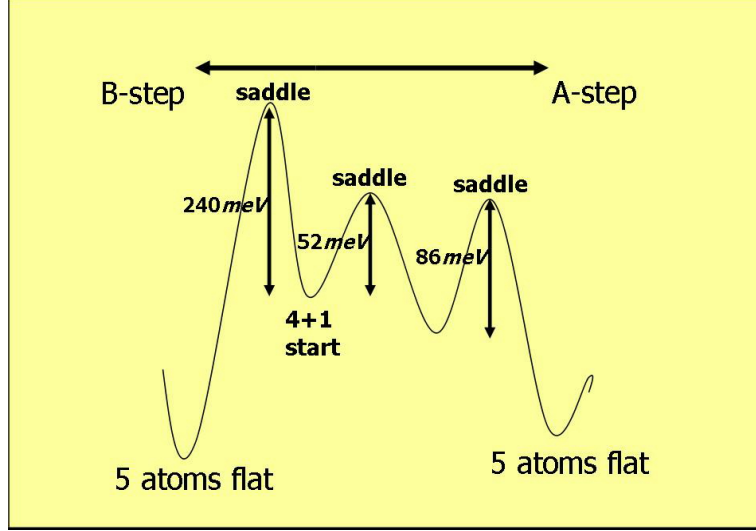


Figure 18: Schematics of the barrier energies

Assuming that the diffusion processes considered here follow an Arrhenius behavior, the diffusion coefficients, D_A , and D_B , to form the A and B type steps are, respectively, given by:

$$D_A = D_{oA} \exp(-E_{bA}/k_B T) \quad (21)$$

$$D_B = D_{oB} \exp(-E_{bB}/k_B T)$$

with E_{bA} and E_{bB} the activation energies to form A and B type step-edges, respectively, 86 and 240meV .

If we now make the usual assumption that both processes have the same pre-exponential factor (i.e., $D_{oA} = D_{oB}$), then, at 300 K, the ratio D_A/D_B is 473:1, in favor of the probability of formation of an A-type step. Even at 500 K, the formation of A-type is favored by a factor of 40.

4.4 Results of Molecular Dynamics Simulations

From the discussion in the previous section, one would expect the formation of A-type edges to be dominant at all temperatures when an adatom descends from a 4-atom island. To test this prediction, we have performed MD simulations of the system at 300, 500, and 700

K, collecting the statistics for each temperature for a large number of initial conditions.

Table 1 shows the number of simulations that ended up with an A-type edge and those that ended up with B-type. While this result is in qualitative agreement with predictions above from considerations of energetics for a static lattice, the probability of finding B-type steps is non-negligible. The situation changes dramatically when the temperature is increased to 500 K, at which 43 out of 81 simulations ended with a B-type edge. At 700 K, 58 out of 100 events resulted in A-type step edges. The probabilities (P) associated with these processes are listed in Table 2. The differences in the calculated ratios of the formation probability of the A and B type steps in Table 1, from the predictions in section 3, indicate that for Arrhenius behavior, the prefactors associated with the two processes cannot be the same.

In order to determine these prefactors, we have calculated the diffusion coefficient for the two processes leading to the formation of either A or B type step, from the descent time (or residence time of the adatom prior to the descent). Table 2 shows the average descent time for the 2 processes at 300, 500, and 700 K. This descent time (DT) is then used to get the frequency of the event and, hence, the diffusion coefficient using:

$$D = \nu\Gamma l^2/2\alpha \quad (22)$$

with l the distance traveled during the exchange process, Γ the frequency of the event, α the dimensionality (2 in this case), and ν the number of possibilities to form an A-type or B-type (2 in this case).

Table 3 shows the diffusion coefficient for the formation of an A-type and B-type edges at different temperatures. It shows that A-type is one order of magnitude more frequent than the B-type at 300 K and a dominance by B-type at 700 K with a crossing around 500 K.

In Fig. 19, we plot the log of these diffusion coefficients as function of $1/k_B T$. Both processes present an arrhenius behavior. This plot also allows us to extract the energy barriers and prefactors. For the formation of an A-type edge by adatom descent, we find an energy barrier of 197meV and prefactor of $3.28 \times 10^{-3}\text{cm}^2/\text{sec}$, while for the B-type

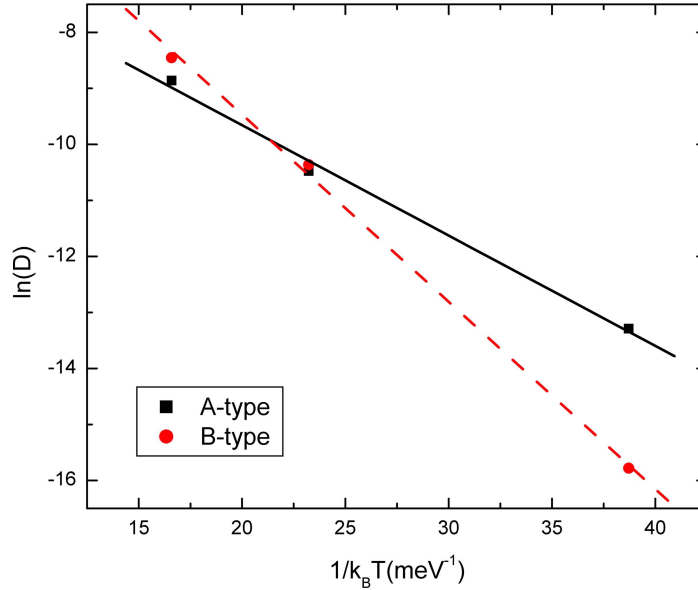


Figure 19: Arrhenius plot of the diffusion coefficient of processes leading to A and B type steps

step-edge the energy barrier is 335meV and the prefactor $6.35 \times 10^{-2}\text{cm}^2/\text{sec}$. Note that the barrier energies extracted from the Arrhenius plot representing the MD results at finite temperatures is about 100meV higher than those calculated with a static system using the grid method. This energy is higher than that associated with the phonons and may be related to frictional forces associated with the island rubbing the substrate. Further studies are needed before we can establish the exact reasons for the differences in the energy barriers in the static and the dynamic calculations. We also find that the prefactor associated with the formation of a B-type edge to be about 20 times larger than that associated with the formation of an A-type edge. This difference in the prefactor is responsible for the inversion in the preference from A-type step formation to B-type at temperatures above 300 K.

Temperature	Number of A-types	Number of B-types	Total
300 K	47	3	50
500 K	38	43	81
700 K	42	58	100

Table 1: M.D. statistics for 4+1 island

Temperature	DT for A-type	DT for B-type	P for A-type	P for B-type
300 K	250×10^{-12} sec	3000×10^{-12} sec	0.94	0.06
500 K	15×10^{-12} sec	13×10^{-12} sec	0.47	0.53
700 K	3×10^{-12} sec	2×10^{-12} sec	0.42	0.58

Table 2: Descending times (DT) and formation probabilities (FP) for A and B types

4.5 Conclusion

In this chapter we have examined the energetics and the dynamics of adatom descent from small two dimensional Ag islands on Ag (111). From considerations of the total energy of the system, we find exchange to be the dominant mechanism for the diffusion of the adatom. Through the usage of a fine computational grid that allows us to map out the potential energy surface in great detail, we find that the minimum energy path for the adatom exchange process is complex. In this coupled motion of the two atoms, both try to maximize their coordination by involving an hcp site in the minimum energy path to diffusion. As a result the process that would lead to the formation of B-type step becomes energetically unfavorable and the A-type step is expected to dominate the growth on this surface. On the other hand, our accompanying molecular dynamics simulations show that the probability of the formation of B-type steps is non-negligible at room temperature and significant at higher temperatures. In addition, these dynamical studies show that pre-exponential factors for the two diffusion processes differ by a factor of 20. These results call into question the application of solely energetic considerations in drawing conclusions about processes at finite temperatures.

Temperature	D for A-type cm^2/sec	D for B-type cm^2/sec
300 K	1.69×10^{-6}	1.40×10^{-7}
500 K	2.82×10^{-5}	3.25×10^{-5}
700 K	1.42×10^{-4}	2.13×10^{-4}

Table 3: Diffusion coefficients (D) for A and B types

CHAPTER V

FLUCTUATIONS OF SURFACE STEPS IN EQUILIBRIUM: A KINETIC MONTE CARLO STUDY

We study the spatial and temporal fluctuations of widely separated step edges on vicinal Cu(1,1,13) and Cu(1,1,19) surfaces using kinetic Monte Carlo simulations of a lattice-gas model, with Effective Medium Theory energy parametrization. By evaluating appropriate correlation functions, we extract the kink formation energy, step stiffness and the temporal dependence of fluctuations. Our results are in excellent agreement with those from continuum theory and experimental data, showing the validity of the atomistic processes used and highlighting the role of mass transport along step edges.

5.1 Introduction

For nanostructuring of materials and controlling epitaxial growth of thin films on substrates, a knowledge of the stability and atomistic quality of the surface is essential. This is particularly important for the case of vicinal surfaces with regular arrays of steps, which can be used, for example, for stabilizing a layer-by-layer Molecular Beam Epitaxy (MBE) growth mode, or for forming quasi-1D nanostructures, by decoration techniques [13]. The ubiquitous presence of steps on surfaces, in general, and the associated equilibrium roughening transitions of vicinal surfaces have been the subject of inquiry for a number of years [52]. However, it is only in the past decade that high quality scanning tunnelling microscopy (STM) measurements have revealed characteristics of microscopic fluctuations at step edges, their variations with time and temperature, and their atomistic nature [53, 15]. Of prime importance are the spatial and temporal autocorrelation functions whose specific power law behavior, and spatial dependence for edge fluctuations, have been thoroughly analyzed based on continuum theory [54, 55, 56]. Interpretation of experimental data in

the light of theory has provided information on energetics at stepped surfaces and possible atomistic processes relevant to them. For example, the spatial correlation function can be used to provide a measure of the kink formation energy and step-step interaction [57], while the time correlation function can be used to identify atomic diffusion processes, and their activation energies [15]. There are also a number of computer simulation studies on the time dependence of equilibrium step fluctuations based on simple models [53, 15] for step energetics and dynamics.

In this work we examine the step fluctuations in a lattice-gas model of regularly stepped Cu(1,1,2 n + 1) surfaces, using Monte Carlo (MC) simulations. Here $n + 1/2$ is the number of atoms across the terrace. This model has recently been used to study Cu adatom island diffusion in equilibrium [58], and the step edge instabilities of Cu(1,1,2 n + 1) surfaces under MBE growth conditions [59, 60], yielding good agreement with experimental data. Because of the availability of specific experimental data [14, 15], we concentrate here on the Cu(1 1 13) and Cu(1 1 19) surfaces both of which have well separated steps and to a first approximation step-step interaction may be ignored. Analysis of the STM data for these cases has already led to predictions about the microscopic mechanisms of surface mass transport and to quantitative determination of the kink formation energy. From the observed evolution of the step profiles, values of key macroscopic parameters such as diffusivity and step stiffness have also been obtained. From our atomistic model study, we also compute the spatial and temporal correlation functions and extract the corresponding relevant step parameters. We find that our atomistic calculations provide results in excellent agreement with experiments.

5.2 *The Model*

Our calculations for the stepped surfaces are based on Monte Carlo (MC) simulations in the framework of the lattice gas approach for fcc(1,1,2 n + 1) vicinal surfaces. Such surfaces consist of (001) terraces separated by the close-packed [110] step edges, as shown in Fig. 20. In the model, an adatom is allowed to hop into the nearest neighbor (NN) site. For the relevant hopping energies we use a parametrization based on the Effective Medium Theory (EMT) [24] for Cu(001) and its (1,1,2 n + 1) vicinal surfaces [61]. The EMT barriers

and their relative ordering are in good agreement with the available experimental data for copper [61, 15]. These barriers are also comparable to others from similar phenomenological methods, for example to those calculated by Mehl *et al.* [62] who used somewhat different interatomic potentials (the largest discrepancy between the barriers is about 0.1 eV). Our barriers from EMT follow a simple bond-counting rule where the hopping rate of an atom to a vacant NN site can be approximated by [61] $\nu = \nu_0 \exp\{-\beta [E_s - \min(0, \Delta_{NN})E_B]\}$, in which the attempt frequency $\nu_0 = 3.06 \times 10^{12} \text{ s}^{-1}$. Here E_s is the barrier for the jump of a single adatom on a flat surface and is equal to 0.399 eV. If there is at least one atom diagonally next to the saddle point, E_s reduces to 0.258 eV leading to fast diffusion along the close-packed step edges. The change in the bond number ($-3 < \Delta_{NN} < 3$) is the number of NN bonds in the final site minus the number of NN bonds in the initial site. Finally, the bond energy is given by $E_B = 0.260 \text{ eV}$. We note that this parametrization has been previously used to study adatom island diffusion on Cu(001) [58] and MBE growth on stepped Cu(1,1,2*n* + 1) surfaces [59, 60].

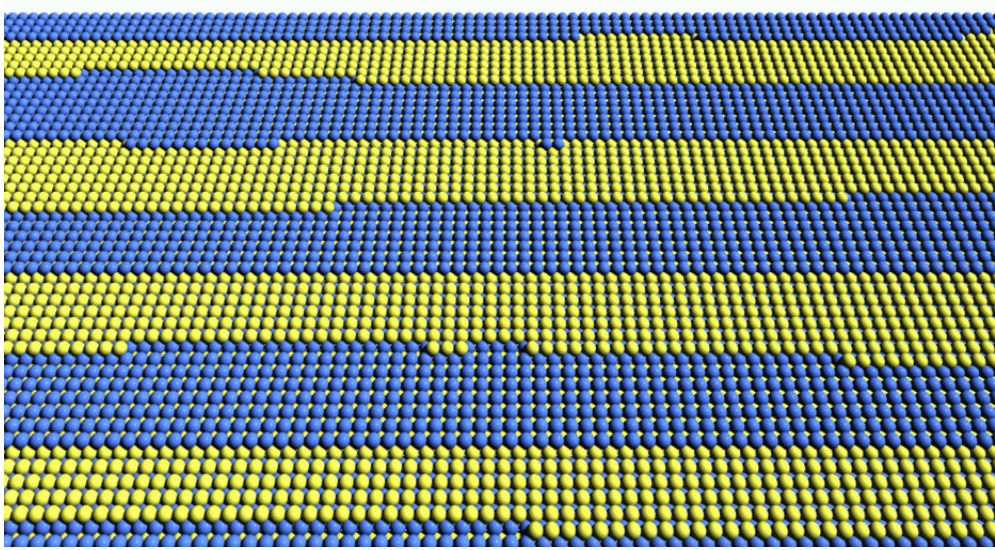


Figure 20: fcc (1 1 13) vicinal surface.

For the MC algorithm we have employed the Bortz-Kalos-Lebowitz (BKL) updating scheme [6], which allows one to reach fully macroscopic time scales that could be up to several seconds of real time scale around room temperature and which has also been used

in the previous works [58, 59]. Periodic boundary conditions were applied in the y direction along the steps and helical boundary conditions in the x direction across the steps. Each simulation was started by first generating rough step edge profiles using the correct Boltzmann probabilities for adatom placement and then equilibrating the profiles by letting the system evolve before starting to measure any observable. The equilibration times were checked by monitoring the saturation of the total transition rate in the system. Typically, such initial equilibration runs required in excess of 10^{-4} sec at $T = 400$ K. Specifically, in our case at $T = 300$ K the equilibration run is 10^{-3} sec long. We note that in analogy with the case of large adatom island diffusion [58], long equilibration runs are required to ensure correct and unbiased equilibrium ensemble averages from the MC simulations.

5.3 *Spatial correlations*

To extract information from microscopic processes it is convenient to use the spatial correlation function of the step profiles. From the Arrhenius behavior of the correlation function one can extract the value of the kink creation energy which is intimately related to the bond energy of the model. The relevant spatial correlation function here is defined as

$$G(y) = \langle [x(y) - x(0)]^2 \rangle, \quad (23)$$

where $x(y)$ is the step profile along the step direction y . The brackets denote a thermal average over (uncorrelated) measurements. The correlation function $G(y)$ measures the spatial fluctuation amplitude of a wandering step. If one assumes that the motion of a step position $x(y)$ can be described by a random walk process, it follows that $G(y)$ is a linear function of the distance y along the step:

$$G(y) = \frac{b^2}{a} y, \quad (24)$$

where b^2 is the mean square deviation of x , or the diffusivity [53] in the units of the lattice constant $a = 2.55 \text{ \AA}$ [54]. At low temperatures the diffusivity equals the (single) kink concentration P_k , from which the kink energy ϵ_k can be obtained as [64]

$$b^2 \approx P_k a^2 = 2 \exp(-\beta \epsilon_k) a^2, \quad (25)$$

with $\beta = 1/k_B T$. On the other hand, the true microscopic kink concentration can also be measured during the simulations by simply counting the number of kinks per unit length. This gives us a consistency check for the kink energy through Eqs. (24) and (25). We note that in our model the kink energy should be given simply by $\epsilon_k = E_B/2 = 0.13$ eV since creating two kinks by atom detachment from the kink site breaks one bond. The step edge stiffness [15] in terms of diffusivity is as follows:

$$\gamma = \frac{ak_B T}{b^2} \quad (26)$$

5.4 Temporal correlations

In addition to static spatial correlations one can also study the temporal correlations through the time-dependent step-step correlation function. This provides an independent way of extracting physical parameters from the simulations. The relevant temporal correlation function of the step profiles is defined as [15]

$$G(t) = \langle [x(y, t) - x(y, 0)]^2 \rangle, \quad (27)$$

This correlation function is expected to follow power law behavior in time, and the corresponding exponent depends on the dominant microscopic process for mass transport along the step edge. With the energetics in our model, diffusion along the close-packed step edges were found to dominate [59] which implies that [53, 15]

$$G(t) \approx 0.464 P_k^{3/4} \Gamma_h^{1/4} t^{1/4}, \quad (28)$$

where $\Gamma_h \propto \exp[-\beta(E_a + 3\epsilon)/4]$ [53] is the mobility along the step edge, and P_k is the kink concentration. Here E_a is the effective hopping barrier, along a kinked step edge, which is obtainable from the results of our simulations.

5.5 Results

Most of the MC simulations here were done on the Cu(1 1 13) and Cu(1 1 19) surfaces where the step separations are 16.58 Å and 24.20 Å, respectively. For such relatively widely separated steps we expect the individual step fluctuations to be almost independent and

elastic step-step interactions not to be important. Note that our lattice-gas model does not include such interactions. Also multi-site hops are not included in our simulations but only jumps to the nearest neighbor sites are allowed. The system size was $L_x \times L_y$, in which $L_x = 52 - 76$ atomic separations in the direction perpendicular to the step edge while $L_y = 1000$ atomic separations in the direction of the step edge. Hence a total of 8 steps were considered in this study. The temperature range studied was $T = 320 - 420$ K. With realistic energy parameters for Cu, the corresponding physical simulation times vary from 10^{-3} s up to 10 s depending on the temperature. In our simulations, a 1 s physical time is equivalent to 10^8 MCS at 320 K, while at higher temperatures such as 390 K, 1 s physical time is roughly equivalent to 1.5×10^{10} MCS.

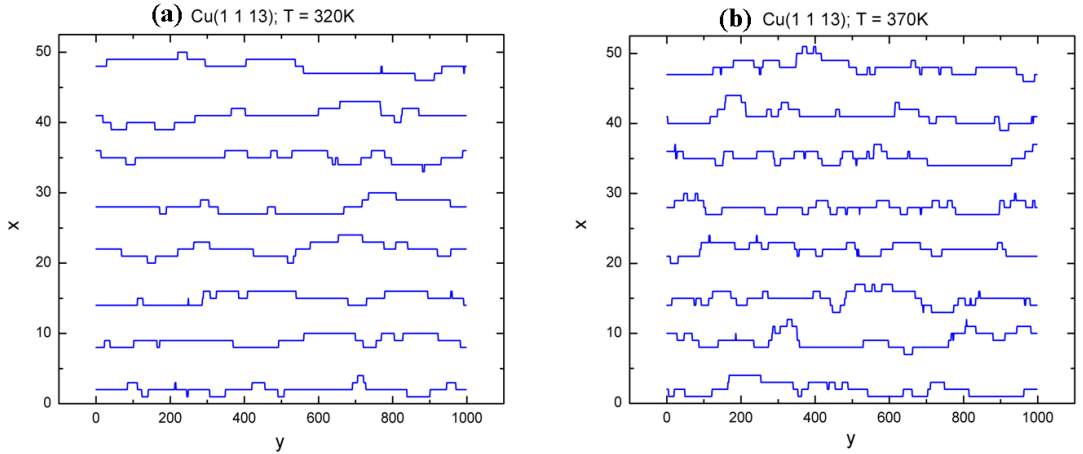


Figure 21: Equilibrium step profiles of the Cu (1,1,13) at (a) $T = 320$ K and (b) $T = 370$ K.

In Figs. 21 (a) and (b) we show typical equilibrium step profiles for the Cu(1,1,13) surface at temperatures $T = 320$ and 370 K. Even at the higher temperatures, there are relatively few kinks present and the correlation times between configurations are rather long, requiring extensive MC simulations. As expected, the profiles at 370 K show more structure than the ones at 320 K. Equilibrium step profiles shown in Figs. 21 (a) and (b) were obtained by extracting x and y positions of sites along the step edge.

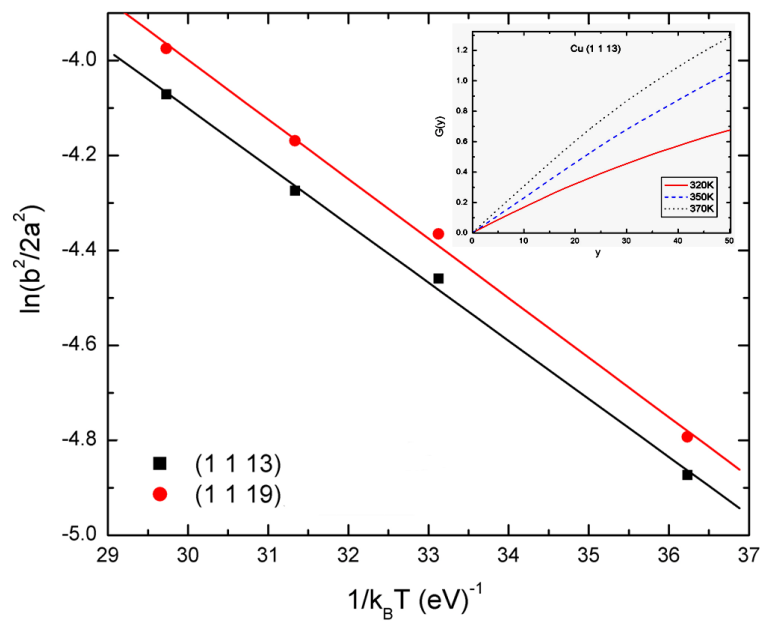


Figure 22: Arrhenius plot of the diffusivities for the Cu (1,1,13) and Cu (1,1,19). The inset displays a series of spatial correlation functions $G(y)$ at several temperatures for Cu (1,1,13).

Surface	T	Diffusivity/a	Diffusivity/a	Stiffness	Stiffness	Kink
Cu	K	(Theory)	(Exp.)[63]	Theory	(Exp.)[63]	Density
		Å	Å	eV/Å	eV/Å	
(1,1,19)	320	0.038	0.049	0.72	0.56	0.017
(1,1,19)	350	0.058	N.A	0.52	N.A	0.026
(1,1,19)	370	0.071	0.080	0.45	0.40	0.032
(1,1,19)	390	0.086	N.A	0.39	N.A	0.038
(1,1,13)	320	0.039	0.050	0.71	0.55	0.018
(1,1,13)	350	0.059	0.071	0.51	0.43	0.027
(1,1,13)	370	0.071	N.A.	0.45	N.A	0.034
(1,1,13)	390	0.087	N.A.	0.38	N.A	0.039

Table 4: Summary of step parameters for the Cu (100) vicinals

In Fig. 22 we show an Arrhenius plot of the diffusivities for the Cu(1,1,13) and Cu(1,1,19) surfaces. The inset displays a series of spatial correlation functions $G(y)$ at different temperatures for the Cu(1,1,13) case. Similar results were found for Cu(1,1,19). In each case, we find that $G(y)$ is well approximated by a linear function of y which allows us to extract the diffusivity parameter $b(T)$. The Arrhenius plot shows that the data are almost independent of the step width. Further, using Eq. 25 we find that the kink formation energies are $\epsilon_k = 123(1)$ meV and $127(1)$ meV for the Cu(1,1,13) and Cu(1,1,19) surfaces, respectively. We have also determined ϵ_k by directly calculating the kink densities at the corresponding temperatures, and obtain $121(3)$ meV and $125(1)$ meV for the two cases (see Table 4). All these results are in excellent agreement with the experimental value of $128(3)$ meV and also very close to the expected value of $E_B/2 = 130$ meV. Note that the kink formation energy obtained from EMT potentials is 107 meV [67], which is 16% smaller than that resulting from the present simulations. A summary of the simulation data and available experimental data is shown in Table 4.

Our calculated temporal correlation functions $G(t)$ are plotted in Fig. 23 on a log-log scale for Cu(1 1 13) at $T = 320, 350, 390, 420$ K. Solid lines in Fig. 23 are obtained by fitting Eq. 28 on the predicted form of the temporal correlation functions. It is clear from the figure that simulation data for $G(t)$ indeed approach the expected $t^{1/4}$ dependence at all temperatures when the simulation time is long enough. This can be also seen by

plotting the running exponent $d \log G / d \log t$ of $G(t)$ which saturates after the temperature-dependent relaxation time, and approaches its asymptotic value from above similar to the solid-on-solid model simulations of Szalma *et al.* [65]. The rate of approach towards the asymptotic behavior is strongly temperature dependent, and very long simulation times are needed at the lowest temperatures studied here. From numerical fits to the prefactor $\Gamma_h(T)$ we obtain that $\Gamma_h(T) \sim e^{-\beta E_t}$, with $E_t = 1.1(1)$ eV. This is again in excellent agreement with the expected result of $4E_B = 1.04$ eV from our model. Also from Arrhenius plots of Γ_h shown in Fig. 24 we have calculated E_a which is the effective hopping barrier along the step. For Cu(1,1,13), $E_a = 0.57(5)$ eV, while for Cu(1,1,19) we find $E_a = 0.49(5)$ eV. This is in very good agreement with the expected kink Ehrlich-Schwoebel barrier of 0.52 eV along the close-packed step edge [59].

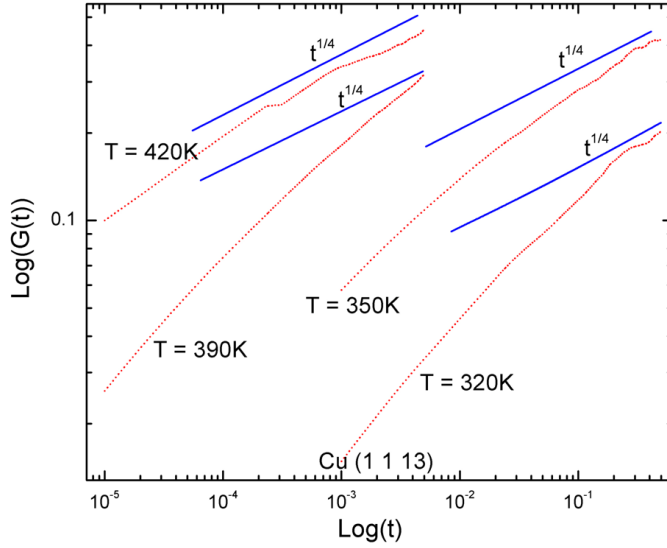


Figure 23: Temporal correlation functions $G(t)$ on a log-log scale for Cu(1,1,13). Solid lines are obtained by fitting the simulation data to Eq. 6.5.

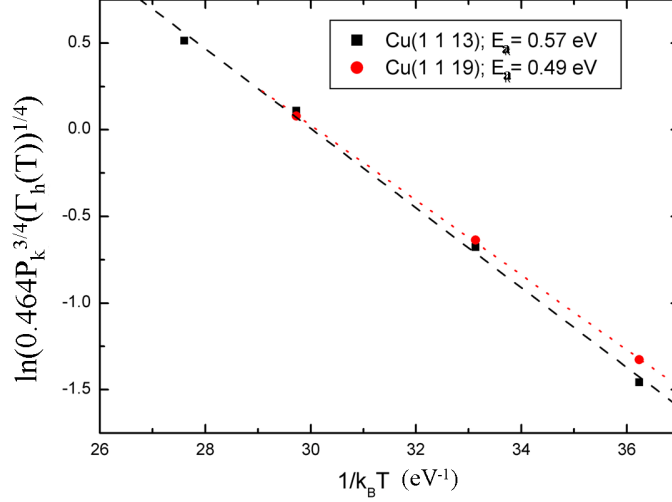


Figure 24: Arrhenius plots of Eq. 6.5 for the Cu(1,1,13) and Cu(1,1,19).

5.6 Summary and conclusions

In this chapter, we have studied the equilibrium step fluctuations of a lattice-gas model of vicinal Cu(1,1, m) surfaces. This model, which has been previously used to study adatom island diffusion and step edge instabilities under MBE growth, gives results which are in excellent agreement with available experimental data on the Cu(1,1,13) and Cu(1,1,19) surfaces [15]. Numerical results for both spatial and temporal correlation functions of the step positions are in quantitative agreement with both theoretical predictions and experimental data, demonstrating the role of mass transport along step edges and kink fluctuations for Cu(1,1, m) surfaces.

Finally, we note that while the results here are in excellent agreement with those from experimental observations and predictions of continuum model, there are some limitations of the present type of models. Solid-on-solid and Ising type of lattice models are unable to quantitatively reproduce the orientational dependence of the step stiffness [66]. Although this is not important for the simple kink excitations here, it demonstrates the importance of including more realistic interactions into the models of fluctuations in low-dimensional nanostructures.

CHAPTER VI

SELF-LEARNING KINETIC MONTE-CARLO METHOD: APPLICATION TO CU(111)

We present a novel way of performing kinetic Monte Carlo simulations that does not require an *a priori* list of diffusion processes and their associated energetics and reaction rates. Rather, at any time during the simulation, energetics for all possible (single or multi-atom) processes, within a specific interaction range, are either computed accurately using a saddle-point search procedure, or retrieved from a database in which previously encountered processes are stored. This self-learning procedure enhances the speed of the simulations along with a substantial gain in reliability because of the inclusion of many-particle processes. Accompanying results from the application of the method to the case of two-dimensional Cu adatom-cluster diffusion and coalescence on Cu(111) with detailed statistics of involved atomistic processes and contributing diffusion coefficients attest to the suitability of the method for the purpose.

6.1 Introduction

The past decade has witnessed a surge in research activities which aim at bridging the gap in length and time scales at which a range of interesting phenomena take place. Some examples of such activities pertain to studies of epitaxial growth, and nanostructuring of materials. The aim in such work is to utilize information obtained at the microscopic level to predict behavior at macroscopic scales. There are thus several key tasks to be undertaken, each of which is a challenge in itself. The first of these is an accurate determination of the energetics and dynamics of the system at the microscopic level. For selected systems this may be achieved through *ab initio* electronic structure calculations [68], which are becoming

increasingly feasible for complex systems, even though they remain computationally intensive. A reasonable alternative, albeit not as reliable or accurate, is the application of one of several genres of many body interatomic potentials [69]. With these interatomic potentials it has been possible to carry out computational and theoretical studies of a range of surface phenomena using techniques like molecular statics and molecular dynamics. Molecular dynamics simulations in particular are capable of revealing the essential details of microscopic phenomena as they unfold as a function of temperature, pressure and other global variables but the application is limited in time and length scales. Since most thermally activated atomistic processes occur in the range of picoseconds, they are best captured with time steps in femtoseconds which limits total simulation time to a few microseconds. These times are many orders of magnitude smaller than processes happening in the laboratory. For example, epitaxial growth and surface morphological changes take place in minutes and hours and are controlled by atomic processes that are infrequent compared to atomic vibrational times of picoseconds. The challenge in molecular dynamics simulations is to find reliable ways which capture infrequent processes and extend to longer time scales with reasonable computational resources.

An alternative to molecular dynamics simulations for examining surface phenomena is offered by the kinetic Monte-Carlo (KMC) technique in which the rates of various eligible atomic processes are provided as input [6, 70, 7]. If this input is accurate and complete, KMC simulations are in good position to mimic experiments. Since the task of accumulating a complete set of atomic processes is non-trivial, standard KMC simulations are typically performed with a set of most obvious simple atom or concerted processes as input, and all others either ignored or included in approximate ways (e-g bond counting models) or added in an *ad hoc* manner to fit experimental data. With a reduced set of barriers, activation energies become effective values rather than actual values, which may be compared with those obtained from experimental data but may not reveal the intervening microscopic processes. This is obviously problematic. Furthermore, it has been shown that novel multiple atom processes may play an important role in providing mass transport on surfaces such as Cu(100) [71, 72], and Ir(111) [73, 74]. Any realistic simulation should have a provision

for uncovering such processes and including their energetics in the evolution of the system.

To overcome these limitations of the two most common approaches for simulating temperature dependent morphological evolutions of surfaces and interfaces, several accelerated schemes have been presented in recent times [75, 76, 33]. In a set of studies, Voter *et al.*, [77] have concentrated on enhancing the time scales achievable in MD simulations through three different strategies: parallel-replica, temperature-accelerated dynamics and hyperdynamics. Fichthorn and co-workers, in related work, apply the bond boost method [78] to extend the time scales in their simulations. The basic principle in these methods is to make the system evolve faster, sampling a larger phase space, either through smartly connected parallel processors, or application of a boost so that the system can overcome energy barriers with relative ease, or by raising the temperature of the system. At the very least, novel and infrequent processes may be revealed through such accelerated schemes. The main issue is the assurance of one-to-one correspondence between the temporal evolution of the accelerated and non-accelerated systems and whether the approach actually leads to a large speed-up for a particular system of interest. The reader is referred to the original papers for further details and suitability of the techniques, to specific cases.

Another promising scheme has focussed on the completeness issue of KMC by allowing the system to evolve according to single and multiple atom processes of its choice. The key to the method is the generation of saddle points in the potential energy surface and benefits from the advances that Jonsson and co-workers [79, 80] have made in procedures for extracting diffusion paths and energy barriers using efficient search procedures. Once a large (sufficient) number of saddle points have been identified, the expectation is that the system will evolve naturally according to its inherent mechanisms. The method we propose here is, in principle, related to the latter approach, with a very important difference. We employ a pattern recognition scheme that allows efficient storage and subsequent retrieval of information from a database of diffusion processes, their paths and their activation energy barriers. The procedure presented here is thus efficient and reliable. The removal of redundancies and repetitions in the calculations of energetics of system dynamics speeds up the simulations by several orders of magnitude making it feasible for a range of applications.

Since the generation of the database and its future usage through recognition patterns is akin to the simulation procedure learning from itself, we call the technique proposed here self learning KMC (SLKMC). While the proposed technique can be applied to any surface systems, our interest is in the examination of atomistic phenomena as related to growth on fcc(111) surfaces. This is a challenging surface since the lack of surface corrugation makes the energy landscape relatively flat with a number of diffusion processes which are equally competitive. Some such atomistic processes may include those with multiatoms which are typically ignored in standard KMC techniques. In this chapter we focus our attention on some characteristics of the proposed technique and its application to homo-epitaxy on fcc(111) surfaces through considerations of the diffusion and coalescence of two dimensional Cu adatom islands on Cu(111).

6.2 Essentials of Self-Learning Kinetic Monte Carlo Method

Although the principle of the proposed technique is generally applicable, we need a specific surface geometry to illustrate its details. For reasons mentioned above our interest is homoepitaxy on fcc(111) surfaces. We provide in this section some details of the model system, together with an outline of the standard kinetic Monte Carlo method for completeness. This is followed by a summary of the pattern recognition and labeling scheme that we invoke to obtain a self-learning KMC methodology.

6.2.1 Model System

To mimic the fcc(111) surface we consider a 2-layer substrate, with periodic boundary conditions in the XY plane (which is parallel to the surface), to uniquely identify the fcc and hcp hollow sites on the surface. The system of interest (such as an adatom island, vacancy island, or any other nanostructure whose morphological evolution or diffusion is to be determined) is placed on top of the substrate. In this initial study only occupancy of fcc sites (i.e. hollow sites with no atom in the layer below) on the substrate is allowed. While there is experimental justification for assuming fcc-site occupancy for Cu adatoms on Cu(111)[82], we are aware that on Ir(111) atoms may also occupy hcp sites (hollow sites with an atom in the layer below) [18]. Infact, even for homoepitaxial growth on

Cu(111) under certain other experimental conditions hcp-site occupancy has been reported [83]. Furthermore, adatoms, dimers, and other smaller clusters may use the hcp site as an intermediate [81] one during its motion. The method we are proposing can easily be generalized to include hcp occupancy. We are also assuming that the diffusion is via hopping. This restriction can be removed in future work. For the moment our interest is in the in-plane (2D) motion of adatoms, vacancies and their clusters on Cu(111), for which diffusion is expected to proceed via hopping.

6.2.2 Some Ingredients of Kinetic Monte Carlo

The goal of kinetic Monte Carlo (KMC) is to mimic real experiments through sophisticated simulations. For these simulations to be realistic, one has to implement increasingly complex scenarios requiring intensive use of state-of-the-art software and hardware. At the heart of a KMC simulation of the time evolution of a given system lie the mechanisms that are responsible for determining the microscopic processes to be performed at any given time. To illustrate the point, consider a system containing N particles at a given time with N_e possible types of processes. Let us also associate with each process-type (i), n_i the number of particles in the system that are candidates for this process-type, the activation energy barrier ΔE_i and a pre-factor ν_i . The microscopic rate associated with process (i), within Transition State Theory (TST) [84], is then,

$$r_i = \nu_i \exp(-\Delta E_i/kT), \quad (29)$$

where k is the Boltzman constant, and T the surface temperature. The total rate R of the system is further given by

$$R = \sum_{i=1}^{N_e} R_i, \quad (30)$$

where $R_i = n_i r_i$ is the macroscopic rate associated with process-type i .

In KMC simulations, the acceptance of a chosen process is always set to one. However, the choice of a given process is dictated by the rates. First, a process-type is chosen

according to its probability $p_i = R_i/R$, and then a particle is randomly chosen from the set n_i to perform this process.

The essential elements of the KMC method are thus the processes 'i' and their activation energy barriers ΔE_i whose determination requires that availability of reliable interatomic interaction, which may be obtained from first principles or from model potentials. In this chapter, all activation energies are determined using the embedded atom method (EAM). This is a semi-empirical, many-body interaction potential [4]. Although the EAM potentials neglect the large gradient in the charge densities near the surface and use atomic charge density for solids, for the six fcc metals Ag, Au, Cu, Ni, Pd, and Pt, and their alloys, it has done a successful job of reproducing many of the characteristics of the bulk and the surface systems[4].

To get back to the issue of the determination of diffusion processes, their paths and their activation energy barriers, we should note that several interesting and appealing approaches have been proposed in the past few years. These methods include the nudged elastic band (NEB) method [79], the step and slide method [85], eigenvector following [86], and temperature accelerated MD [87]. Each of these methods has its own computational demand and measure of accuracy whose balance dictates the choice of the approach. For the studies presented in this chapter, we find the simple 'drag' method to be adequate, as we shall see. This is, of course, a rudimentary method in which the moving entity is dragged in very small steps towards a probable (aimed) final state. The dragged atoms is constrained in the direction towards the aimed position while the other two degrees of freedom (perpendicular to this direction) and all degrees of freedom of the rest of the atoms in the system are allowed to relax. The other atoms are thus free to participate in the move, thereby activating many-particle processes (when neighbor adatoms start to follow a central leading atom). In connection with SLKMC, the central atom is always dragged towards one of its vacant fcc site. A more general way to map out the potential energy surface is to use the grid method which, has been successful in finding non-trivial diffusion paths and saddle points [28].

6.2.3 Self Learning Kinetic Monte Carlo Method

As we have already mentioned, the limitation of standard KMC is its reliance on an *ad hoc* choice of processes and hence lack of completeness. For these reasons and also because of experimental observations of complex and unforeseen processes, the predictive power of KMC is in question. A rethinking of the way we perform KMC has become a necessity. Simulations with an a priori chosen catalogue of processes need to be replaced by a continuous identification of possible processes as the environment changes. For these innovations in the KMC procedure, the local environment is the key issue and its complexities need to be exploited. With this in mind we are proposing a methodology in which the base ingredient is the collection of local environments of undercoordinated atoms found automatically during the simulations and labeled and stored for subsequent usage in the simulation. As a concrete example of our approach we have chosen the fcc(111) surface with a six-fold symmetry. For simplicity, we assume that any process in this system will involve a central (undercoordinated) atom and atoms in the next 3-shells as illustrated in Fig. 25. The motif in Fig. 25 is to serve as a 'cookie cutter' and is placed on all active atoms in the system to define their local environment. We further assume, without loss of generality that any process may be described in terms of the central atom moving to a neighboring vacancy accompanied by the motion of any other atom or atoms in the 3 surrounding shells. The labeling of the surrounding atoms is done in binary and a base ten number is then associated with the first shell configuration. The same procedure is followed for atoms in the second and third shell. Hence, for an atom in the system to be active (i.e. central atom for a given process), it should have a vacancy in its first shell (or an occupancy number less than 63 for the cookie cutter); as illustrated in Fig. 25 (b).

Once the atoms are classified as active and non-active and encrypted within the 3-shell scheme, we proceed by determining all possible processes associated with every active atom. Next the determination of the activation energy and pre-factor is performed for all processes. Examples of how processes are labeled and stored in the database are given in Fig.26. In this figure, full circles represent occupied sites and open circles vacancy sites.

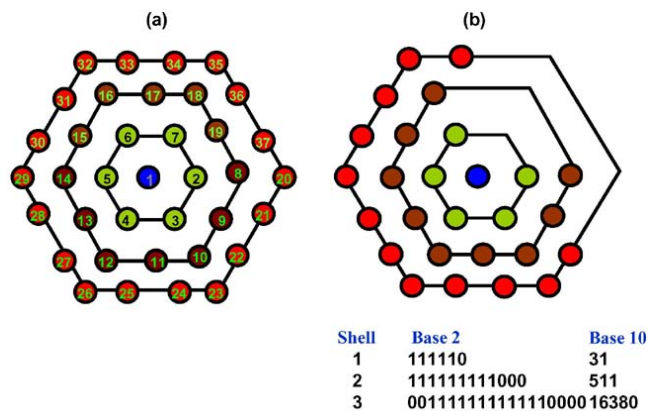


Figure 25: (a) The three-shell indexing around the central atom labeled 1; (b) signature of a particular 2D cluster configuration in base 2 and base 10

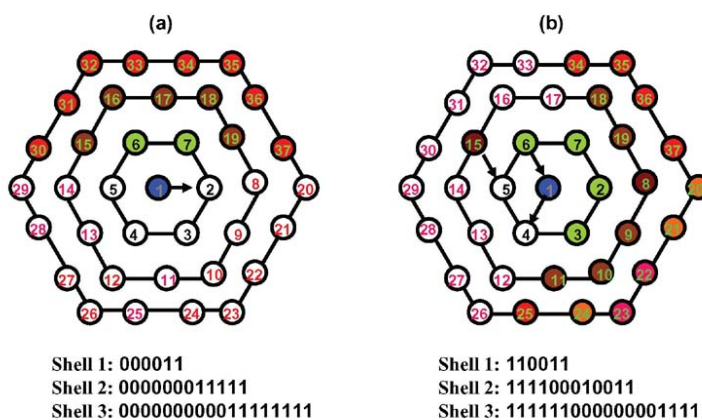


Figure 26: Sample (a) single-atom and (b) multiple-atom processes involved in the diffusion of 2D clusters presented with their specific labels for our database

Fig. 26 (a) illustrates the "diffusion along a step" process where the central atom labeled 1 moves to the vacant site 2 along the step formed by atoms numbered 30, 15, 6, 7, 19 and 37 in the cookie cutter. The initial configuration for this process is recorded in base 10 as (48,3968,261120) in the database and shown with the base 2 label in the figure. The move in Fig. 26 (a) is recorded as atoms 1 going to position 2 (1,2) and the activation energy barrier for the process in Fig. 26 (a) is found to be 0.31 eV. Similarly, for the multi-atom process illustrated in Fig. 26 (b), the initial configuration in base 10 is recorded along with the sequence of motion of atoms involved in the process which in this case is 1 going to 4, 6 to 1 and 15 to 15, which is recorded as (1,4;6,1;15,5). This multi-atom process was found during the coalescence of two islands and will be discussed later. Its activation energy barrier of 0.595 eV is also recorded with the label.

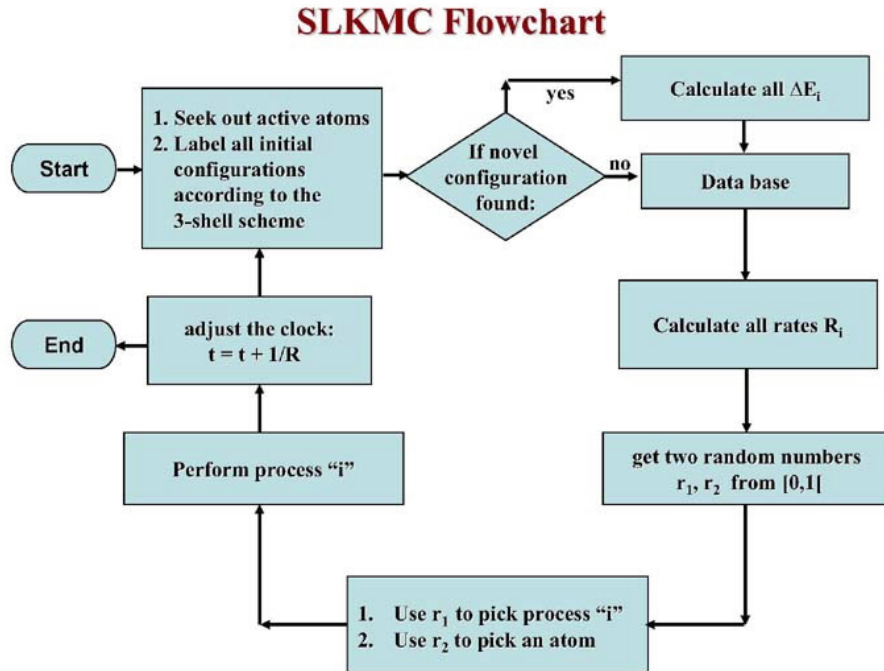


Figure 27: Flow chart for SLKMC simulation

The bottleneck for the simulation is the determination of the activation energy and the prefactor for all possible processes. Even when we make the widely-used assumption

that all the processes have the same pre-factor, the calculation of the activation energy is very expensive if one needs accurate values. Note that since the activation energy is in the exponential, any small variation in the activation energy results in a substantial change in the relative probabilities and hence the outcome of the whole simulation. In standard KMC these energy barriers are provided as input. If, however, as we and others [76] are proposing that these barriers be calculated on-the-fly, the process will be sped-up if provisions are made to avoid recalculations. In the method proposed here this is achieved through the storage of activation energy barriers tagged to specific atomic processes in the database. This is the basis of our KMC in which "self-learning" is achieved by the system through the ability to: (1) calculate activation energies on the fly; (2) store them in a database; and (3) recognize and retrieve them using the labeling described above. Step 1 is not new. It was already proposed by Henkelman and Jonsson *et al* [76] and Voter, Montalenti, and Germann [77]. Step 2 and 3 are unique to our approach and help remove redundancies in the calculations. At any given time, after all the processes have been sorted out, a search for the activation energies in the database is launched. If a new process is encountered, the actual calculation is performed and this process with its activation energy is added to the database. Once the processes are classified and macroscopic rates are calculated, we proceed to perform one Monte Carlo step in which a randomly selected process is executed. The entire simulation process is summarized in a flowchart (Fig. 27). At later times in the simulation, when the system encounters environments for which some of the possible processes have been met earlier, a retrieval process of the activation energy from the database substitutes for the actual calculation. This gives a tremendous gain in the execution times as evident in our application to the diffusion of 2D Cu clusters on Cu(111). With modest computational resources, it was possible to carry out the simulation for a number of MC steps, large enough to provide good statistics. The exact number of steps may vary from problem to problem.

In the next section, we discuss some key features of the database collected during an extended simulation along with the results obtained from applying the SLKMC to post-deposition analysis of homoepitaxy on Cu(111).

6.3 Application of SLKMC to Morphological Evolution of 2D islands on Cu(111)

Since the devil is generally in the details, we present below results of the application of SLKMC to study Cu cluster diffusion and coalescence on Cu(111). After giving some specifics of the model system, we present an analysis of the database, which includes an evaluation of the accuracy of the calculated energy barriers and other factors affecting the simulation (CPU) time. We also comment of the presence and importance of multi-atom processes. This is followed by the results and discussion of the diffusion and coalescence of 2D clusters on Cu(111).

6.3.1 Model Systems

In the first example, i.e. the study of the diffusion of 2D adatom islands of Cu(111) we have chosen four specific sizes (19, 26, 38 and 100 Cu atoms) for which we already have results for comparison with a KMC simulation using a fixed data base of logical processes involving single atom periphery diffusion [89]. For the second application to the process of cluster coalescence, our model system consists of 2 adatom islands, one consisting of 78 atoms and the other 498 atoms placed on top of the 2-layer substrate.

6.3.2 Examination of the collected database

To check the reliability of the data in the created database, we have compared in Table 5 the energy barriers that we obtained for some typical diffusion processes presented in Fig. 28, using both the drag and the NEB methods. We also include in the Table values available in the literature. The comparison in the Table attests to the reliability of the drag method as compared to the more time-consuming NEB procedure. For example, with the drag method we were able to achieve speed-up of at least an order of magnitude in the CPU time for the calculation of the energy barriers, as compared to one in which we applied the spherical repulsion method [88] to obtain the final states for a given initial state followed by application of NEB method for the calculation of the activation energies.

As an illustration of the richness of the database that we collect, we plot in Fig. 29 the

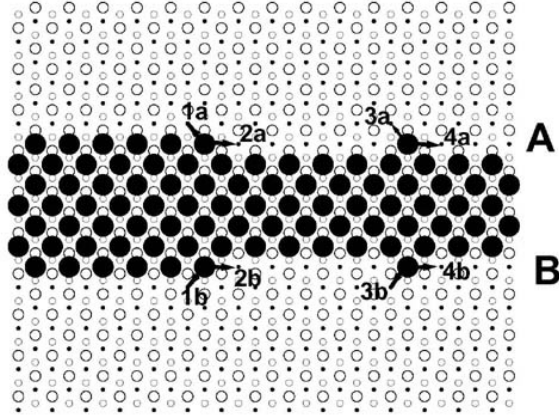


Figure 28: Selected single atom processes on the two types of steps A (100 microfaceted) and B (111 microfaceted), on fcc (111) surface. Process 1 is kink-detachment from a step, and 4 is adatom diffusion along step. The labels a and b refer to steps A and B, respectively.

Process	Drag Method (eV)	NEB Method (eV)	Ref. [93] (eV)
1a	0.68	0.66	-
2a	0.53	0.52	-
3a	-	0.65	-
4a	0.25	0.25	-
1b	0.60	0.59	0.59
2b	0.58	0.56	0.54
3b	0.68	0.67	0.67
4b	0.32	0.30	0.29

Table 5: Diffusion energy barriers for selected mechanisms as shown in Fig. 6.4

energy distribution of about 5000 diffusion processes that have been accumulated during a simulation containing several hundreds of millions of Monte Carlo steps. Note from Fig. 29 that the distribution is very wide covering activation energies as small as few tens of a meV to about 1 eV. Unlike the highly energetically corrugated surfaces like Cu(100)[93], energy barriers cannot be classified into groups. Note that in the calculations of the energy barriers differences are introduced when the effect of next nearest neighbors of the local environment is included in the calculation, as we have done. Note also that the accumulation of the database does not proceed uniformly with time, as reflected in the insert of Fig. 30. The SLKMC starts, in this case, by accumulating about 400 different processes during the very first MC step, after which the database is "quasi-saturated" for a certain period of CPU time. This is followed by an other phase of accumulation of about 600 processes, and so on. It is clear from the slope in Fig. 30 that when the simulation runs with a "quasi-saturated" database, the number of KMC steps/CPU time increases dramatically. During a heavy buildup of the database, the yield is about 80 KMC steps per second and can go up to several thousands of KMC steps per seconds as the database saturates. The onset of new events in the database after a certain duration of simulation does raise the issue of measures that would assure that the data base is complete. So far we have found the database to saturate after runs of about 100 - 500 million MC steps. Actually, for the systems under study we have rarely found new processes to set in after 10 million time steps.

One of the most important features of the method, as we have seen, is its ability to treat many-particle processes, the so called "concerted atomic motion". The recent version of the code allows inclusion of simultaneous displacements for atoms up to the third shell. From our simulations of several types of local environments (straight steps with kinks, compact islands, fractal like islands) we found that in some cases many particle processes play an important role in providing atomic transport [89]. They are especially important in the case of low coordination systems, like fractal islands. In such cases atoms are weakly bound and prefer to perform concerted motion rather than single atomic jumps. Furthermore, the importance of concerted motion increases with decreasing size of the cluster. In fact,

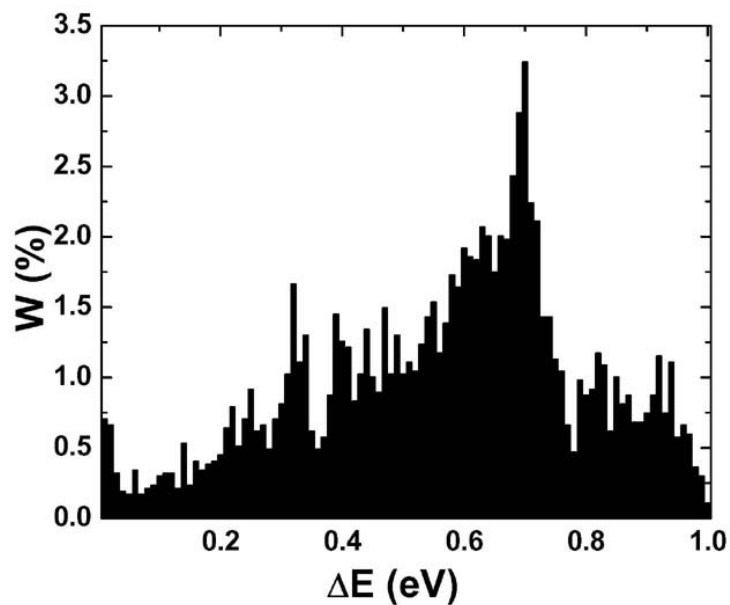


Figure 29: Distribution (percentage) of activation energies of stored processes in the database during a SLKMC simulation

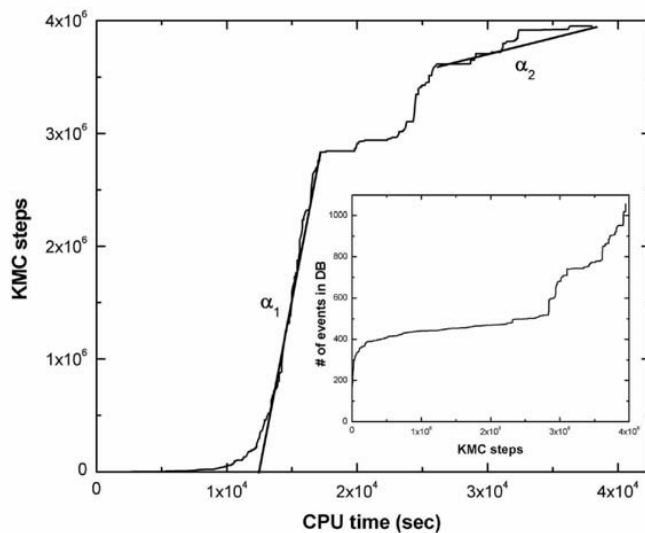


Figure 30: Variations in the number of KMC steps per CPU time (i.e., performance) and the buildup of the database as a function of the number of KMC steps (inset)

cluster Size	300K	500K
19	0.196	1.67×10^5
26	0.170	8.05×10^4
19	0.117	4.27×10^4
19	0.016	1.02×10^4

Table 6: Diffusion coefficient for 2D Cu islands on Cu(111) ($\text{\AA}^2/\text{sec}$)

molecular dynamics simulations simulations of a 10-atom Cu island on Cu(111) at 700K and 900K, show that the island moves by concerted displacement rather than through single atoms motion [90]. We next move on to examination of the results for two specific applications of SLKMC method.

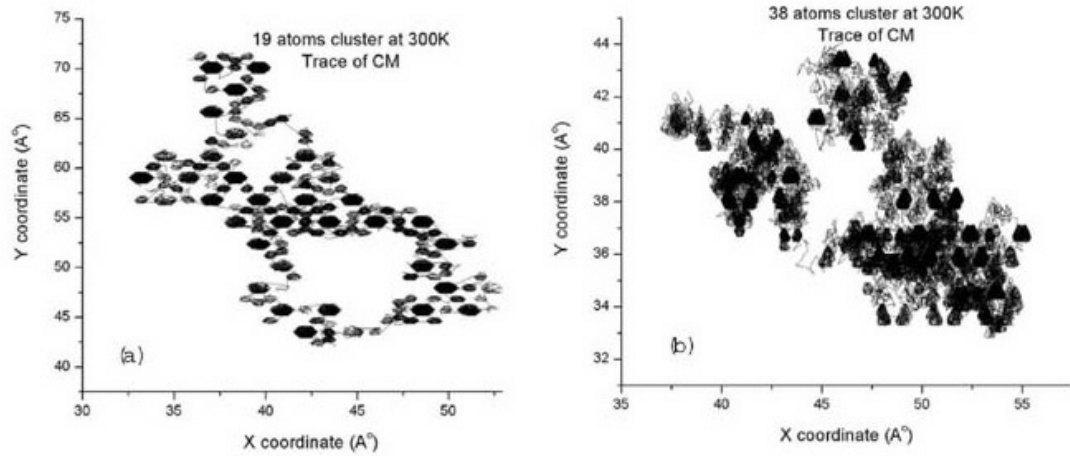


Figure 31: Trace of center of mass of 19- and 38-atom Cu clusters on Cu (111) at 300K as obtained from SLKMC simulations (10 million steps)

6.3.3 Morphological Evolution

6.3.3.1 Diffusion of 2D islands

As a first application of the SLKMC method, we present results for the diffusion of 2D Cu islands on Cu(111) of four sizes: 19, 26, 38 and 100 atoms. These simulations were performed using 10-100 million MC-steps at 300K and 500K. During the simulation, the position of the center of mass was recorded at each MC step along with the performed process. After 10 million MC steps, the islands have moved far enough that their diffusion

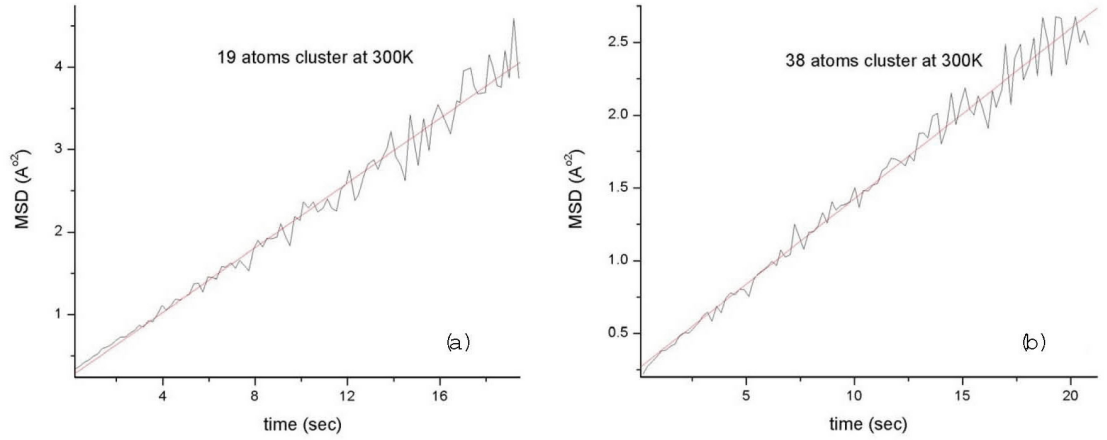


Figure 32: Mean square displacement (MSD) for 19- and 38-atom Cu clusters on Cu (111), as function of time at 300 K

coefficient may be extracted from the mean square displacement of the center of mass. In Fig. 31 we show the trace of the position of the center of mass on the (x, y) plane for both 19 and 38 atoms clusters at 300K. Note the dark spots for both cases indicating a stick-slip type motion of the center of mass. The corresponding mean square displacement, for these two atoms, as a function of time show a linear behavior (within statistical errors) and is shown in Fig.32. The extracted slope from the mean square displacement plot gives the coefficient diffusion. In Table 6, we report the diffusion coefficient for the four cluster sizes at 300K and 500K. Note that the diffusion coefficient increases exponentially with temperature. The decrease of the diffusion coefficient with the cluster size follows a power law ($D = N^{-1.57}$ at 300K and $D = N^{-1.64}$ at 500K), which is in good agreement with previous results [91]. The virtue of our calculation is that the atomic processes leading to cluster diffusion were picked by the system itself during the simulation. The frequencies of the contributing processes vary with cluster size and, more importantly, with surface temperature (see Table 7) Detailed descriptions of the processes in Table 7 are found in Ref.[94].

Processes	Energy Barrier		300K		500K	
	(eV) NEB	(eV) Drag	KMC	SLKMC	KMC	SLKMC
Step Edge A	0.252	0.250	0.62	0.6797	0.42	0.511
Step Edge B	0.295	0.310	0.17	0.0954	0.24	0.1403
Kink Detach along Step A	0.519	0.521	0.0	0.0	0.0020	0.0016
Kink Detach along Step B	0.556	0.538	0.0	0.0	0.0	0.0008
Kink Detach along small Step A	0.608	0.620	0.026	0.0106	0.012	0.0
Kink Detach along small Step B	0.680	0.693	0.0016	0.0007	0.0023	0.0018
Kink Incorp. A	0.220	0.220	0.0	0.0001	0.0020	0.0025
Kink Incorp. B	0.265	0.287	0.0	0.0	0.0	0.0009
Kink Incorp. (small) A	0.0075	0.009	0.025	0.0	0.011	0.002
Kink Incorp. (small) B	0.0810	0.108	0.0	0.0	0.0012	0.0
AA corner detachment	****	0.440	****	0.0007	****	0.0063
Kink Detach out of Step B	0.590	0.600	0.0	0.0091	0.0	0.0098
Kink Fall into Step A	0.074	0.102	0.0	0.0007	0.0	0.0016
Kink Fall into Step B	0.0069	0.015	0.0	0.0109	0.0	0.0101
BB corner detachment	****	0.344	****	0.0322	****	0.0451
All multiple atom processes			****	0.00015	****	0.0042
KESE A	0.374	****	0.0	****	0.0011	****
Corner Rounding at AA stage 1	0.313	0.325	0.0	0.0001	0.0	0.0017
Corner Rounding at AA stage 3	0.0096	0.014	0.0	0.0	0.0	0.0017
Corner Rounding at BB stage 1	0.374	0.393	0.0	0.0	0.0	0.0002
Corner Rounding at BB stage 3	0.052	0.072	0.0	0.0	0.0	0.0002
Corner Rounding at AB stage 1	0.317	0.328	0.066	0.0579	0.11	0.0894
Corner Rounding at AB stage 2	0.0839	0.113	0.0053	0.0023	0.024	0.0158
Corner Rounding at BA stage 1	0.396	0.421	0.0047	0.0013	0.023	0.0095
Corner Rounding at BA stage 2	0.0148	0.021	0.067	0.0884	0.12	0.1348
AB corner detachment to B	****	0.619	****	0.0003	****	0.0017
AB corner detachment to A	****	0.689	****	0.0	****	0.0002

Table 7: Frequencies of diffusion processes for the 19 atom cluster at two temperatures

Process	Barrier (eV)	Frequency ($0 - 1 \times 10^5$ steps)	Frequency ($1 - 2 \times 10^5$ steps)
2a	0.530	7.41	0.03
Rev. 2a	0.220	8.43	0.04
4a	0.25	69.66	95.88
others	-	14.50	4.05

Table 8: Frequency of selected processes during the coalescence of 2 islands

6.3.3.2 Island coalescence

As a second example of application of the SLKMC method, we present here results of simulation of the coalescence process in which two adatom islands join together to form a larger island with an equilibrium shape on Cu(111). This simulation was performed at 300K using a small island containing 78 atoms and with an arbitrary shape, put close to a larger island containing 498 atoms with a circular shape. Successive snapshots of the system during the SLKMC simulation are shown in Fig. 33, for a total number of forty millions KMC steps. From this figure, one notes that a neck between the two islands forms during the first 100000 KMC steps, corresponding to a physical time of 0.25s. After this time, the neck grows until the two islands form an elongated single island after about 10 seconds. Finally, the shape of the island evolves to a quasi-triangle with mostly (111)-steps (A-type), which is a result of the asymmetry in the activation energy barriers associated with A and B-type steps (see Table 5). In order to get an insight in the mechanisms involved in the neck formation, we have analyzed the frequency distribution of key processes during the first and second 100000 KMC steps. Three types of processes appear prominent in the coalescence of these two clusters: kink detachment on an A-type step (2a in Fig. 28), the reverse of 2a (Rev. 2a in Table 6) also called kink incorporation, and diffusion along A-type step (4a in Fig. 28). Listed in Table 8 are the frequencies for these processes. We note from Table 8 that during the formation of the neck, kink detachment and kink incorporation count for about 15% of the performed processes, another 70% involve diffusion along A-type step and other single and multiple atom processes including kink-rounding and two atoms diffusion along steps constitutes the remaining 15%. For the second 100000 KMC steps, the simulation is mostly dominated by diffusion along the A-type step (about 96%), with about 4% counting for various mechanisms. The important fact to note here is that kink-detachment and kink-incorporation contributions drop to almost zero after the neck has been formed. Detailed analysis of similar simulations involving islands of various sizes and shapes are actually in the processes of being performed and will be published elsewhere. A similar process for our simulations of cluster island coalescence are in qualitative agreement with the observations made by M. Giesen [92] using scanning tunneling microscopy.

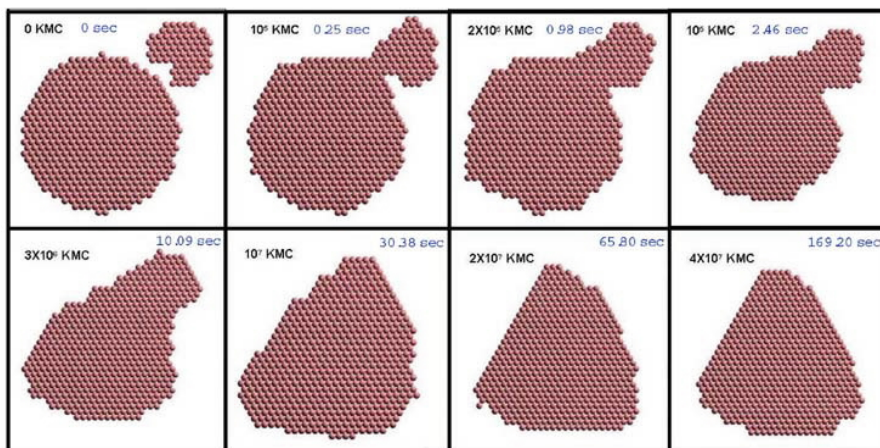


Figure 33: Coalescence of a small Cu cluster (78 atoms) with a larger one (498 atoms) on Cu (111) at 300 K, using the SLKMC simulation (10 million steps).

6.4 *Conclusion*

We have addressed the issue of completeness of KMC simulations by proposing a method in which the system finds, calculates, and collects the energetics of all possible diffusion processes that the moving entities are capable of performing. What separates our technique from others recently proposed is the provision for storing and retrieving the environment-dependent activation energy barriers from a database. Examination of the database shows that the simulation proceeds much faster when the set of processes is "quasi-saturated" and that after sampling such regions the system has the ability to trigger the participation of new diffusion processes requiring enhanced CPU's for the calculation of new activation energy barriers. The system eventually settles down and the number of MC steps needed to do this depends on the system and the number of entries already in the data base (about $10^7 - 10^8$ steps). With the use of the pattern recognition scheme we are able to identify and calculate the frequency of occurrence of individual single and multiple atom diffusion processes that actually participate in the evolution of a particular entity. The microscopic details of the processes involved in surface morphological evolution can thus be documented for a system that has the freedom to evolve on its own accord. We show this through application to the diffusion and coalescence of 2D adatom islands on Cu(111) for which the simulation began with an empty database. Once a substantial accumulation has occurred, the simulation time speeds up by orders of magnitudes and allows the calculation of system dynamics for time scales relevant to those phenomena happening in the laboratory. Interestingly, the two simple examples that we have presented here show that only a few dozen diffusion processes are in the end vital for a diffusion event. The question of course is: which ones? Our approach answers this question. As we have already alluded to, the task of calculating diffusion prefactors is still ahead of us. This is particularly important since we find many competing processes to differ only slightly in energy and differences in their vibrational entropy contributions to the prefactors can make a difference in the ultimate evolution of the film morphology. Another important result from our simulations with the open database is that dynamical evolution of the system with prejudged diffusion processes may yield erroneous results. Also, the pattern recognition schemes to be a prudent way

to develop a database of diffusion processes and their energetics. It does involve a lot of work in the beginning but once the data base is compiled, it can be used for any type of simulation of the system. Of course, for realistic simulations of thin films we need to incorporate exchange and other processes which involve motion in 3D. We have already alluded to the importance of inclusion of hops and occupancies of the hcp site. Such efforts are currently underway. In fact, preliminary results have already been obtained for the diffusion of small clusters (2-10 atoms) in which the SLKMC code with the both fcc and hcp occupancy[94],[95]. In the same vein, this work focuses on homoepitaxy. But this is not a limitation of the method because with well-defined changes the SLKMC method can be adapted to extend to heteroepitaxy. We will also discuss our results of heteroepitaxy later in this dissertation.

CHAPTER VII

DIFFUSION OF SMALL TWO-DIMENSIONAL CU ISLANDS ON CU (111)

Diffusion of small two-dimensional Cu islands containing up to 10 atoms on Cu 111 has been studied using the newly developed self-learning Kinetic Monte Carlo SLKMC method, which is based on a database of diffusion processes and their energetics accumulated automatically during the implementation of the SLKMC code. Results obtained from simulations in which atoms hop from one fcc hollow site to another are compared with those obtained from a parallel set of simulations in which the database is supplemented by processes revealed in complementary molecular dynamics simulations at 500 K. They include processes involving the hcp stacking-fault sites, which facilitate concerted motion of the islands with simultaneous motion of all atoms in the island . A significant difference in the scaling of the effective diffusion barriers with island size is observed in the two cases. In particular, the presence of concerted island motion leads to an almost linear increase in the effective diffusion barrier with size, while its absence accounts for strong size-dependent oscillations and anomalous behavior for trimers and heptamers. We also identify and discuss in detail the key microscopic processes responsible for the diffusion and examine the frequencies of their occurrence, as a function of island size and substrate temperature.

7.1 Introduction

Acquiring a precise knowledge of the microscopic mechanisms responsible for island diffusion or mass transport on surfaces is an important step toward the understanding of phenomena such as thin film growth and its morphological evolution. Motivated by experimental observations, initially using field ion microscopy (FIM) [96] - [100], and more recently with the use of the scanning tunneling microscope (STM) [101]- [106], the study of adatom and

vacancy island diffusion as a function of size has been an important concern also for many theorists [72], [107]. Because of the inherent differences in the microscopic processes responsible for the diffusion and its scaling behavior with size, the discussion has naturally bifurcated into those for the larger islands, usually containing more than 20 atoms, and the smaller ones ($N < 20$). For the larger islands, the diffusion coefficients appear to scale as a function of the size and the scaling exponent is expected to reflect the intervening atomistic processes responsible for the diffusion [16, 17]. However, for the smaller islands a consistent knowledge of the variation of their mobility with size and the details of the responsible atomistic processes has not yet been fully established, especially on the (111) surfaces of fcc metals.

One of the distinguishing geometrical features of the fcc(111) surface is the presence of two types of hollow sites: the so called fcc site under which there is no atom in the second layer and whose occupancy by an adatom maintains the crystal stacking order, and the hcp site under which there is an atom in the second layer and its nucleation can lead to a stacking fault. Whether or not an adatom or adatoms in an adatom island occupy one or the other of these two sites depends on their relative occupation energies and has significant consequences for epitaxial growth and the morphological evolution of the surface. Although Ag, Cu, Pt, and Ir are all fcc crystals there is no guarantee that the adatom would prefer to sit in the fcc site. In fact, experiments show that the hcp site is preferred on Ir(111) [18, 106], while on Cu(111) the fcc site appears to be favored [81], although the small difference in the occupation energy (a few meV) between the two sites does not rule out the occupation of the hcp sites. For dimers, trimers, and other larger islands, mixed occupancy of the two sites is also possible. The relative probability of occupancy of these two sites on fcc(111) surfaces continues to be the subject of much discussion and debate.

For small adatom islands earlier experimental studies point to a general decrease in mobility with increasing island size, except for some cases of anomalously large mobility [96] - [100]. For larger islands short-range diffusion of the atoms around the periphery, followed by adjustment of island shape, has been proposed to be the dominant mechanism for the diffusion [18, 19]. In the case of small Ir islands on Ir(111), concerted gliding motion

of the island has also been reported [18]. Subsequent molecular dynamics (MD) simulations using many-body potentials based on the embedded atom method (EAM) [4] have further disclosed that in addition to gliding, there is simultaneous motion of a portion of the island from the fcc to the hcp sites, creating a stacking fault [108]. The motion of the island could result from the rest of the atoms shifting also to the available hcp site. On Ni(111), for example, the smaller islands reportedly find the fcc to hcp transition to be critical to their diffusion, although gliding of the island as a whole and periphery motion has also been seen [108]. In agreement with the experimental results of Wang and Ehrlich on the higher mobility of tetramers as compared to trimers for Ir on Ir(111), Chang *et al.* [110] find the barrier for diffusion for the tetramer to be lower than that for the trimer for a number of fcc metals. They also predict a zigzag motion to be the dominant one for the dimer and the tetramer, while predicting a concerted motion as a whole for the trimer. Recent theoretical studies of the energetics and dynamics of 1 – 7 atom Cu islands on Cu(111) have once again highlighted the role of the concerted motion of the island in controlling its diffusion characteristics [112]. In the very recent work of Mueller *et al.* [107] good agreement with experimental data on submonolayer epitaxy on Ir(111) is also obtained with the inclusion of concerted motion of islands (with the stacking fault sites). Issues about the relative importance of the proposed diffusion mechanisms, the relevance of the occupation of the hcp sites, and the observed anomalous diffusion for certain sizes, are striking aspects of the diffusion of small 2D islands on fcc(111) surfaces and may control the subsequent growth patterns on these surfaces.

Our purpose here is to determine the microscopic factors that control the diffusion of small Cu islands on Cu(111) in an unbiased manner. We should hasten to mention that some results for such systems have recently been presented by Marinica *et al.* [112] who focussed on the application of a newer version of the EAM potentials [113] to calculate diffusion barriers and pre-exponential factors for a small set of likely processes that they find from their MD simulations to be responsible for island diffusion. The work ignores the contribution of mechanisms associated with atom-by-atom motion in small islands and

attributes the diffusion to specific collective island motion. The diffusion coefficient is simply obtained from application of the Arrhenius law to the activation energy barrier and the diffusion prefactor calculated for the chosen diffusion process. The natural question is whether such *a priori* selection of the responsible process precludes the contributions of other processes and whether such exclusion makes any difference in the predicted trends in island diffusion. The deeper question is, of course, whether it is possible to allow adatom islands to evolve as a function of time with mechanisms of their own choosing and thereby provide an unbiased illustration of the rate limiting step in the diffusion and the relative contributions of various mechanisms. We have recently developed a self-learning approach to kinetic Monte Carlo (KMC) simulations (*SLKMC*) in which the combination of an automatic generation of a database of single and multiple atom (2 or more atoms) processes during the evolution of the system, and a pattern recognition scheme provides a possible answer to the above question [32]. Application [17] of this method to the diffusion of 2D Cu islands on Cu(111) containing 19 – 100 atoms has shown the diffusion coefficient D to scale with the number of atoms N in the island as $D \propto N^{-1.57}$. Periphery diffusion in which single atoms hopped from one fcc site to another was the dominant mechanism. Several types of single and multiple atom processes were also revealed in the collected database. However, the frequency of occurrence of multiple atom processes was small even for the smaller islands (19-20 atoms) and their contribution to the diffusion process decreased further with increasing size and decreasing temperature. The situation may be different for islands with fewer atoms in which concerted island motion might dominate the diffusion process [112]. These processes necessarily involve occupation or transit through the hcp sites, although their exact nature is not known *a priori*. Our aim here is to apply *SLKMC* to examine the trends in the diffusion of small (2-10 atoms) Cu islands on Cu(111). Since in the original version of the code adatoms are assumed to occupy only fcc hollow sites, and in the light of the possible importance of the hcp site from the discussion above, we have also carried out MD simulations for further insights into the mechanisms controlling island diffusion. Indeed, the MD simulations reveal the importance of processes involving concerted island motion. A second set of *SLKMC* simulations with an enhanced database is

then performed and comparisons of the results of the two sets of KMC simulations provide an understanding of the factors that control the trends in the behavior and the atomistic processes that determine the diffusive motion of small Cu islands on Cu(111). In particular, our results provide interesting insights into the conditions that may lead to anomalous diffusion coefficients for certain sizes of islands. Also, since the issue of the relative importance of the fcc and hcp site may be system specific, by carrying out these two sets of simulations, the results presented here should have significance for other surfaces.

7.2 *Calculational Details*

The first set of calculations is based on the recently developed Self Learning Kinetic Monte Carlo (*SLKMC*) [32, 31] technique, in which we have implemented a pattern recognition scheme that assigns a unique label to the environment of the diffusing atom up to several neighbors for efficient storage and retrieval of information on activation energy barriers of possible processes that the system may choose to undergo. Provisions are made for automatic calculation of the energy barrier when a process is first identified and the result stored in a database. These energy barriers are calculated using a simple method that maps out the total energy of the system as the diffusing entity moves from the initial fcc site to the aimed final fcc site, in small steps. During the ensuing energy minimization procedure, all atoms in the system are allowed to relax in all directions, except for the diffusing atom whose motion is constrained along the reaction path. Processes involving multiple atoms can thus be revealed naturally. Extensive comparisons of the resulting energy barriers [32] with those obtained using the more sophisticated nudged elastic band method show only minor differences. The simpler method gives a gain of almost two orders of magnitude in the time taken to acquire a comprehensive data base. To ensure that the principle of detailed balance is rigorously obeyed, the barriers of the forward processes are used, together with the total energies of the system in the initial and final states, to determine the energy barriers for the reverse processes. For the calculation of the total energy of the system, interatomic potentials based on the embedded atom method (EAM) are used. The initial step in the simulation is the acquisition of the data base. Once it has become stable,

i.e. no new processes appear for some time (for the islands under consideration the data base saturated after about ten million KMC steps), the system evolves smoothly through atomistic processes of its choice and statistics are collected for calculating quantities like the mean square displacement of the center of mass of the island, correlation functions, and the frequencies of the atomistic processes.

In the *SLKMC* code that is extensively used here, we allow island atoms to occupy only fcc hollow sites. Also, interlayer exchange processes are not considered as the pattern recognition scheme for them is more complex than the one implemented here for diffusion via atomic hops. For the diffusion of 2D islands on Cu(111), such exchange processes are not expected to play a major role as their energy barriers are relatively high. Further, they have not been identified in either experiments or in the accompanying MD simulations performed at 500 K.

Assuming the validity of the transition state theory, the rate for an atom to hop to a vacant site is given by $r_i = \nu_i \exp(-\Delta E_i/k_B T)$. Here ΔE_i is the activation energy barrier, k_B is the Boltzmann constant, and ν_i is the attempt frequency or the so-called prefactor, which in principle can be sensitive to the details of the atomic environment. The prefactors for the various processes can thus be expected to be different. However, calculation of prefactors is non-trivial although the methodology is well defined [23]. Recent calculations of the prefactors for concerted island motion containing 2 – 7 atoms show some variation with size [112], particularly for the 7-atom island, and thus we have varied the prefactor for the 7-atom island by one order of magnitude and find the results reported here to remain essentially unchanged. In principle it would be preferable to calculate the prefactors for all the processes present in the database. We leave these calculations for the future, and invoke here the often used assumption of a standard value of 10^{12}sec^{-1} for all prefactors. For further efficiency in the KMC algorithm, we have employed the Bortz-Kalos-Lebowitz (BKL) updating scheme [6] which allows one to reach macroscopic time scales of seconds or even hours for simulations at, say, room temperature as has been shown in recent works [58, 59].

For reasons discussed in the Introduction, MD simulations were also carried out to

identify novel processes that can not be automatically picked up in *SLKMC* runs because of its restrictions to fcc site occupancy. The MD simulations were carried out using standard techniques and, naturally, with the same EAM interatomic potentials as in the rest of the work. For efficiency, these simulations were performed at 500K. As we shall see, collective island motion was revealed in the MD simulations and the hcp sites were found to be occupied particularly in transiting from one set of fcc sites to another. The message from the MD simulations is clear: the occupancy of the hcp site has to be allowed in KMC simulations of small islands. The first step in the direction is to replace the original 3-shell pattern recognition scheme in *SLKMC* with a 9-shell one which provides labels to all fcc and hcp sites in the vicinity of the moving atoms. The labels of all processes collected in the *SLKMC* database can then be converted to the 9-shell scheme. For the 2-4 atom islands this was not a problem and all processes in the database were relabeled and new ones from MD simulations accordingly labeled and their energy barriers calculated and stored. This newer version of the code named *SLKMC2* is fully equipped for the examination of the diffusion of these small Cu clusters on Cu(111). For islands containing 5 or more atoms, however, the database collected by *SLKMC* was far too extensive to manually convert each one into the new 9-shell labeling scheme. We have thus refrained from developing manually a data base of all single and multiple atom and collective island diffusion processes for these larger Cu islands. Work is underway to equip *SLKMC2* with an efficient and robust saddle point search routine such that in the future it will be able to acquire automatically the data base of all relevant diffusion processes for two dimensional islands of any size. For purposes here we have used *SLKMC2* to examine the diffusion of 2-4 atom Cu islands on Cu (111) in the presence of all possible single and multiple atom, and collective island diffusion processes. The results of such simulations are compared with those obtained from *SLKMC*. Note that, although concerted island motion is a type of multiple atom process, throughout this chapter we have made a distinction between it and other multiple atom processes.

In the case of clusters with 5-10 atoms, we have proceeded along another route. We have retained the original *SLKMC* code and supplemented its database with processes that allow us to mimic collective island motion through an indirect procedure for the inclusion

of the fcc-hcp jumps. The rationale for the indirect procedure is as follows. We know that the first step in a concerted island motion is the collective jump of all island atoms from fcc to hcp sites. For the island sizes in questions we calculate the activation energy barriers ΔE_{hf} for all such collective processes (fcc-hcp). MD simulations have been very helpful in revealing the shapes of the islands before the jumps from fcc to hcp sites. In particular islands are found to assume more or less compact shapes before the collective jumps. The rate of the concerted island motion from fcc to hcp sites is $\nu_{hf} \exp(-\Delta E_{hf}/k_B T)$, where ν_{hf} is the pre-exponential factor, as noted above. As will be seen in Figs. 40 and 42, once the island atoms are in hcp sites, each one can hop to one of three equivalent fcc sites. We calculate the energy barriers for such collective hcp to fcc transitions. The relative magnitude of these barriers determines the relative probability for the particular hcp-fcc hop. If the energy barrier for all three processes is the same, then the probability for each is 1/3. In such a scenario the rate for fcc-hcp-fcc concerted island motion could be written as $1/3 \nu_{hf} \exp(-\Delta E_{hf}/k_B T)$ and in general as $P_{hf} \nu_{hf} \exp(-\Delta E_{hf}/k_B T)$, where P_{hf} is the probability of the particular hcp to fcc hop, which lies between 1 and 1/3. We now have a recipe for including concerted island motion from fcc to fcc sites in the database of *SLKMC*. To check whether the indirect procedure of including concerted island motion in *SLKMC* is reliable, we have carried out simulations for the 2-4 atoms islands using this recipe and compared the results obtained from *SLKMC2*. In Table 9 we have summarized the results of KMC simulations for trimers and tetramers by using the direct and indirect methods. As can be seen both yield almost the same diffusion coefficients.

As for the model system, we consider a fcc(111) substrate with an adatom island on top, as shown in Fig. 34. The gray circles are substrate atoms which stay rigid during the simulation, whereas the dark (colored on-line) circles are the island atoms, placed on fcc sites, which are the hollow sites having no atoms underneath them in the layer below. A KMC simulation step begins by placing an adatom island of desired size, in a randomly chosen configuration, on the substrate. The system evolves by performing a process of its choice, from the multitude of possible single or multiple adatom jumps at each KMC step. We performed about 10^7 such steps at 300 K, 500 K, and 700 K. Typically, at 500 K, 10^7

KMC steps were equal to 10^{-3} sec in physical time. The diffusion coefficient of an adatom island is calculated by $D = \lim_{t \rightarrow \infty} \langle [R_{\text{CM}}(t) - R_{\text{CM}}(0)]^2 \rangle / 2dt$, where D is the diffusion coefficient, $R_{\text{CM}}(t)$ is the position of the center of mass of the island at time t , and d is the dimensionality of the system.

7.3 Results and Discussions

We present first the results that are obtained from the *SLKMC* method with single and multiple atom processes involving jumps from one fcc site to another, which are automatically accumulated and performed during the simulation. The calculated diffusion coefficients of the islands at 300 K, 500 K, and 700 K are summarized in Table 10. These are the numerical values in the first entry for each size type in Table 10 and range from $8.82 \times 10^{10} \text{ \AA}^2/\text{sec}$ for the dimer to $4.12 \text{ \AA}^2/\text{sec}$ for the 10-atom island. A log-log plot of D vs N in Fig. 35a shows oscillations in the diffusion coefficient with size. This hint for magic sizes of islands signifying reduced mobility is also seen in the Arrhenius plot of $\ln D$ vs $1/k_B T$. The effective diffusion barriers extracted for each island size from the Arrhenius plot (Fig. 36) also display oscillatory behavior. As can be seen in Table 10, the 3, 7, and 10-atom islands display higher effective barriers than the others. The barrier for diffusion is particularly high for the perfect hexagon (7-atom) island.

As we mentioned in Sec. II, MD simulations carried out at 500 K revealed several new concerted moves of the islands which involved occupation of the hcp sites, too. Before discussing the details of the atomistic processes let us examine the results for the diffusion coefficients once these processes are included in the database of *SLKMC*. The calculated diffusion coefficients, effective energy barriers, and the prefactors for the second set of KMC simulations are summarized in Table 10. These values are given in the square brackets underneath the corresponding ones obtained when hcp-site assisted processes are not included. The size dependence of the diffusion coefficients at three different temperatures with the inclusion of concerted moves from MD are also shown in Fig. 35(b) for comparison of the case already discussed in Fig. 35(a). Further comparison of the results of the two sets of simulations is in Fig. 36, in which the effective diffusion energy barrier appears to scale with

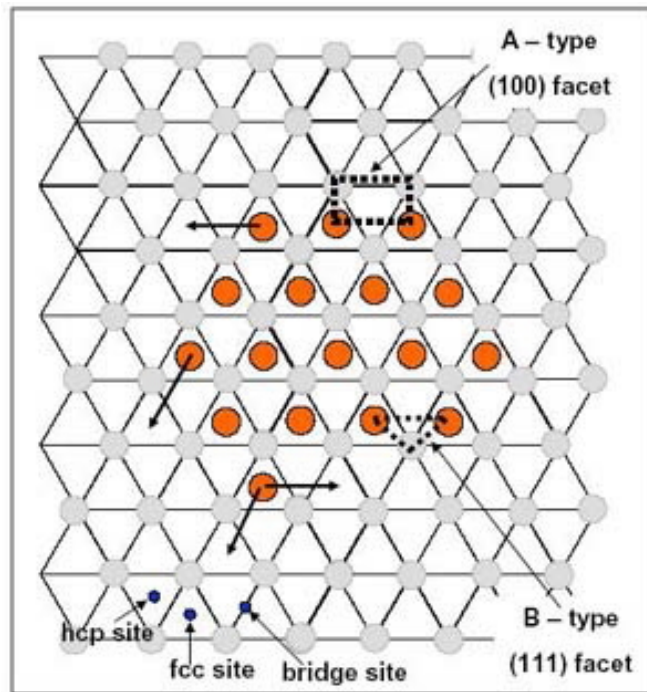


Figure 34: Some examples of adatom diffusion and hops on the fcc (111) surface. Dark-colored atoms are active and placed at fcc sites, whereas light-colored atoms serve as the substrate. The lower edge of the layer containing active atoms forms a (111) microfacet, so it is called the B-type step edge while the upper edge of the layer containing active atoms forms a (100) microfacet which is called an A-type step.

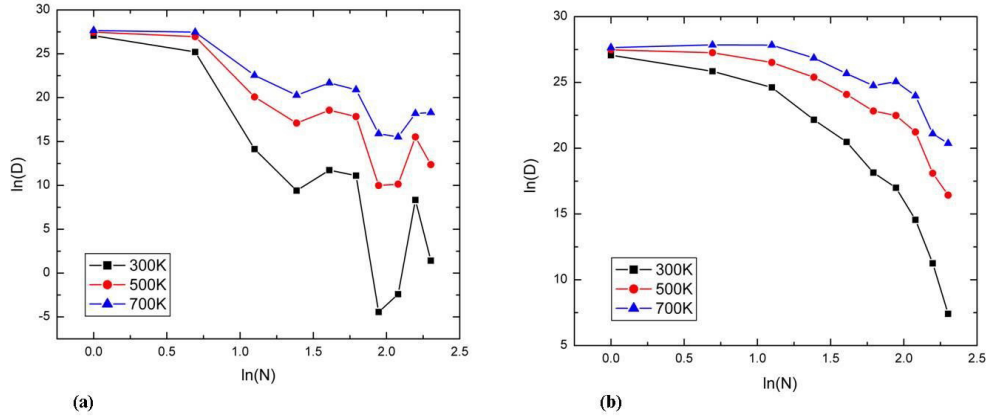


Figure 35: Diffusion coefficients as a function of the island size; (a) KMC results without including concerted motion mechanisms; (b) KMC results after including concerted motion mechanisms obtained from MD simulations.

Island	Temperature	SLKMC	(SLKMC) with	[SLKMC2] with
	K		concerted motion	concerted motion
			Indirect results	Direct results
Trimer	300	1.37×10^6	(2.78×10^{10})	$[4.89 \times 10^{10}]$
	500	5.26×10^8	(1.83×10^{11})	$[3.27 \times 10^{11}]$
	700	6.17×10^9	(4.55×10^{11})	$[1.22 \times 10^{12}]$
Tetramer	300	1.21×10^4	(3.40×10^9)	$[4.19 \times 10^9]$
	500	2.66×10^7	(9.17×10^{10})	$[1.06 \times 10^{11}]$
	700	6.35×10^8	(3.38×10^{11})	$[4.60 \times 10^{11}]$

Table 9: Diffusion coefficients of a trimer and a tetramer at different temperatures.

the island size once the hcp-assisted concerted motion is taken into account. The striking result is that there is no longer any oscillation in the quantities and the 3 and 7 atom islands diffuse just like the others, in proportion to their size. We now turn to an analysis of the details of the single and multiple atom mechanisms involved in the diffusion of the islands, one by one.

7.3.1 Monomer

For completeness we begin with a few comments on the diffusion of an adatom on Cu(111). The primary motion for a single atom is simply the process of hopping between the fcc and the hcp sites. We find an activation energy barrier of $E = 29$ meV for the process,

Island size (atoms)	D ($\text{\AA}^2/\text{sec}$)			Effective barrier E_a (eV)	Diffusion prefactor D_0 ($\text{\AA}^2/\text{sec}$)
	KMC 300 K	[KMC with 500 K	concerted motion] 700 K		
1	5.70×10^{11}	8.50×10^{11}	1.02×10^{12}	0.026	1.56×10^{12}
2	8.82×10^{10} [1.68×10^{11}]	5.07×10^{11} [6.90×10^{11}]	8.50×10^{11} [1.24×10^{12}]	0.104 [0.091]	5.14×10^{12} [5.58×10^{12}]
3	1.37×10^6 [4.89×10^{10}]	5.26×10^8 [3.27×10^{11}]	6.17×10^9 [1.22×10^{12}]	0.380 [0.141]	3.52×10^{12} [1.06×10^{13}]
4	1.21×10^4 [4.19×10^9]	2.66×10^7 [1.06×10^{11}]	6.35×10^8 [4.60×10^{11}]	0.492 [0.211]	2.31×10^{12} [1.50×10^{13}]
5	1.25×10^5 [7.81×10^8]	1.16×10^8 [2.87×10^{10}]	2.60×10^9 [1.40×10^{11}]	0.440 [0.234]	4.13×10^{12} [6.73×10^{12}]
6	6.66×10^4 [7.57×10^7]	5.58×10^7 [8.15×10^9]	1.19×10^9 [5.60×10^{10}]	0.440 [0.300]	1.69×10^{12} [8.22×10^{12}]
7	1.18×10^{-2} [2.40×10^7]	2.18×10^4 [5.80×10^9]	8.00×10^6 [7.60×10^{10}]	0.922 [0.362]	3.80×10^{13} [2.90×10^{13}]
8	9.00×10^{-2} [2.10×10^6]	2.53×10^4 [1.65×10^9]	5.49×10^6 [2.59×10^{10}]	0.800 [0.430]	3.70×10^{12} [3.61×10^{13}]
9	4.18×10^3 [7.72×10^4]	5.50×10^6 [7.20×10^7]	8.00×10^7 [1.45×10^9]	0.448 [0.444]	1.55×10^{11} [2.24×10^{12}]
10	4.12 [1.65×10^3]	2.33×10^5 [1.37×10^7]	8.82×10^7 [7.02×10^8]	0.731 [0.580]	7.24×10^{12} [1.06×10^{13}]

Table 10: Diffusion coefficients of 1 to 10 atom islands at different temperatures and their effective diffusion barriers with diffusion prefactors.

while with a slightly different EAM potential Marinica *et al.* [112] find it to be 41 meV. As already mentioned, exchange processes between the adatom and the substrate atoms are not included in our KMC simulations, neither do they appear in the accompanying MD simulations. The effective diffusion barrier inferred from the Arrhenius plot of the monomer diffusivities from our KMC simulations is $E_a = 26 \pm 3$ meV, which is consistent with the calculated energy barrier contained in our database. This value is also in agreement with that obtained from MD simulations ($E_a = 31.0 \pm 0.8$ meV) by Hynninen *et al.* [111]. Experimental results report the adatom activation energy on Cu(111) to be $E_a = 37.00 \pm 5$ meV [81]. Our results are thus in agreement with experimental data.

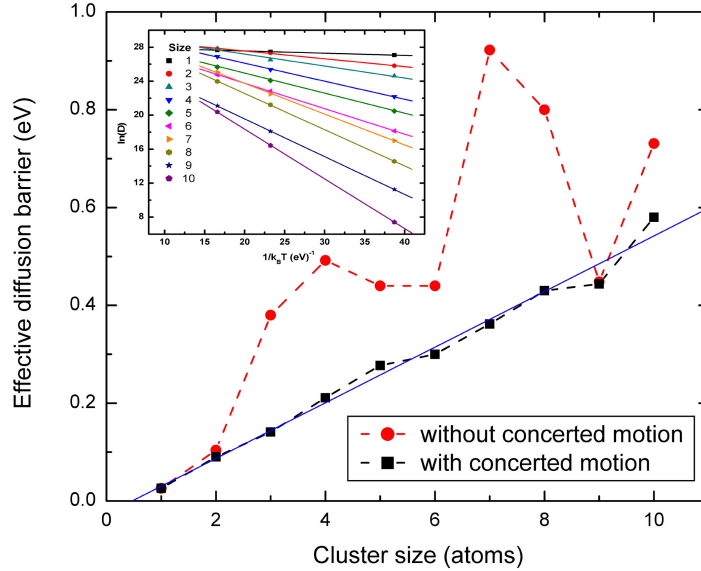


Figure 36: Effective diffusion barriers of 1-10 atom islands plotted as a function of island size. The dotted line with squares represents full KMC simulation results including concerted motion, whereas the dotted line with circles shows results of the KMC simulation without including concerted motion mechanisms. The inset shows Arrhenius plots of diffusion coefficients as a function of temperature.

7.3.2 Dimer

In the case of the motion of the dimer the *SLKMC* code picked up only two mechanisms which permit jumps from fcc to fcc sites. These are labeled *Dimer A* and *Dimer B* in

Fig. 37 (a), and their energy barriers are 101 meV and 15 meV, respectively. Results of diffusion coefficients with these two processes at three different temperatures are in Table 10. The effective diffusion barrier for the dimer from the Arrhenius plot is 104 meV. Of course, the dimer motion is actually nontrivial since in reality both dimer atoms could also occupy the hcp sites or they could occupy mixed sites with one atom on the fcc and the other on the hcp site. The MD simulations actually revealed 13 more mechanisms for the dimer diffusion which are shown in Fig. 37 (b). These illustrations show transitions between the sites occupied by the dimer atoms. Simultaneous occupation of mixed sites is slightly favorable because of the somewhat lower energy (by 1 – 3 meV), as compared to both atoms occupying the same type of sites.

Let us have a critical look at mechanisms shown in Fig. 37 (b). Processes describing sliding and rotational motion, D_2, D_3, D_4, D_6 , and D_8 , have lower energy barriers as compared to the others shown in Fig. 37 (b). Process D_2 , in which both atoms are initially on hcp sites and one jumps to the fcc site by crossing the bridge site, has the lowest energy barrier of 5 meV, The second low energy mechanism is D_6 , (9 meV), in which both atoms occupy fcc sites initially and one of them jumps to hcp site by crossing the bridge site. The energy barrier for the same mechanism from the experimental data reported by Repp *et al.* [81] is 18 ± 3 meV, which is larger than what we find. Marinica *et al.* [112] find this barrier to be 16 meV. Process D_4 describes dimer atoms as initially occupying mixed sites and finally both atoms occupy hcp sites. We find its energy barrier to be 18 meV while Marinica *et al.* [112] reported it to be $E = 26$ meV. We also observed long jump mechanisms (D_7, D_{10}, D_{11} , and D_{13}) for dimer diffusion in our MD simulations.

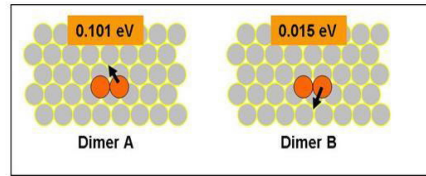
The sliding motion between fcc and hcp sites has diffusion barriers of the same order of magnitude as that for the long jump motion of the dimer. On the other hand, the rotational motion, D_3 , has a diffusion barrier (20 meV) closer to the value of a single atom hopping barrier, which is 29 meV. Finally, we included all of these 13 mechanisms in our *SLKMC* database that had only two mechanisms (*Dimer A* and *Dimer B*) initially. As we can see from Table 10, with the inclusion of concerted motion the effective diffusion barrier reduces to $E_a = 92$ meV, which is closer to the value of barrier representing concerted motion of the

dimer. Although a dimer performs low energy mechanisms (D_2, D_3, D_4, D_6 , and D_8) more frequently, the change in the center of mass position is small as compared to the long jump mechanisms (D_7, D_{10}, D_{11} , and D_{13}) and also concerted motion mechanism (D_1 and D_{12}). Hence a small frequency of relatively high energy mechanisms (long jumps) can greatly change the center of mass position of the dimer. This is why the effective diffusion barrier of a dimer is closer to the diffusion barrier of long jumps and concerted motion mechanisms (D_7, D_{11}, D_{13}).

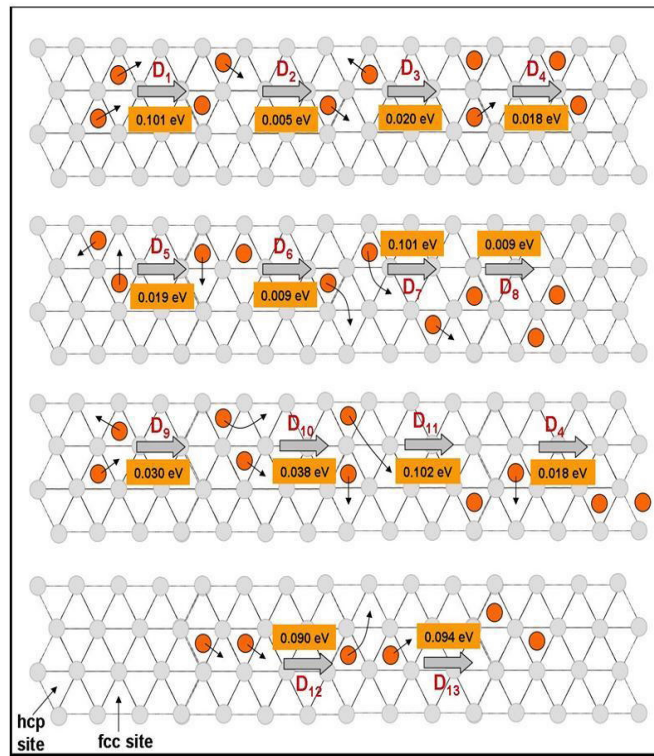
7.3.3 Trimer

We have done a detailed study of trimer diffusion using *SLKMC* simulations. There are only nine possible atom-by-atom motion mechanisms that were identified by our *SLKMC* code. These mechanisms and their corresponding energy barriers are shown in Fig. 38 (a). With only fcc to fcc jumps the effective diffusion barrier for the trimer is 380 meV (see Table 10). Actually the atom-by-atom motion produces a shape change but does not facilitate the diffusion of the trimer. We obtained quite interesting results when we included mechanisms describing concerted motion of trimer as shown in Fig. 38 (b). The trimer moves from one fcc site to the neighboring hcp site by performing concerted gliding and rotation mechanisms. The energy barrier for concerted gliding of the trimer from 3fB to 3hA is found to be 125 meV, whereas the reverse mechanism has a barrier of 115 meV. The rotation of the trimer has the lowest energy barrier of all: 38 meV from 3hA to 3fA and 62 meV from 3fA to 3hA, respectively. With the inclusion of these additional processes the effective diffusion barrier is found to be 141 meV.

This is a dramatic reduction from 380 meV found earlier and the effect is impressively represented in Fig. 35b and Fig. 36b which shows the trimer to be relatively mobile. In Fig. 39 we plot the distribution of the frequency of events with and without rotation and concerted motion, represented, respectively by filled and open symbols. We find that the occurrence frequencies of added mechanisms (concerted motion and rotation) are much higher than the occurrence frequencies of all other nine mechanisms because concerted motion and rotation mechanisms have low energy barriers as compared to the mechanisms



(a)



(b)

Figure 37: (a) Illustration of two simple mechanisms for dimer diffusion and their energy barriers, where atoms jump from fcc to fcc sites. (b) 13 mechanisms for dimer diffusion via fcc to hcp sites and their energy barriers. These mechanisms were found from MD simulations.

such as *Opening From A* and *Opening From B*. Although rotation dominates, it does not play a key role in trimer diffusion because it is not responsible for the center of mass motion of the trimer. We expect concerted motion to dominate diffusion, and thus we can predict that the value of the effective diffusion barrier should be closer to the value of the concerted motion barrier, which is indeed true here. In Table 10, we can clearly see the difference between results before and after including rotation and concerted motion mechanisms in our primary database of nine processes.

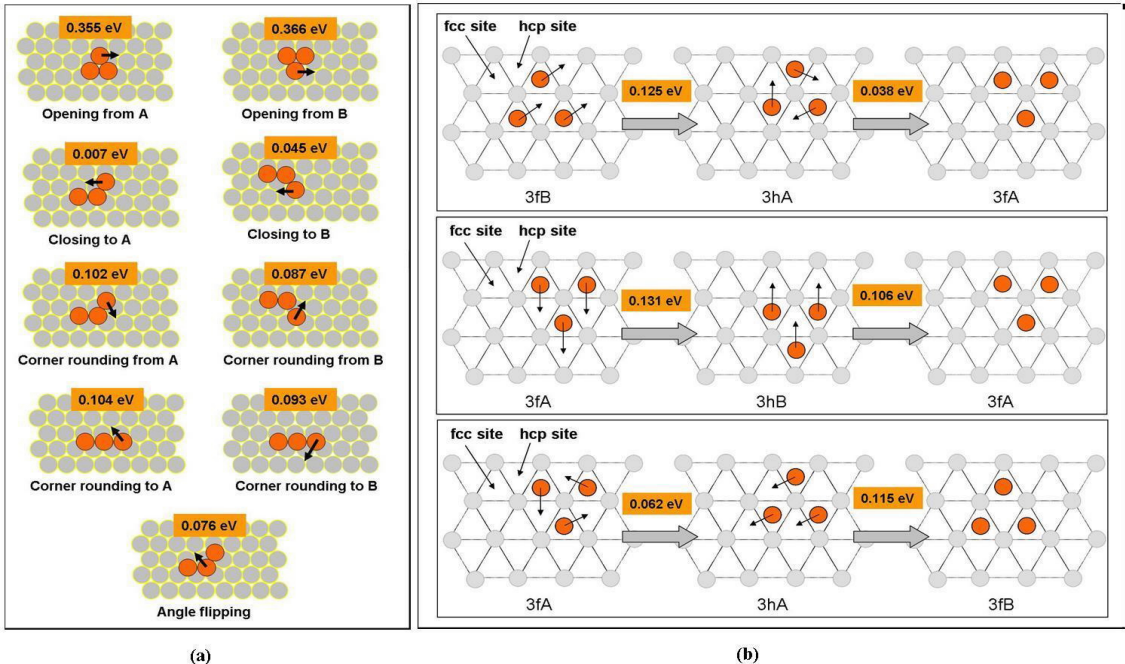


Figure 38: (a) Nine mechanisms for trimer diffusion with their corresponding energy barriers, where atoms are allowed to jump from fcc to fcc sites. (b) Trimer diffusion mechanisms observed during MD simulations. These mechanisms are conducted through a collective motion of three atoms by rotation and gliding over the bridge sites from fcc to hcp sites, or vice versa.

7.3.4 Tetramer

In the case of the tetramer we have 28 possible, fcc to fcc, atom-by-atom jump processes which together with their energy barriers are shown in Fig. 40 (a). As noted in Table 10, KMC simulations performed with these mechanisms led to an effective diffusion barrier of

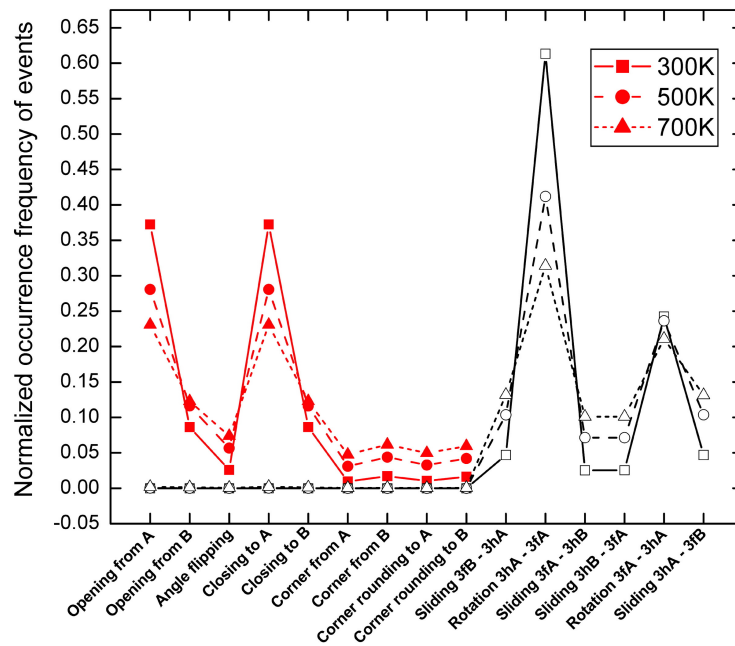


Figure 39: Distribution of normalized frequencies of event occurrences in the case of trimer diffusion. The lines with filled symbols show the distributions of events at different temperatures when only single atom mechanisms were included, and lines with open symbols show the distributions of all events including the collective motion of three atoms by rotation and gliding.

492 meV. Three mechanisms exhibiting concerted motion and shearing of a diamond shaped tetramer, revealed in MD simulations, and their corresponding diffusion barriers, are shown in Fig. 40(b). Concerted motion of a diamond shaped tetramer takes place through sliding between the fcc and the hcp sites, along its small and large diagonals. The ones along the small diagonal (Fig. 40b-1) have lower energy barrier (167 meV for fcc to hcp and 125 meV for hcp to fcc) than those along the large diagonal (Fig. 40b-2). These processes have also been discussed by Marinica *et al.* [112]. However, the case of diamond shape tetramer diffusion through the shearing mechanism shown in Fig. 40b-3 with energy barrier 230 meV was not taken into account by them. When we included these three mechanisms in our database of 28 single atom mechanisms and performed KMC simulation, we found significantly different values for the diffusion coefficients. In Table 10, these values are written in square brackets and the effective diffusion barrier for tetramer is $E_a = 212$ meV.

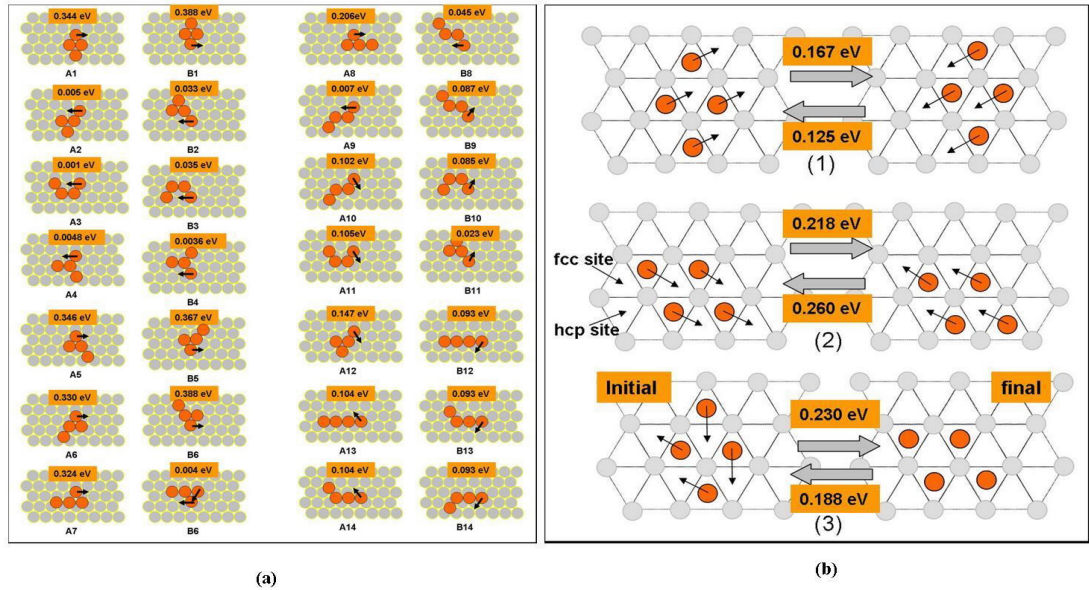


Figure 40: (a) Illustration of 28 mechanisms and their corresponding energy barriers for tetramer diffusion, where jumps are allowed from fcc to fcc sites only. (b) Tetramer diffusion mechanisms revealed from MD simulations: (1) diagonal glide, (2) vertical glide of 4 atom island over the bridge sites and the corresponding energy barriers, and (3) shearing mechanism.

7.3.5 Islands containing 5 to 10 atoms

A few examples of single atom processes collected in the database of our KMC simulations, for the islands containing 5 to 10 atoms, are shown in Fig. 41 with the corresponding energy barriers. The diffusion coefficients calculated from KMC simulations based on these single atom mechanisms are very low as shown in Table 10. This is particularly the case for the 7 and 8 atom islands whose effective diffusion barriers are consequently the largest. This is understandable because we find that processes such as *AB Corner Detachment A* and *AB Corner Detachment B*, shown in Fig. 41, play a key role in the island diffusion by contributing the most to the change in the center of mass position. Processes such as *Step Edge A* and *Step Edge B* occur more frequently, but they do not contribute significantly to the motion of the center of mass of the island; rather the atoms move around and around along the periphery of the island. In Fig. 42 we show the concerted motion processes revealed from MD simulations. Their energy barriers were determined from molecular static calculations by dragging the central atom of the island from the fcc site to the nearest hcp site. Other atoms in the island followed its motion by gliding over the bridge sites. The different shapes and geometries of these islands contribute to the differences in the energy barriers for the processes. For example in our MD simulations we found that the 10 atom island can move as a single entity from fcc to hcp sites whenever it appears into one of the three shapes shown in Fig. 42. The energy barriers associated with these processes are slightly different. Clearly, the barriers of these concerted motion mechanisms, (for 5 to 10 atom islands) are comparatively lower (270 meV to 590 meV) than the energy barriers of the single atom mechanisms *AB Corner Detachment A* and *AB Corner Detachment B*, also considered essential for island diffusion. After the inclusion of new low energy concerted motion mechanisms in our database, the high energy single atom mechanisms become less frequent in KMC simulations and high values of diffusion coefficients and correspondingly low values of the effective diffusion barriers were obtained (see Table 10). The size dependent oscillations of the diffusion coefficients and the effective diffusion barriers also disappeared from the plots shown in Fig. 35(b) and Fig. 36, respectively. We can thus conclude that the absence of the low energy concerted motion mechanisms is responsible for the oscillatory

behavior of diffusion coefficients as a function of size. Finally, our complete KMC results show that the effective diffusion barriers increase almost monotonically with increasing island size.

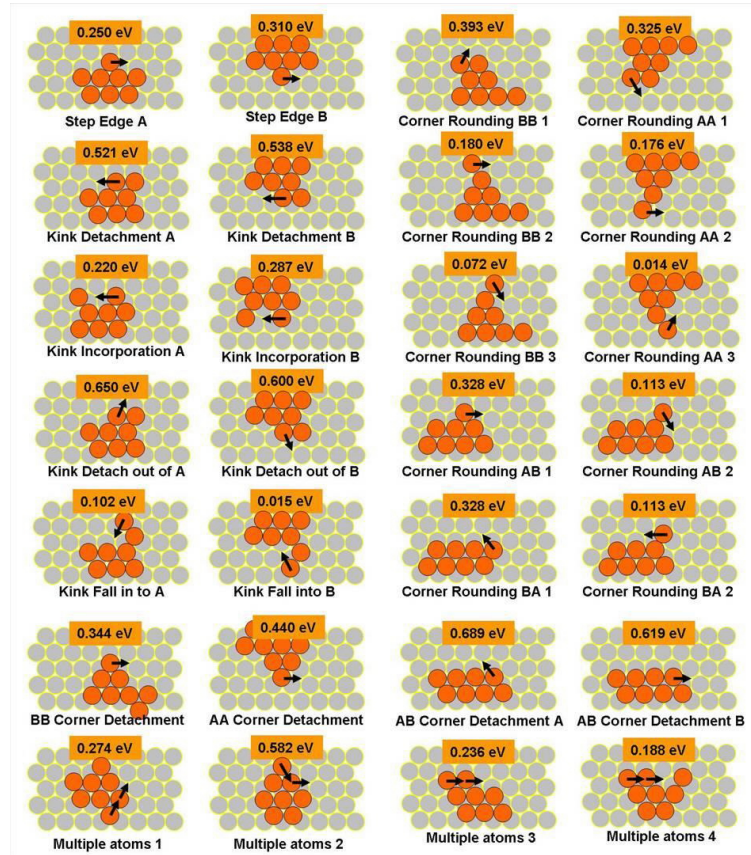


Figure 41: A few examples of single and multiple atom mechanisms and their corresponding energy barriers used in our KMC simulations for island larger than 4 atoms. Jumps are allowed from fcc to fcc sites only.

7.3.6 Key mechanisms and their occurrence frequencies

In Fig. 43 we show the normalized frequencies of all events from the extended *SLKMC* data that were performed during the simulations. Lines with open symbols in Fig. 43 show the occurrence frequencies of the all concerted motion mechanisms, at three different temperatures, as the function of the island size, while those with filled symbols all show single atom mechanisms. For the dimer case, most of the single atom mechanisms have the same effective barriers as compared to the barriers associated with concerted motion

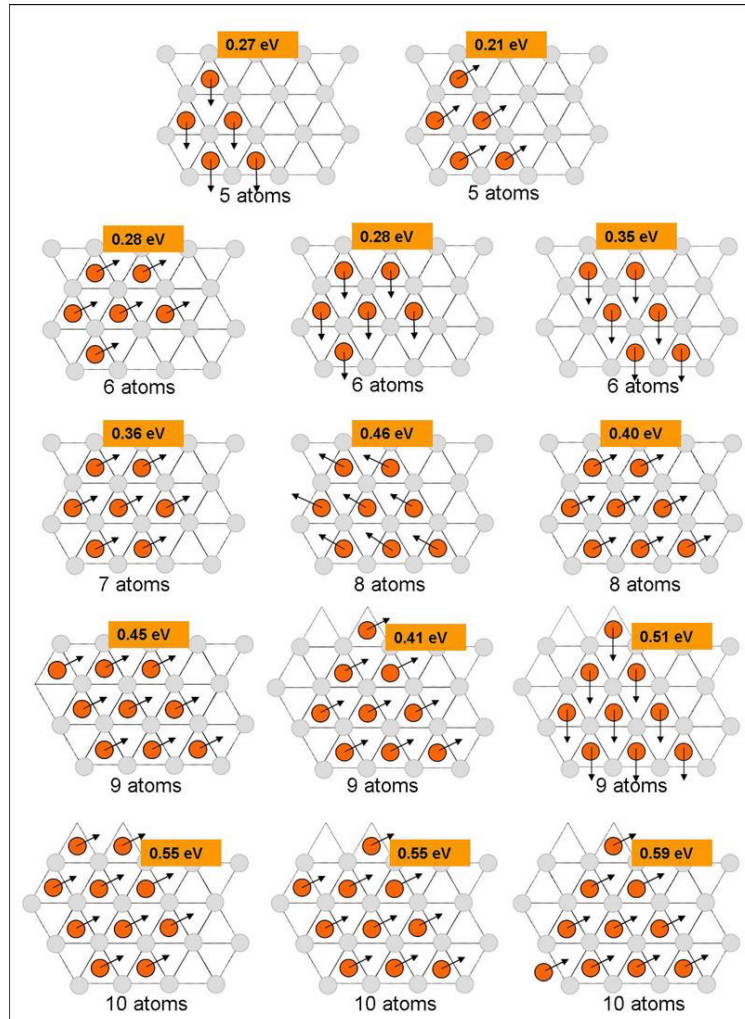


Figure 42: Diffusion mechanisms found by performing MD simulations for the island sizes of 5-10 atoms and their corresponding energy barriers when they glide over the bridge sites exhibiting collective motion of all atoms.

mechanisms. Thus, the occurrence frequencies of single and multiple atom mechanisms are almost the same for dimer diffusion. In the case of 3 to 7 atom islands, concerted motion processes are associated with significantly lower energy barriers as compared to the single atoms, and therefore concerted motion occurs more frequently. A six atom island has an effective barrier for concerted motion that is closer to barriers of some single atom mechanisms, which play a role in the motion of the center of mass position to some extent (*i.e.* *Step Edge A* and *Step Edge B* processes). Because of the close competition between concerted motion and single atom mechanisms, we find a narrow gap between their occurrence frequencies in the case of the 6 atom island. A similar, narrow gap can be seen in the case of the 8 atom island. In this case there is close competition between concerted motion and the motion of the single atom going around the periphery of the island (*i.e.* *BB Corner Detachment* and *AA Corner Detachment* processes). In the case of 9 and 10 atom islands the low energy single atom mechanisms (*i.e.* *Step Edge A* and *Step Edge B* processes) occur more frequently, but they do not play a key role in island diffusion. On the other hand, since the barriers of the concerted motion mechanisms are higher (410 meV to 590 meV), they occur rarely but still play an important role in the diffusion.

7.4 Conclusions

To summarize, we have performed a systematic study of the diffusion of small Cu islands on Cu(111), using a recently developed self learning KMC simulations in which the system is allowed to evolve through mechanisms of its choice with the usage of a self generated database of single and multiple atom diffusion processes. Complementary molecular dynamics simulations carried out for a few cases provided further details of several new mechanisms for small island diffusion that were not automatically picked up by our *SLKMC* method because of the initial restriction of fcc site occupation. We found significant changes in the size dependent variations of diffusion characteristics of the islands after including concerted motion mechanisms that were revealed from MD simulations. We find that these small sized islands diffuse primarily through concerted motion with a small contribution from single atom processes, even though for certain cases the frequency of single atom processes is large

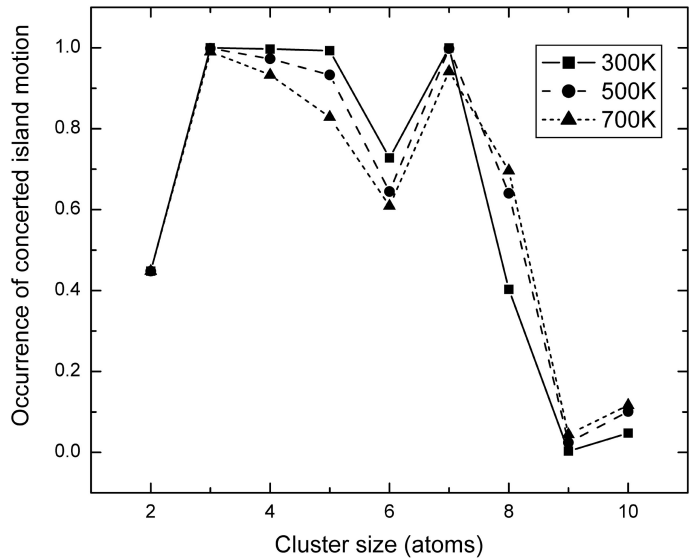


Figure 43: Distribution of normalized frequencies of concerted motion events as a function of island size.

because of lower activation energies. By allowing the system the possibility of evolving in time through all types of processes of its choice, we are able to establish the relative significance of various types of atomistic processes through considerations of the kinetics and not just the energetics and/or the thermodynamics, as is often done. For small Cu islands on Cu(111), we find the effective barriers for diffusion to scale with island size. We await experiments to verify our findings.

CHAPTER VIII

THE CROSSOVER FROM COLLECTIVE MOTION TO PERIPHERY DIFFUSION FOR ADATOM-ISLANDS ON CU(111) AND AG(111)

In this chapter the diffusion of two dimensional Cu islands (larger than 10 atoms) and Ag islands (up to 100 atoms) on Cu(111) and Ag(111) has been studied respectively. A variety of multiple and single atom processes are revealed in the simulations. Also the size dependence of the diffusion coefficients and effective diffusion barriers are calculated. From the tabulated frequencies of events found in the simulation, we show a crossover from diffusion due to a collective motion of the island to a regime in which the island diffuses through a periphery dominated mass transport. This crossover occurs for island sizes of 8 to 11 atoms. For islands containing 19 to 100 atoms the scaling exponent is approximately $3/2$, which is in good agreement with previous work. The diffusion of islands containing 2 to 10 atoms can be explained primarily on the basis of a linear increase of the barrier for the collective motion with the size of the island.

8.1 Introduction

The study of adatom and vacancy island diffusion as a function of size has been an important concern also for many theorists [72], [107]. Because of the inherent differences in the microscopic processes responsible for diffusion and its scaling behavior with size, the discussion has naturally bifurcated into those for the larger islands, usually containing more than 10 atoms, and the smaller ones ($N < 10$). For islands of sizes ($N > 15$), a very important study of diffusion on metal surfaces was done by Voter [7]. He showed that the diffusion coefficient D obeys the following scaling law with a constant scaling exponent α .

$$D \propto \exp(-E_{eff}/k_B T) N^{-\alpha}, \quad (31)$$

where E_{eff} is an effective energy barrier for island diffusion and N is the size of the island. The scaling exponent is expected to reflect the intervening atomistic processes responsible for the diffusion [16, 17]. For larger islands short-range diffusion of the atoms around the periphery, followed by adjustment of island shape, has been proposed to be the dominant mechanism for the diffusion [18, 19]. On the theoretical side, Khare *et al.* [56] explained island diffusion in terms of the shape fluctuations of the outer boundary, thereby establishing a relation between the macroscopic motion of islands and the atomistic processes responsible for their motion. In their work, they considered various types of single atom diffusion mechanisms such as periphery diffusion, terrace diffusion etc. By allowing island diffusion only through the motion of periphery atoms they obtain the scaling exponent $\alpha = 3/2$.

As we have already seen in Chapter 7, the above scaling law is not valid for small island diffusion. For small adatom islands earlier experimental studies point to a general decrease in mobility with increasing island size, except for some cases of anomalously large mobility [96] - [100]. In the case of small Ir islands on Ir(111), concerted gliding motion of the island has been reported [18]. Recent theoretical studies of the energetics and dynamics of 1 – 10 atom Cu islands on Cu(111) have once again highlighted the role of the concerted motion of the island in controlling its diffusion characteristics [112]. For small islands a consistent knowledge of the variation of their mobility with size and the details of the responsible atomistic processes has been established in the previous chapters.

In this chapter we will show through systematic size dependent studies of Cu islands on Cu(111) and Ag islands on Ag(111) that there is a crossover in size dependence of the diffusion and the processes responsible for island diffusion. We will show that the effective diffusion barriers of small islands are much smaller than those of the large ones. In other words for the smaller islands the effective diffusion barrier scales linearly with the size. On the other hand, the effective barrier for large island diffusion is constant, around $0.79eV$ for Cu islands on Cu(111) and $0.465eV$ for Ag islands on Ag(111) with scaling

exponent $\alpha \approx 3/2$. This value of the effective diffusion barrier is closer to the values of high energy processes, like corner detachments or kink detachments, participating in periphery dominated mass transport.

Our purpose in this chapter is two fold. First through a size dependent study of the island diffusion coefficient, we establish the range of sizes of Cu and Ag islands that correspond to specific trends in their diffusion coefficients. Second, through detailed analysis of the frequencies of events for atomistic processes and their energy barriers we provide an evidence for the crossover collective motion to periphery diffusion for adatom-islands on Cu(111) and Ag(111).

8.2 Computational Details

We used the same model system as discussed in the previous chapter (see Fig. 34) considering a fcc(111) substrate with an adatom island on top for both cases of Cu on Cu and Ag on Ag. The gray circles are substrate atoms which stay rigid during the simulation, whereas the dark (colored on-line) circles are the island atoms, placed on fcc sites, which are the hollow sites having no atoms underneath them in the layer below. A KMC simulation step begins by placing an adatom island of desired size, in a randomly chosen configuration, on the substrate. The system evolves by performing a process of its choice, from the multitude of possible single or multiple adatom jumps at each KMC step. We performed about 10^7 such steps at 300 K, 500 K, and 700 K. Typically, at 500 K, 10^7 KMC steps were equal to 10^{-3} sec in physical time. The diffusion coefficient of an adatom island is calculated by $D = \lim_{t \rightarrow \infty} \langle [R_{CM}(t) - R_{CM}(0)]^2 \rangle / 2dt$, where D is the diffusion coefficient, $R_{CM}(t)$ is the position of the center of mass of the island at time t , and d is the dimensionality of the system.

8.3 Results and Discussions

Our results for the calculated size dependence of the diffusion coefficients for Cu islands on Cu(111) and Ag islands on Ag(111) at 300K, 500K, and 700K are shown in Fig. 44. The actual data together with the calculated effective diffusion barriers are also compiled

in Table 11. For island sizes larger than 13 (in the case of Cu), and 7 (in the case of Ag) we clearly observe a crossover region in the behavior of the diffusion coefficients at all temperatures of interest here. In case of Cu, for the size window $19 \leq N \leq 100$, D follows Eq. 31 and we obtain a scaling exponent α that weakly depends on temperature, i.e., $1.49 \leq \alpha \leq 1.64$, in the above mentioned range of temperatures. Consistently, we also found a similar type of crossover in the behavior of effective diffusion barriers as function of size, as shown in Fig. 45. These effective diffusion barriers are calculated from Arrhenius plots of island diffusivity. The effective diffusion barriers are constant in the crossover region of island sizes greater than 13 atoms and 7 atoms in the case of Cu and Ag respectively, as shown in Fig. 45 (a) and (b). For the larger islands the results are in agreement with the predictions of Eq. 31.

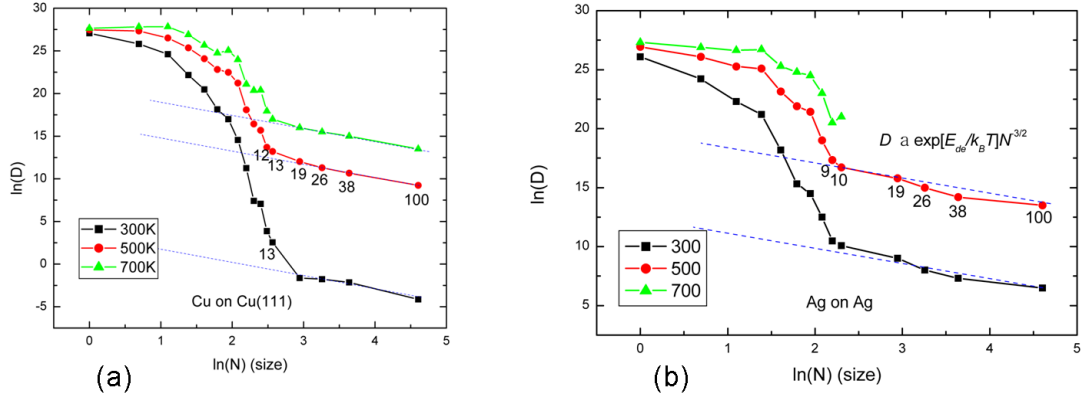


Figure 44: Adatom island diffusion coefficient D vs N for $1 \leq N \leq 100$ at $T = 300\text{K}$, 500K , and 700K , a) Cu on Cu(111), b) Ag on Ag(111).

The behavior of D for the smaller island sizes ($13 \geq N$) where Eq. 31 is not valid is interesting. Contrary to the previous work [58], [116] we have not found any size dependent oscillations in D in this crossover region. On the other hand, the effective diffusion barrier increases linearly with size up to 13 and 7 atom islands in the cases of Cu and Ag, respectively (see Fig. 45 (a) and (b)). This trend in the behavior of the effective diffusion barriers is correlated with the presence of collective island motion for such small islands as already

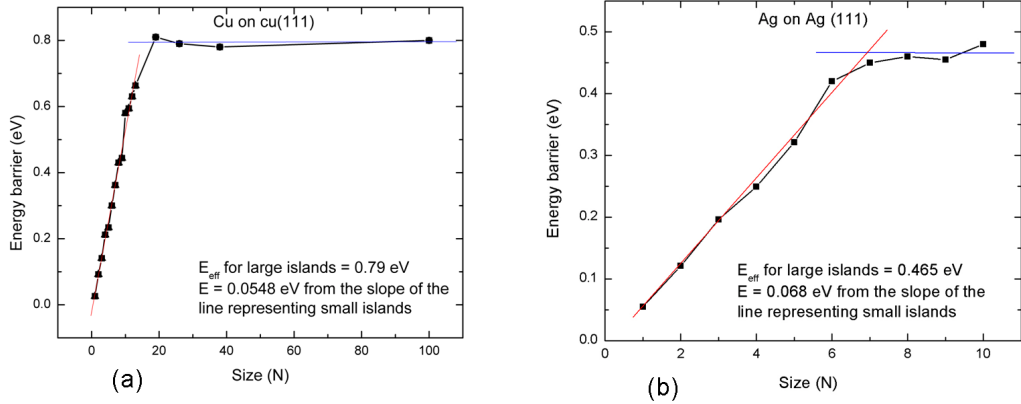


Figure 45: Effective diffusion barriers as a function of the island size, a) Cu on Cu(111), b) Ag on Ag(111).

seen in Chapter 7. Energy barriers of collective motion processes also display a linear increase in their values with size. As shown in Fig. 46 (a) and (b), the activation energy for collective island motion and the effective diffusion barriers overlap in the crossover region for small islands sizes up to 13 and 10 atoms, for Cu and Ag, respectively. We will discuss later the region for larger islands (more than 13 atoms) in which these energy barriers do not overlap. As we see for both Cu and Ag, the effective diffusion barrier increases linearly with size. We may define the effective barrier as $E_{eff} = \xi N + C$ where ξ is the slope of the line representing effective diffusion barriers of smaller islands and C is a constant, as shown in Fig. 45. The values of ξ are 0.0548 eV and 0.060 eV for Cu and Ag, respectively, with C s -0.021 eV and 0.006 eV. Using these parameters, ξ and C , for the linear fit of the effective diffusion barriers we can fit the equation, $(D \propto \exp(E_{eff}/k_{\beta}T))$, on our data for D for small islands. This fit is shown in Fig. 47 with error bars of 5% for smaller island sizes can be easily understood from the fact of linear dependence of the effective diffusion barrier on size.

Now we turn to discussion of the microscopic mechanisms for island diffusion. Here we will try to understand the crossover on the basis of microscopic mechanisms and their frequencies. For simplification, we divide all microscopic mechanisms into three categories, 1) collective motion, 2) single atom processes, and 3) multiple atom processes. From Fig.

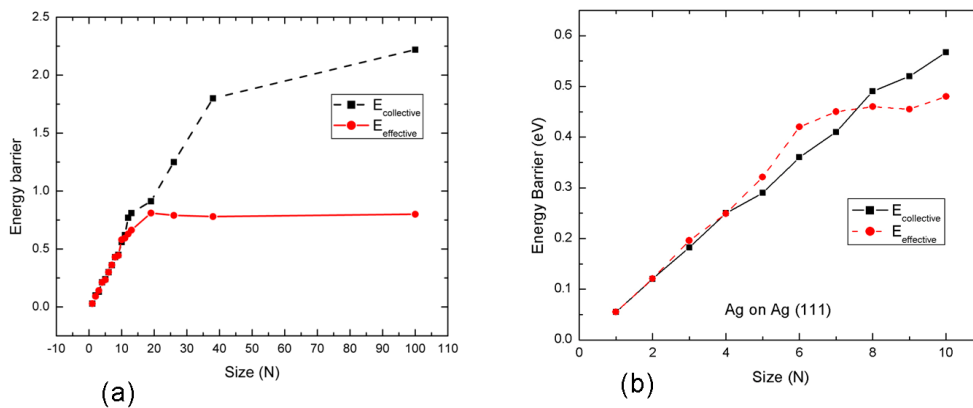


Figure 46: Comparison of effective and collective diffusion barriers as function of the island size, a) Cu on Cu(111), b) Ag on Ag(111).

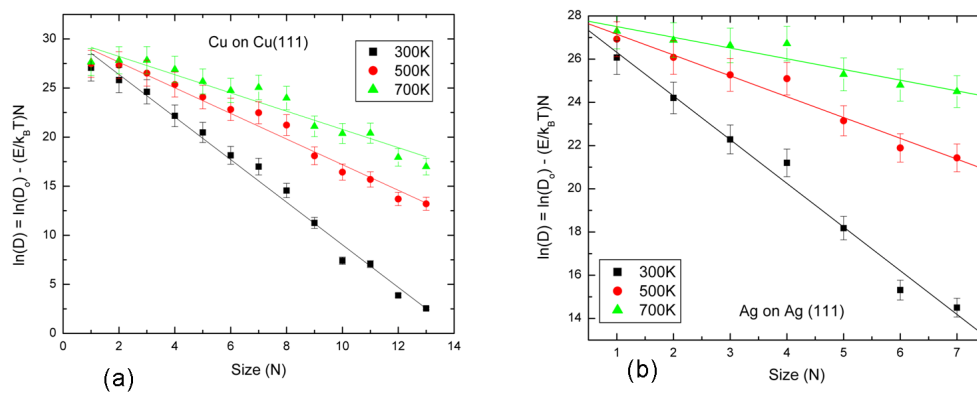


Figure 47: Fit of the proposed theoretical model on simulation data of D , a) Cu on Cu(111), b) Ag on Ag(111).

46 we see that the energy barriers for collective motion of smaller islands are comparatively lower than those of other types of processes and hence collective motion is favorable for them. The frequencies of events that occur in the KMC simulation, plotted in Fig. 48 verify this conclusion for islands containing up to 8 atoms. In Fig. 48, the frequency of events was multiplied by the factor $(\Delta CM_i/\Delta CM_{max})$, to boost up those processes that play a role in the change of the center of mass position. For smaller islands, single atom processes do not make a significant change in the center of mass position, whereas the collective motion significantly changes it. This factor, $(\Delta CM_i/\Delta CM_{max})$, is also useful in eliminating non diffusive processes like trimer rotation. In Fig. 48 we can clearly see a crossover region at 9 and 10 atoms islands in the case of Cu, and at 8 atom islands in the case of Ag. In this region all types of processes have competing energy barriers. For the larger islands having more than 13 atoms the collective motion barriers are very high (see Fig. 45) so the diffusion takes place mostly through single atom processes like corner detachments, kink detachments, or corner rounding, participating in periphery dominated mass transport. We observe a crossover in size dependence of the frequency of events and diffusion coefficients in the regime where the island size is big enough that its barrier of collective motion approaches in a competition with high energy processes participating in periphery mass transport. Fig. 49 show few important multiple atom processes that play an important role in 9 and 10 atoms island diffusion because of their competing barriers with collective motion processes. Also a detailed comparison of Cu and Ag energetics is shown in Figs. 50, 51, 52, 53.

8.4 Conclusions

To summarize, we have performed a systematic study of the crossover from collective island motion to periphery atom diffusion for adatom islands on Cu(111) and Ag(111) using a recently developed self learning KMC simulations in which the system is allowed to evolve

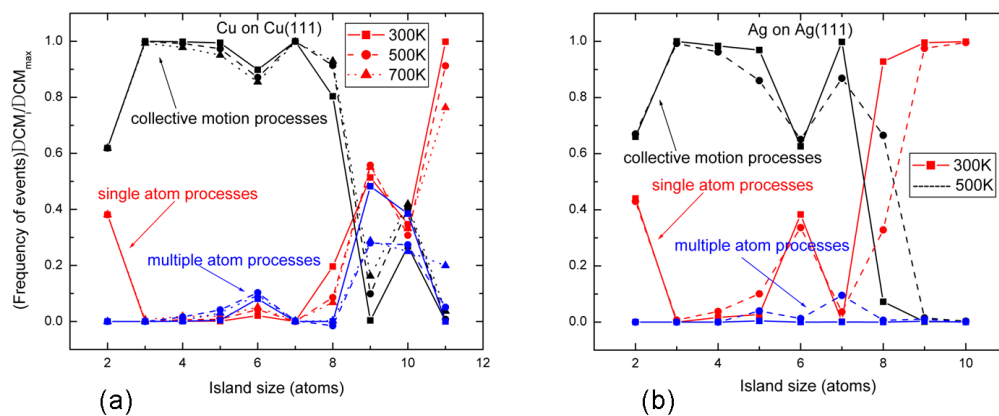


Figure 48: Frequencies of different processes as function of the island size, a) Cu on Cu(111), b) Ag on Ag(111).

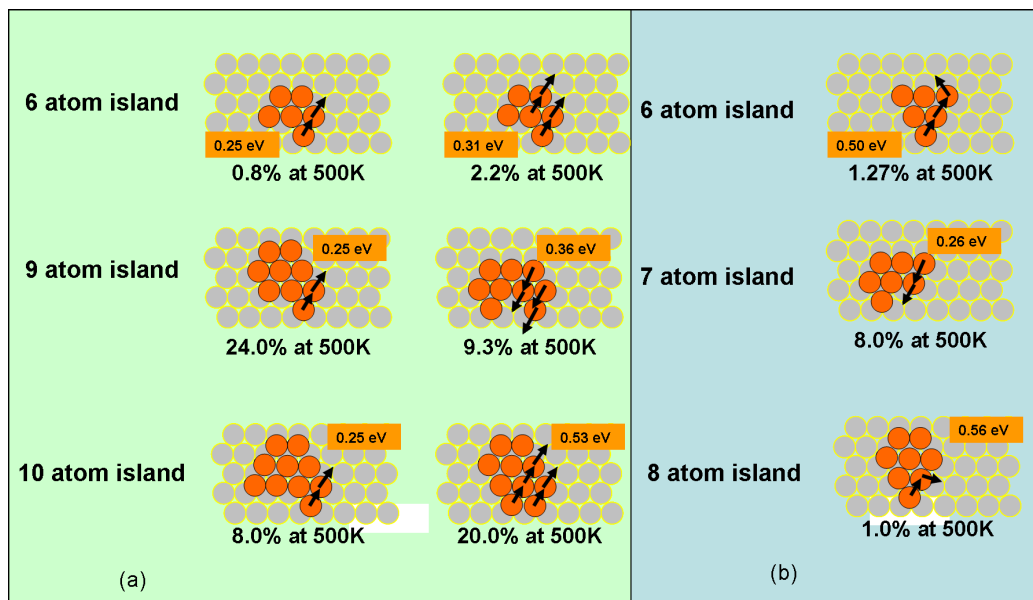


Figure 49: Some important multiple atom mechanisms for island diffusion, a) Cu on Cu(111), b) Ag on Ag(111).

Island size (atoms)	Diffusion coefficient $D(\text{\AA}^2/\text{sec})$ {Ag on Ag (111), [Cu on Cu (111)]}			Effective barrier E_a (eV)
	300 K	500 K	700 K	
1	{ 2.11×10^{11} } [5.70×10^{11}]	{ 4.94×10^{11} } [8.50×10^{11}]	{ 7.16×10^{11} } [1.02×10^{12}]	{0.055} [0.026]
2	{ 3.25×10^{10} } [1.68×10^{11}]	{ 2.12×10^{11} } [6.90×10^{11}]	{ 4.72×10^{11} } [1.24×10^{12}]	{0.121} [0.091]
3	{ 4.77×10^9 } [4.89×10^{10}]	{ 9.45×10^{10} } [3.27×10^{11}]	{ 3.70×10^{11} } [1.22×10^{12}]	{0.196} [0.141]
4	{ 1.61×10^9 } [4.19×10^9]	{ 7.92×10^{10} } [1.06×10^{11}]	{ 4.02×10^{11} } [4.60×10^{11}]	{0.249} [0.211]
5	{ 7.87×10^7 } [7.81×10^8]	{ 1.13×10^{10} } [2.87×10^{10}]	{ 9.71×10^{10} } [1.40×10^{11}]	{0.321} [0.234]
6	{ 4.46×10^6 } [7.57×10^7]	{ 3.22×10^9 } [8.15×10^9]	{ 5.89×10^{10} } [5.60×10^{10}]	{0.420} [0.300]
7	{ 1.98×10^6 } [2.40×10^7]	{ 2.05×10^9 } [5.80×10^9]	{ 4.37×10^{10} } [7.60×10^{10}]	{0.450} [0.362]
8	{ 2.68×10^5 } [2.10×10^6]	{ 1.78×10^8 } [1.65×10^9]	{ 9.74×10^9 } [2.59×10^{10}]	{0.460} [0.430]
9	{ 3.59×10^4 } [7.72×10^4]	{ 3.34×10^7 } [7.20×10^7]	{ 7.99×10^8 } [1.45×10^9]	{0.450} [0.444]
10	{ 2.31×10^4 } [1.65×10^3]	{ 1.78×10^7 } [1.37×10^7]	{ 1.31×10^9 } [7.02×10^8]	{0.480} [0.580]
11	[1.17×10^3]	[6.5×10^6]	[7.23×10^8]	[0.594]
12	[48]	[8.87×10^5]	[6.18×10^7]	[0.630]
13	[12.18]	[5.42×10^5]	[2.40×10^7]	[0.663]
19	{ 8.10×10^3 } [0.196]	{ 7.27×10^6 } [1.67×10^5]	[8.88×10^6]	[0.81]
26	{ 2.98×10^3 } [0.170]	{ 3.26×10^6 } [8.05×10^4]	[5.38×10^6]	[0.79]
38	{ 1.48×10^3 } [0.117]	{ 1.46×10^6 } [4.27×10^4]	[3.26×10^6]	[0.78]
100	{ 6.65×10^2 } [0.016]	{ 7.29×10^5 } [1.02×10^4]	[7.29×10^5]	[0.80]

Table 11: Diffusion coefficients of 1 to 10 atom islands at different temperatures and their effective diffusion barriers.

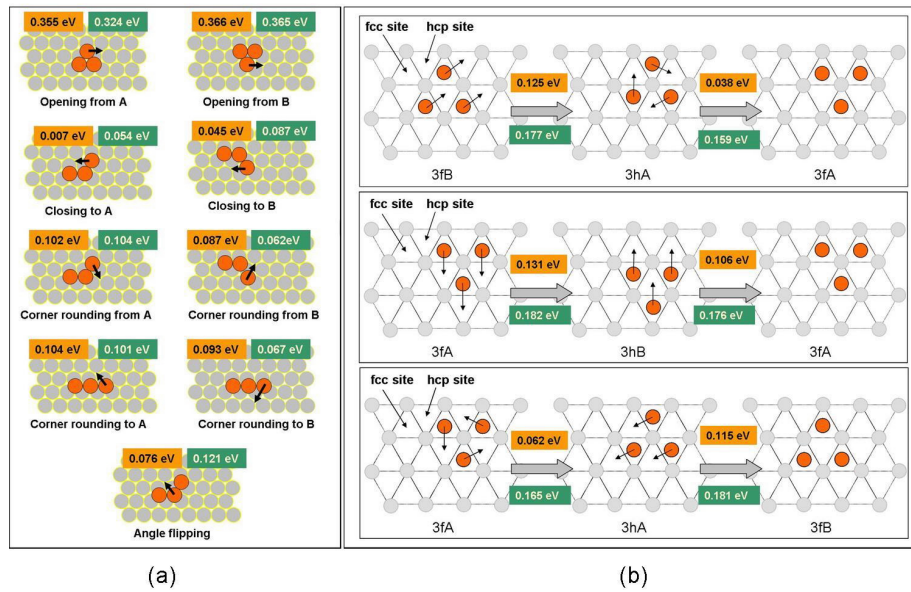


Figure 50: Comparison of Cu and Ag trimer energetics, light colored labels represent energetics of Cu, whereas dark colored labels represent energetics of Ag. (a) Nine mechanisms for trimer diffusion with their corresponding energy barriers, where atoms are allowed to jump from fcc to fcc sites. (b) Trimer diffusion mechanisms observed during MD simulations. These mechanisms are conducted through a collective motion of three atoms by rotation and gliding over the bridge sites from fcc to hcp sites, or vice versa.

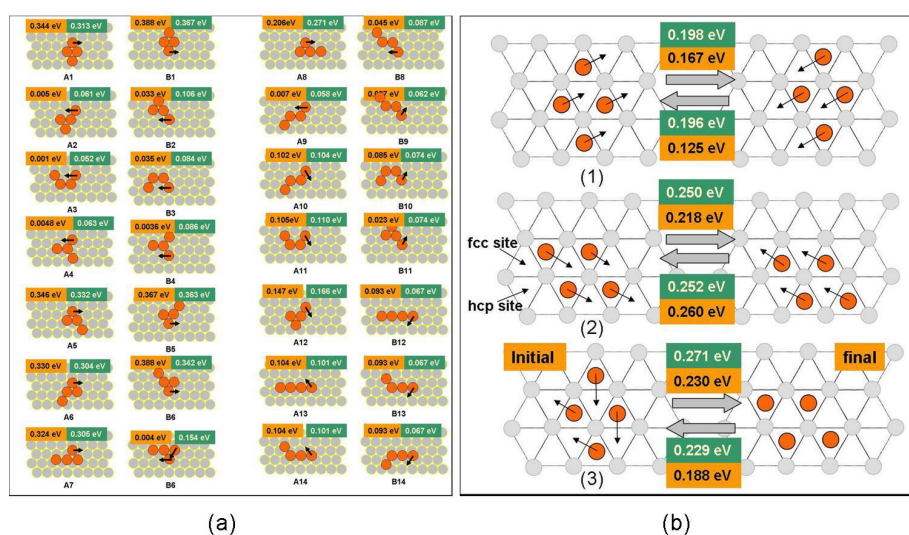


Figure 51: Comparison of Cu and Ag tetramer energetics, light colored labels represent energetics of Cu, whereas dark colored labels represent energetics of Ag. (a) Illustration of 28 mechanisms and their corresponding energy barriers for tetramer diffusion, where jumps are allowed from fcc to fcc sites only. (b) Tetramer diffusion mechanisms revealed from MD simulations: (1) diagonal glide, (2) vertical glide of 4 atom island over the bridge sites and the corresponding energy barriers, and (3) shearing mechanism.

through mechanisms of its choice with the usage of a self generated database of collective motion, single, and multiple atom diffusion processes. Our simulations for large islands (13 to 100 atoms) show a size dependence of diffusion coefficients based on Eq. 31. The effective barrier for large island diffusion is constant in our results, and is around $0.79eV$ for Cu and $0.465eV$ for Ag. These values are closer to the values of high energy processes, like corner detachments or kink detachments, participating in periphery dominated mass transport. We also confirm that the scaling rule from Eq. 31 is not valid for small island diffusion. Effective diffusion barriers for these small islands are significantly smaller than the effective diffusion barriers for large islands. Contrary to the case of the large islands, which have almost constant effective diffusion barriers, the small islands show a trend of increasing effective diffusion barrier with island size. In this case, processes representing the collective motion of the whole island are responsible for small island diffusion because of their comparatively low energy barriers. We observe a crossover in size dependence of diffusion coefficients in the regime where the island size is big enough that its barrier

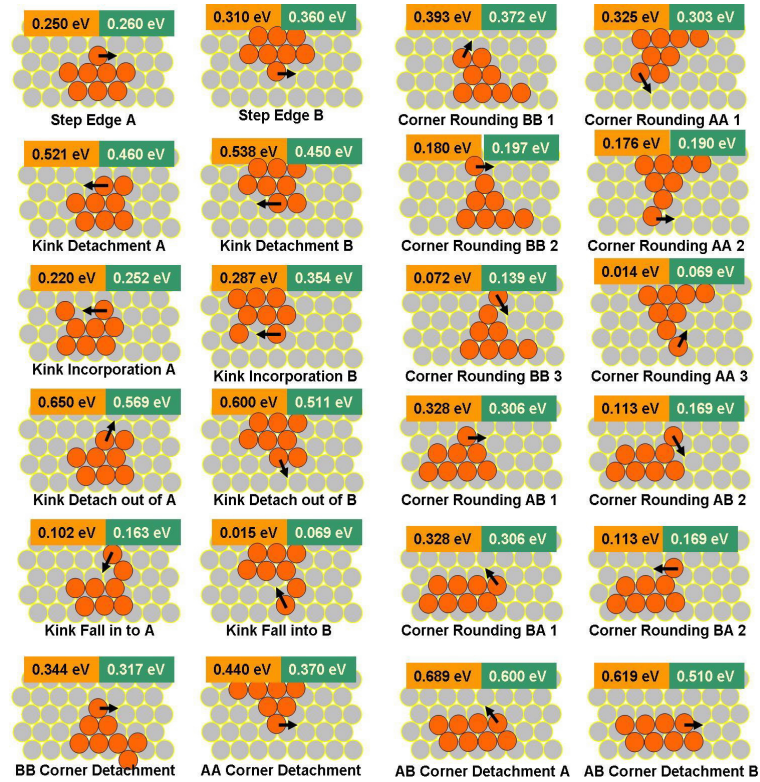


Figure 52: Comparison of Cu and Ag single atom energetics, light colored labels represent energetics of Cu, whereas dark colored labels represent energetics of Ag. A few examples of single and multiple atom mechanisms and their corresponding energy barriers used in our KMC simulations for island larger than 4 atoms. Jumps are allowed from fcc to fcc sites only.

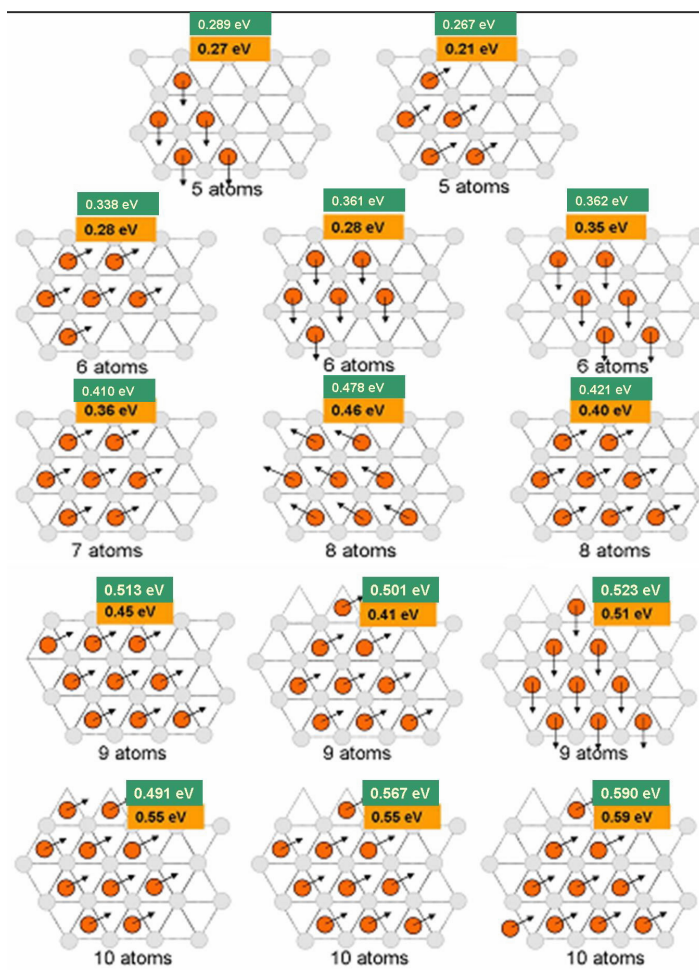


Figure 53: Comparison of Cu and Ag concerted motion energetics, light colored labels represent energetics of Cu, whereas dark colored labels represent energetics of Ag. Diffusion mechanisms found by performing MD simulations for the island sizes of 5-10 atoms and their corresponding energy barriers when they glide over the bridge sites exhibiting collective motion of all atoms.

for collective motion approaches a competition with high energy processes participating in periphery mass transport.

CHAPTER IX

CONCLUSIONS

In this dissertation a comprehensive study of morphological evolution of surfaces based on a detailed analysis of atomistic processes and their energetics is presented. During the examination of the energetics and dynamics of adatom descent from small two dimensional Ag islands on Ag(111), we found that the pre-exponential factors for the two diffusion processes (A-type and B-type step) differ by a factor of 20. These different pre-exponential factors play a big role in defining the probabilities of A-type and B-type steps at different temperatures. MD simulations concluded that the A-type step formation is a favorable process at low temperature, while it is not favorable at high temperatures because of the significantly growing probability of B-type step formation with temperature. These results call into question the application of solely energetic considerations in drawing conclusions about processes at finite temperatures.

Further, to understand the macroscopic properties of a system on the basis of its atomic scale information, spatial and temporal fluctuations of step edges on vicinal Cu(1,1,13) and Cu(1,1,19) surfaces is studied using kinetic Monte Carlo (KMC) simulations. Numerical results of quantities like step edge diffusivity, step edge stiffness, and kink formation energy derived from spatial and temporal correlation functions of the step positions are in quantitative agreement with both theoretical predictions and experimental data, demonstrating the role of mass transport along step edges and kink fluctuations for Cu(1,1, m) surfaces. Finally, we would like to note that while the results here are in excellent agreement with those from experimental observations and predictions of continuum models, there are some limitations for the present type of models. It has been shown that solid-on-solid and Ising type of lattice models are unable to quantitatively reproduce the orientational dependence of the step stiffness [66]. Although this is not important for the simple kink excitations

here, it demonstrates the importance of including more realistic interactions in the models of fluctuations in low-dimensional nanostructures. Since energetics of atomistic processes were determined from bound counting formula in these simulations, realistic simulations may not be performed with high reliability using simple models for KMC simulations.

We have also addressed the issue of completeness of KMC simulations by proposing a method in which the system finds, calculates, and collects the energetics of all possible diffusion processes that the moving entities are capable of performing. What separates our technique from others recently proposed is the provision for storing and retrieving the environment-dependent activation energy barriers from a database. Examination of the database shows that the simulation proceeds much faster when the set of processes is "quasi-saturated" and that after sampling such regions the system has the ability to trigger the participation of new diffusion processes requiring enhanced CPU's for the calculation of new activation energy barriers. The system eventually settles down and the number of MC steps needed to do this depends on the system and the number of entries already in the data base (about $10^7 - 10^8$ steps). With the use of a pattern recognition scheme we are able to identify and calculate the frequency of occurrence of individual single and multiple atom diffusion processes that actually participate in the evolution of a particular entity. The microscopic details of the processes involved in surface morphological evolution can thus be documented for a system that has the freedom to evolve on its own accord. We showed this through application to the diffusion and coalescence of 2D adatom islands on Cu(111) for which the simulation began with an empty database. Once a substantial accumulation has occurred, the simulation time speeds up by orders of magnitudes and allows the calculation of system dynamics for time scales relevant to those phenomena happening in the laboratory. Interestingly, the two simple examples that we have presented here show that only a few dozen diffusion processes are in the end vital for a diffusion event. The question, of course, is: which ones? Our approach answers this question. As we have already alluded to, the task of calculating diffusion prefactors is still ahead of us. This is particularly important since we find many competing processes to differ only slightly in energy and differences in their vibrational entropy contributions to the prefactors can make a difference in the

ultimate evolution of the film morphology. Another important result from our simulations with the open database is that dynamical evolution of the system with prejudged diffusion processes may yield erroneous results. Also, the pattern recognition schemes are a prudent way to develop a database of diffusion processes and their energetics. It does involve a lot of work in the beginning but once the database is compiled, it can be used for any type of simulation of the system.

Using the new SLKMC techniques, we have performed a systematic study of the diffusion of small Cu islands on Cu(111). The beauty of the technique is that the system is allowed to evolve through mechanisms of its choice with the usage of a self generated database of single and multiple atom diffusion processes. Complementary molecular dynamics simulations carried out for a few cases provided further details of several new mechanisms for small island diffusion that were not automatically picked up by our *SLKMC* method because of the initial restriction of fcc site occupation. We found significant changes in the size dependent variations of diffusion characteristics of the islands after including concerted motion mechanisms that were revealed from MD simulations. We find that these small sized islands diffuse primarily through concerted motion with a small contribution from single atom processes, even though for certain cases the frequency of single atom processes is large because of lower activation energies. By allowing the system the possibility of evolving in time through all types of processes of its choice, we are able to establish the relative significance of various types of atomistic processes through considerations of the kinetics and not just the energetics and/or the thermodynamics, as is often done. For small Cu islands on Cu(111), we find the effective barriers for diffusion to scale with island size.

Further, we have extended our research to perform a systematic study of the crossover from collective motion to periphery diffusion for adatom islands on Cu(111) and Ag(111). Our simulations for large islands (19 to 100 atoms) show a size dependence of diffusion coefficients based on the scaling law. The effective barrier for large island diffusion is constant in our results, and is around $0.79eV$ for Cu and $0.465eV$ for Ag. This value is closer to the values of high energy processes, like corner detachments or kink detachments, participating in periphery dominated mass transport. Whereas the above mentioned diffusion law is not

valid for small island diffusion. Effective diffusion barriers for these islands are significantly smaller than the effective diffusion barriers of large islands. Contrary to large islands, which have almost constant effective diffusion barriers, the small islands show a trend of increasing effective diffusion barrier with island size. In this case, processes representing the collective motion of whole island are responsible for small island diffusion because of their comparatively low energy barriers. These collective motion barriers linearly increase with island size. We observe a crossover in size dependence of diffusion coefficients in the regime where the island size is big enough that its barrier of collective motion approaches a competition with high energy processes participating in periphery mass transport.

Bibliography

- [1] G. Binnig, H. Rohrer, Ch. Gerber, and E. Weibel, *Appl. Phys. Lett.* **40**, 178 (1982).
- [2] G. Binnig, H. Rohrer, Ch. Gerber, and E. Weibel, *Phys. Rev. Lett.* **49**, 57 (1982).
- [3] M.C. Payne, M.P. Teter, D.C. Allen, T.A. Arias and J.D. Joannopoulos, *Rev. Mod. Phys.* **64**, 1045 (1992).
- [4] S.M. Foiles, M.I. Baskes, and M.S. Daw, *Phys. Rev. B* **33**, 7983 (1986).
- [5] A.F. Voter, F. Montalenti, T. C. Germann, *Annu. Rev. Mater. Res.* **32**, 321 (2002).
- [6] A. B. Bortz, M. H. Kalos, and J. L. Lebowitz, *J. Comp. Phys.* **17**, 10 (1975); M. Kotrla, *Comp. Phys. Commun.* **97**, 82 (1995); J. L. Blue, I. Beichl, and F. Sullivan, *Phys. Rev. E* **51**, R867 (1995).
- [7] A.F. Voter, *Phys. Rev. B* **34**, 6819 (1986).
- [8] P.A. Maksym, *Semicond. Sci. Technol.* **3**, 594 (1988).
- [9] J.Y. Tsao, *Materials Fundamentals of Molecular Beam Epitaxy*, World Scientific, Singapore, (1993)
- [10] A.-L. Barabasi and H.E. Stanley, *Fractal Concepts in Surface Growth*, Cambridge University Press, New York (1995).
- [11] N.C. Metropolis, A.W. Rosenbluth, M.N. Rosenbluth, A.H. Teller, and E. Teller, *J. Chem. Phys.* **21**, 6 (1953).
- [12] T. Michely, M. Hohage, M. Bott, and G. Comsa, *Phys. Rev. Lett.* **70**, 3943 (1993).
- [13] C. Teichert, *Phys. Rep.* **365**, 335 (2002).
- [14] M. Geisen-Seibert, R. Jentjens, M. Poensgen, H. Ibach, *Phys. Rev. Lett.* **73**, 911 (1994), and references therein; M. Giesen-Seibert, F. Schmitz, R. Jentjens, and H. Ibach, *Surf. Sci.* **329**, 47 (1995).

- [15] M. Giesen, Prog. Surf. Sci. **68**, 1 (2001).
- [16] A. Bogicevic, S. Liu, J. Jacobsen, B. Lundqvist, and H. Metiu, Phys. Rev. B **57**, R9459 (1998).
- [17] T.S. Rahman, A. Kara, O. Trushin, A. Karim, unpublished (2004).
- [18] S.C. Wang, and G. Ehrlich, Surf. Sci. **239**, 301 (1990).
- [19] C. L. Liu and J. B. Adams, Surf. Sci. **268**, 73 (1992).
- [20] P. Hohenberg and W. Kohn, Phys. Rev. B **136**, 864 (1964).
- [21] R. Car and M. Parrinello, Phys. Rev. Lett. **55**, 2471 (1985).
- [22] Z.J. Tian and J.E. Black, Surf. Sci. **303**, 395 (1994).
- [23] U. Kurpick, P. Kurpick, and T.S. Rahman, Surf. Sci. **383**, L713 (1997).
- [24] K. W. Jacobsen, J. K. Norskov, and M. J. Puska, Phys. Rev. B **35**, 7423 (1987).
- [25] W. Murray Gill, P.E. and M.H. Wright. Practical Optimization. Academic Press, London, 1981.
- [26] O. Trushin, E. Granato, S.C. Ying, P. Salo, T. Ala-Nissila, Phys. Rev. B **65**, 241408 (2002).
- [27] H. Jonsson, G. Mills and K. W. Jacobsen, in Classical and Quantum Dynamics in Condensed Phase Simulations, ed. by B. J. Berne et al World Scientific, Singapore, 1998.
- [28] T.S. Rahman, A. Kara. A. Karim, and A. Al-Rawi, in *Collective Diffusion on Surfaces: Correlation Effects and Adatom Interactions*, ed. by M.C. Tringides and Z. Chvoj (Kluwer Academic Publishers, Netherlands) 327 (2001).
- [29] M. P. Allen and D. J. Tildesley, Computer Simulation of Liquids (Clarendon, Oxford, 1987).

- [30] G.W. Gear, *Numerical initial value problems in ordinary differential equations*, Prentice Hall, Englewood Cliffs, 1971.
- [31] T.S. Rahman, C. Ghosh, O. Trushin, A. Kara, A. Karim, in *Nanomodeling*, edited by Akhlesh Lakhtakia, Sergey A. Maksimenko, Proceedings of SPIE, Vol. **5509** (SPIE, Bellingham, WA, 2004).
- [32] O. Trushin, A. Karim, A. Kara, T. S. Rahman, Phys. Rev. B **72**, 115401 (2005).
- [33] G. Henkelman and H. Jonsson, Phys. Rev. Lett. **90**, 116101 (2003).
- [34] G. H. Vineyard, J. Phys. Chem. Solids **3**, 121 (1957).
- [35] U. Kürpick, A. Kara and T.S. Rahman, Phys. Rev. Lett. **78**, 1086 (1997).
- [36] U. Kürpick and T.S. Rahman, Phys. Rev. B **57**, 2482 (1998).
- [37] J. H. Block, A. M. Bradshaw, P. C. Gravelle, J. Haber, R. S. Hansen, M. W. Roberts, N. Sheppard, and K. Tamaru, Pure & Appl. Chem., Vol. **62**, No. **12**, pp. 2297-2322,1990.
- [38] P. Hofmann, Lecture Notes on Surface Science, 2005.
- [39] T. Fu and T.T. Tsong, Phys. Rev. B **61**, 4511 (2000).
- [40] P. Feibelman, Phys. Rev. B **62**, 17020 (2000), and references therein.
- [41] A. Bogicevic, J. Strömquist, and B.I. Lundqvist, Phys. Rev. Lett. **81**, 637 (1998).
- [42] S. Ovesson, A. Bogicevic, and B.I. Lundqvist, Phys. Rev. Lett. **83**, 2608 (1999).
- [43] F. Maca, M. Kotrla, and O.S. Trushin, Surf. Sci. **454-456**, 579 (2000).
- [44] A. Kara, T.S. Rahman, to be published.
- [45] M.S. Daw, S.M. Foiles, and M.I. Baskes, Mat. Sci. Rep. **9**, 251 (1993).
- [46] K.P. Bohnen and K.M. Ho, Surface science Reports **19**, 99 (1993).

- [47] T.S. Rahman, in Condensed Matter Theories, eds. J. Clark, K. Shoaib, and A. Sadiq, Vol. **9**, Nova, NY, 299, (1994).
- [48] A. Kara, S. Durukanoglu, and T.S. Rahman, J. Chem. Phys. **106**, 2031 (1997).
- [49] S. Durukanoglu, A. Kara, and T.S. Rahman, Phys. Rev. B **55**, 13894 (1997).
- [50] U. Kürpick, A. Kara, and T.S. Rahman, Phys. Rev. Lett. **78**, 1086 (1997); U. Kürpick and T.S. Rahman, Surf. Sci. **383**, 137 (1997).
- [51] A.F. Voter and S.P. Chen, Proc. Mat. Res. Soc. **82**, 175 (1986).
- [52] J. Lapujoulade, Surf. Sci. Rep.**20**, 191 (1994).
- [53] H.C. Jeong and E. D. Williams, Surf. Sci. Rep. **34**, 171 (1999).
- [54] N. C. Bartelt, T. L. Einstein, and E. D. Williams, Surf. Sci. **240**, L591 (1990).
- [55] N.C. Bartelt, J.L. Goldberg, T.L. Einstein, and E.D. Williams, Surf. Sci. 273 (1992) 252.
- [56] S. V. Khare, N. C. Bartelt, and T. L. Einstein, Phys. Rev. Lett. **75**, 2148 (1995); S. V. Khare and T. L. Einstein, Phys. Rev. B **54**, 11752 (1996).
- [57] E. Le Goff, L. Barbier, B. Salanon, Surf. Sci. **432**, 139 (1999).
- [58] J. Heinonen, I. Koponen, J. Merikoski, and T. Ala-Nissila, Phys. Rev. Lett. **82**, 2733 (1999).
- [59] M. Rusanen, I. T. Koponen, J. Heinonen, and T. Ala-Nissila, Phys. Rev. Lett. **86**, 5317 (2001).
- [60] M. Rusanen, I. T. Koponen, T. Ala-Nissila, C. Ghosh, and T. S. Rahman, Phys. Rev. B **65**, 041404(R) (2002).
- [61] J. Merikoski, I. Vattulainen, J. Heinonen, and T. Ala-Nissila, Surf. Sci. **387**, 167 (1997); J. Merikoski and T. Ala-Nissila, Phys. Rev. B **52**, R8715 (1995).

- [62] H. Mehl, O. Biham, I. Furman and M. Karimi, Phys. Rev. B **60** 2106 (1999).
- [63] M. Giesen, Surf. Sci. **370**, 55 (1997).
- [64] M. Poensgen, J. F. Wolf, J. Frohn, M. Giesen, and H. Ibach, Surf. Sci. **274**, 430 (1992).
- [65] F. Szalma, W. Selke, and S. Fischer, Physica A **294**, 313 (2001).
- [66] S. Dieluweit, H. Ibach, M. Giesen, and T. L. Einstein, Phys. Rev. B **67** 121410 (2003).
- [67] P. Stoltze, J. Phys. Cond. Matt. **6** (1994) 9495.
- [68] B.D. Yu and M. Scheffler, Phys. Rev. Lett. **77**, 1095 (1996).
- [69] F. Ercolessi, M. Parrinello, and E. Tosatti, Phil. Mag. A **58**, 213 (1988); M.S. Daw, S.M. Foiles, and M.I. Baskes, Mater. Sci. Rep. **9**, 251 (1993).
- [70] D.T. Gillespie, J. Comput. Phys. **22**, 403 (1976).
- [71] O.S. Trushin, P. Salo, T. Ala-Nissila, Phys. Rev. B **62**, 1611 (2000).
- [72] P. Salo, J. Hirvonen, I.T. Koponen, O.S. Trushin, J. Heinonen, T. Ala-Nissila, Phys. Rev. B **64**, 161405 (2001).
- [73] S.C. Wang, U. Kurpick, G. Ehrlich, Phys. Rev. Lett. **81** 4923 (1998).
- [74] S.C. Wang, G. Ehrlich, Phys. Rev. Lett. **79** 4234 (1997).
- [75] M.R. Sorensen and A.F. Voter, J. Chem. Phys. **112**, 9599 (2000).
- [76] G. Henkelman and H. Jonsson, J. Chem. Phys. **115**, 9657 (2001).
- [77] A.F. Voter, F. Montalenti, T. C. Germann, Annu. Rev. Mater. Res. **32**, 321 (2002).
- [78] R.A. Miron and K.A. Fichthorn, J. Chem. Phys. **119**, 6210 (2003); R.A. Miron and K.A. Fichthorn, Phys. Rev. Lett. **93**, 138201 (2004).

- [79] H. Jónsson, G. Mills and K. W. Jacobsen, in *Classical and Quantum Dynamics in Condensed Phase Simulations*, ed. by B. J. Berne *et al* (World Scientific, Singapore, 1998).
- [80] G. Henkelman and H. Jonsson, *J. Chem. Phys.* **115**, 7010 (1999).
- [81] J. Repp, G. Meyer, K. H. Rieder, and P. Hyldgaard, *Phys. Rev. Lett.* **91**, 206102 (2003).
- [82] M. Giesen and H. Ibach, *Surf. Sci.* **529**, 135 (2003).
- [83] J. Camarero, J.D.L. Figuera, J.J.D. Miguel, R. Miranda, J. Alvarez, S. Ferrer, *Surf. Sci.* **459**, 191 (2000).
- [84] S. Glasstone, K.J. Laidler, and H. Eyring, *The Theory of Rate Processes* (Mc Graw-Hill, New York, 1941); D. A. King, *J. Vac. Sci. Technol.* **17**, 241 (1980).
- [85] R.A. Miron and K.A. Fichtthron, *Molecular Simulation* **30**, 273 (2004).
- [86] L. J. Munro and D. J. Wales, *Phys. Rev. B* **59**, 3969 (1999), and references therein.
- [87] A.F. Voter, *J. Chem. Phys.* **106**, 4665 (1997).
- [88] O. S. Trushin, P. Salo, T. Ala-Nissila, and S. C. Ying *Phys. Rev. B* **69**, 033405 (2004).
- [89] T.S. Rahman, A. Kara, A. Karim, and O. Trushin, *Mater. Res. Proceedings* (2004).
- [90] A. Al-Rawi and T.S. Rahman, unpublished.
- [91] A. Bogicevic, C. Liu, J. Jacobsen, H. Metiu, *Phys. Rev. B* **57**, R9459-R9462 (1998).
- [92] M. Giesen, *Step and Island Dynamics* (internal report)
- [93] M. Karimi, T. Tomkowski, G. Vodali, O. Biham, *Phys. Rev. B* **52**, 5364 (1995).
- [94] C. Ghosh, A. Kara, and T. S. Rahman, to be published; C. Ghosh. Ph. D. thesis, Kansas State University, 2003.
- [95] P. Vikulov, O. Trushin, A. Kara, and T.S. Rahman (unpublished).

- [96] D. W. Bassett, J. Phys. C **9**, 2491 (1976).
- [97] T. T. Tsong and R. Casanova, Phys. Rev. B **22**, 4632 (1980).
- [98] S.C. Wang and G. Ehrlich, Phys. Rev. Lett. **68**, 1160 (1992).
- [99] S.C. Wang, U. Kuerpick, and G. Ehrlich, Phys. Rev. Lett. **81**, 4923 (1998).
- [100] G.L. Kellogg, Appl. Surf. Sci. **67**, 134 (1993)
- [101] J.M. Wen, S.L. Chang, J.W. Burnett, J.W. Evans, and P.A. Thiel, Phys. Rev. Lett. **73**, 2591 (1994).
- [102] K. Morgenstern, G. Rosenfeld, B. Poelsema, and G. Comsa, Phys. Rev. Lett. **74**, 2058 (1995).
- [103] W.W. Pai, A.K. Swan, Z. Zhang, and J.F. Wendelken, Phys. Rev. Lett. **79**, 3210 (1997).
- [104] M. Giesen, G. Schulze Icking-Konert, and H. Ibach, Phys. Rev. Lett. **80**, 552 (1998).
- [105] H.A. van der Vegt, J. Alvarez, X. Torrelles, S. Ferrer, and E. Vlieg, Phys. Rev. B **52**, 17443 (1995).
- [106] C. Busse, C. Polop, M. Muller, K. Albe, and U. Linke, Phys. Rev. Lett **91**, 056103 (2003).
- [107] M. Mueller, K. Albe, C. Busse, A. Thoma, and T. Michely, Phys. Rev. B **71**, 075407 (2005).
- [108] J.C. Hamilton, M.S. Daw, and S.M. Foiles, Phys. Rev. Lett. **74**, 2760 (1995).
- [109] D.S. Sholl and R.T. Skodje, Phys. Rev. Lett. **75**, 3158 (1995).
- [110] C.M. Chang, C.M. Wei, and S.P. Chen, Phys. Rev. Lett. **85**, 1044 (2000).
- [111] A. Hynninen, A. Al-Rawi, T. Ala-Nissila, and T. S. Rahman, unpublished (2002).

- [112] M. Marinica, C. Barreteau, M.C. Desjonqeres, and D. Spanjaard, Phys. Rev. B **70**, 075415 (2004).
- [113] Y. Mishin, M.J. Mehl, D.A. Papaconstantopoulos, A.F. Voter, and J.D. Kress, Phys. Rev. B **63**, 224106 (2001).
- [114] We have now developed a *SLKMC* code which inherently uses the 9-shell pattern recognition scheme.
- [115] A. Karim, A. Al-Rawi, A. Kara, T. S. Rahman, O. Trushin, T. Ala-Nissila, Phys. Rev. B **73**, 165411 (2005).
- [116] K.A. Fichthorn and S. Pal, Bull. Am. Phys. Soc. **43**, 850 (1998); (unpublished).

APPENDIX A

LIST OF PUBLICATIONS

The following is a list of publications that I have authored/co-authored during my career at Kansas State University. This dissertation is composed of results presented in the first 5 publications of the list.

1. A. Karim, A. Kara, and T. S. Rahman, "The crossover from collective motion to periphery diffusion for adatom-islands on Cu (111) and Ag (111)", to be submitted to Phys. Rev. Lett. (2006).
2. A. Karim, A. Al-Rawi, A. Kara, T. S. Rahman, O. Trushin, and T. Ala-Nissila, "Diffusion of small two-dimensional Cu islands on Cu(111) studied by a self-learning kinetic Monte Carlo method", Phys. Rev. B 73, 165411 (2006).
3. O. Trushin, A. Karim, A. Kara, and T. S. Rahman, "Self-learning kinetic Monte Carlo method: Application to Cu(111)", Phys. Rev. B 72, 115401 (2005).
4. A. Karim, M. Rusanen, I. T. Koponen, T. Ala-Nissila, and T. S. Rahman, "Fluctuations of Surfaces Steps in Equilibrium: A kinetic Monte Carlo Study". Surface Science 554, L113 (2004).
5. T. S. Rahman, A. Kara, A. Karim, and A. Al-Rawi, "Paths, Barriers, and Prefactors for Adatom Descent from Ag Cluster on Ag (111)". Collective Diffusion on Surfaces: Correlation Effects and Adatom Interactions, 327-338, 2001 Kluwer Academic Publishers. Printed in the Netherlands.
6. A. Karim, A. Al-Rawi, A. Kara, T. S. Rahman, "Decay of Ag ad-atom island inside vacancy island on Ag (111)", to be submitted to Phys. Rev. B (2006).
7. M.O. Jahma, M. Rusanen, A. Karim, I.T. Koponen, T. Ala-Nissila, and T.S. Rahman,

"Diffusion and Submonolayer Island Growth During Hyper Thermal Deposition on Cu(100) and Cu(111)", Surface Science 598, 246-252 (2005).

8. T. S. Rahman, A. Kara, O. Trushin, A. Karim, "Cluster Diffusion and Coalescence on Metal Surfaces: application of a Self-teaching Kinetic Monte-Carlo method", 2004 MRS Fall Meeting Proceedings.
9. T. S. Rahman, C. Gosh, O. Trushin, A. Kara, A. Karim, "Atomistic studies of thin film growth", Proc. SPIE 5509, 1-14, Nanomodeling.